USGS
science for a changing world

National Cooperative Geologic Mapping Program

A Three-Dimensional Geologic Framework Model of the Northern Great Plains Region of Montana, North Dakota, South Dakota, and Wyoming, USA

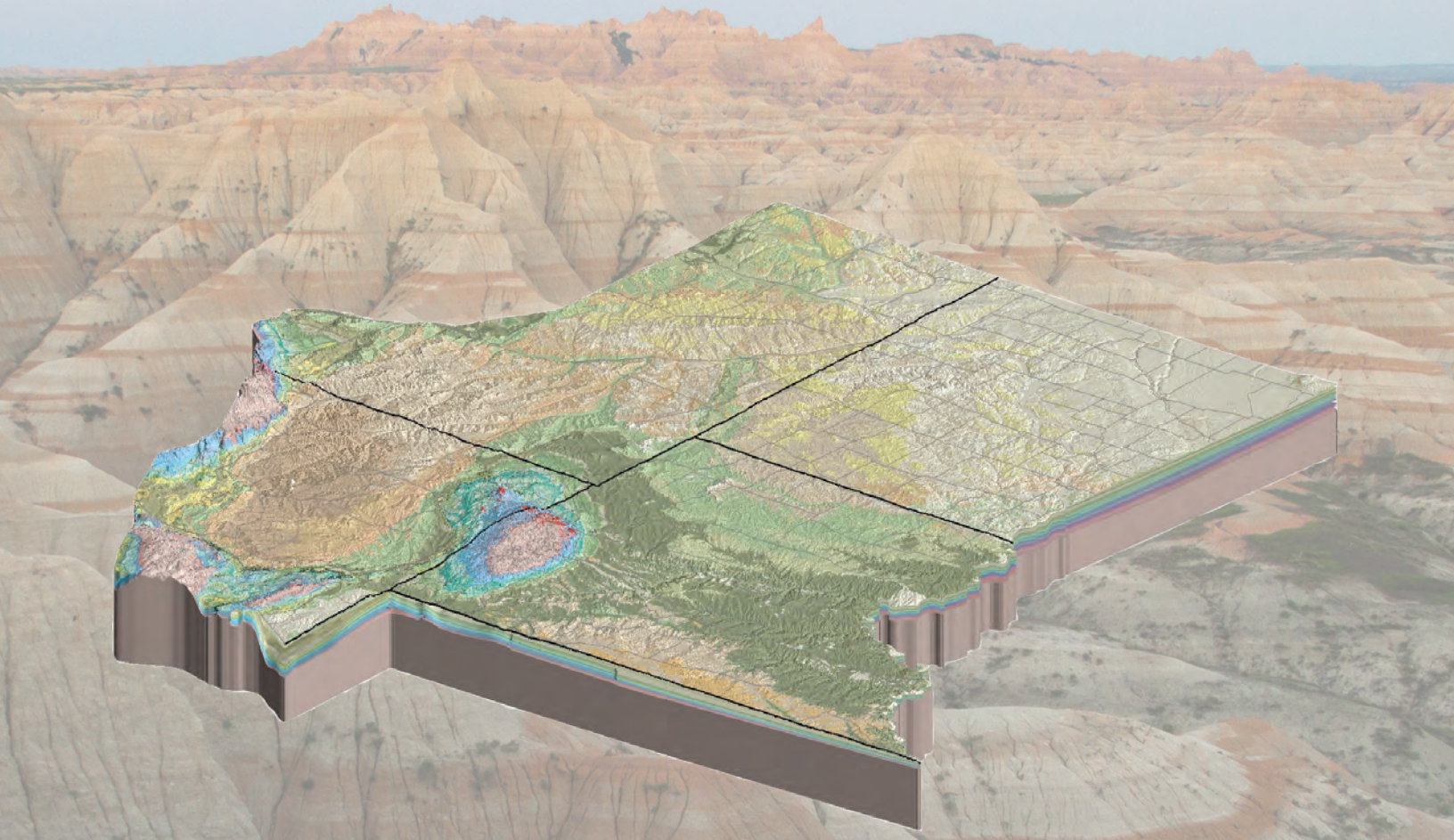

Scientific Investigations Report 2026–5127

U.S. Department of the Interior
U.S. Geological Survey

Cover: Background photograph of Badlands National Park by David Restivo, National Park Service. Overlaying image showing a perspective view of the northern Great Plains three-dimensional geologic framework model from Leland Spangler, U.S. Geological Survey.

A Three-Dimensional Geologic Framework Model of the Northern Great Plains Region of Montana, North Dakota, South Dakota, and Wyoming, USA

By Leland R. Spangler

National Cooperative Geologic Mapping Program

Scientific Investigations Report 2026–5127

U.S. Department of the Interior
U.S. Geological Survey

U.S. Geological Survey, Reston, Virginia: 2026

For more information on the USGS—the Federal source for science about the Earth, its natural and living resources, natural hazards, and the environment—visit https://www.usgs.gov.

For an overview of USGS information products, including maps, imagery, and publications, visit https://store.usgs.gov/ or contact the store at 1–888–275–8747.

Suggested citation:
Spangler, L.R., 2026, A three-dimensional geologic framework model of the northern Great Plains region of Montana, North Dakota, South Dakota, and Wyoming, USA: U.S. Geological Survey Scientific Investigations Report 2026–5127, 51 p., https://doi.org/10.3133/sir20265127.

Associated data for this publication:
Spangler, L.R., 2024a, Digital database of a 3D geological model of the Powder River Basin and Williston Basin regions, USA: U.S. Geological Survey data release, https://doi.org/10.5066/P13RSCBV.

Spangler, L.R., 2024b, Digital data for a 3D geological model of western South Dakota, USA: U.S. Geological Survey data release, https://doi.org/10.5066/P9LK4QHJ.

ISSN 2328-0328 (online)

Acknowledgments

This study was funded by the U.S. Geological Survey's (USGS) National Cooperative Geologic Mapping Program.

I would like to extend my gratitude to Jesse Melick (Montana State University), Sarah Gelman (USGS), the South Dakota Geological Survey, the Montana Bureau of Mines and Geology, the Wyoming Geological Survey, and the North Dakota Geological Survey for their technical consultation and openness to sharing data which significantly enhanced the quality of the study. Special thanks are due to Don Sweetkind, Judd Goldberg, and Jaime Hirtz of the USGS for their invaluable support in data compilation, synthesis, and technical consultation. I would like to additionally thank Jeremy Havens (USGS) and Brooklyn Smout (USGS) for assistance with data organization and drafting figures.

This manuscript was greatly improved by the thoughtful peer reviews provided by Theresa Schwartz (USGS), and Tyson Smith (USGS). Their insights and suggestions were invaluable in refining the final product.

Contents

Plates

[Available for downloading from https://doi.org/10.3133/sir20265127]

1. Elevation from sea level for the uppermost horizon of the Precambrian basement rock unit produced in the three-dimensional geological model
2. Elevation from sea level for the uppermost horizon of the Interlake Dolomite unit produced in the three-dimensional geological model
3. Elevation from sea level for the uppermost horizon of the Madison Group unit produced in the three-dimensional geological model

4. Elevation from sea level for the uppermost horizon of the Minnelusa Formation and Tensleep Sandstone unit produced in the three-dimensional geological model
5. Elevation from sea level for the uppermost horizon of the Inyan Kara Group unit produced in the three-dimensional geological model
6. Elevation from sea level for the uppermost horizon of the Greenhorn Formation unit produced in the three-dimensional geological model
7. Elevation from sea level for the uppermost horizon of the Pierre Shale unit produced in the three-dimensional geological model

Figures

Tables

Conversion Factors

International System of Units to U.S. customary units

Multiply	By	To obtain
	Length	
meter (m)	3.281	foot (ft)
kilometer (km)	0.6214	mile (mi)
meter (m)	1.094	yard (yd)
	Area	
square meter (m^2)	0.0002471	acre
square kilometer (km^2)	247.1	acre
square meter (m^2)	10.76	square foot (ft^2)
square kilometer (km^2)	0.38610.003861	square mile (mi^2)
	Mass	
gram (g)	0.03527	ounce, avoirdupois (oz)

Datums

Vertical coordinate information is referenced to the North American Vertical Datum of 1988 (NAVD 88).

Horizontal coordinate information is referenced to the North American Datum of 1983 (NAD 83).

Altitude, as used in this report, refers to distance above the vertical datum.

Supplemental Information

Elevation, in this report refers to the vertical distance (in meters) above or below average sea level (2025).

Arc-second refers to the unit of angular measurement equivalent to 1/3600 of a degree.

Heat flow is given in milliwatts per square meter (mW/m^2).

The term “Precambrian” in this report is intended to refer to any rock older than the earliest Paleozoic. Previous studies compiled for this study commonly do not differentiate beyond the informal term "Precambrian," so we have retained this designation.

Abbreviations

2D	two dimensional
3D	three dimensional
3DEP	3D Elevation Program
API	American Petroleum Institute
ArcPro	ArcGIS Pro
ASCII	American Standard Code for Information Interchange
COSUNA	Correlation of Stratigraphic Units of North America
DEM	Digital Elevation Model
ESRI	Environmental Science Research Institute
GFM	geologic framework model
GIS	geographic information system
GSO	geological survey organizations
Ma	mega-annum
MBOGC	Montana Board of Oil and Gas Conservation
PDF	Portable Document Format
RBF	radial basis function
SGMC	State Geological Mapping Compilation
TIFF	Tagged Imaged File Format
USGS	U.S. Geological Survey
VE	vertical exaggeration
WOGCC	Wyoming Oil and Gas Conservation Commission
WSGS	Wyoming State Geological Survey

A Three-Dimensional Geologic Framework Model of the Northern Great Plains Region of Montana, North Dakota, South Dakota, and Wyoming, USA

By Leland R. Spangler

Abstract

This report presents a new three-dimensional geologic framework model (GFM) of the northern Great Plains region, encompassing parts of Montana, North Dakota, South Dakota, and Wyoming. The model provides a regionally consistent, geographic information system (GIS)-ready representation of Phanerozoic sedimentary strata, major fault systems, and Precambrian basement geometry across two sedimentary basins and adjacent uplifts. More than 300,000 geologic and geophysical data inputs were synthesized to model 41 stratigraphic horizons and 47 faults, yielding an internally coherent, sealed-volume interpretation of the subsurface. The modeling workflow developed for this study demonstrates an efficient and scalable approach for constructing basin- to regional-scale GFMs in geologically complex and data-variable settings. Although model fidelity varies with data density and quality, the resulting geometry is broadly consistent with 1:500,000-scale geologic mapping and highlights areas where additional geologic study is most needed. The three-dimensional GFM provides a foundational framework to support groundwater, energy, and mineral resource assessments, and offers a transferable methodology for potential future U.S. Geological Survey efforts to build large-area subsurface models in underexplored regions of the United States.

Plain Language Summary

This report presents a new three-dimensional map of underground rock layers and faults in the northern Great Plains, covering parts of Montana, North Dakota, South Dakota, and Wyoming. The model was built from thousands of data points collected from wells, maps, and geophysical surveys. It shows the shape, depth, and thickness of multiple rock layers—many of which are important for water, energy, and mineral resources. The map helps scientists, land managers, and decisionmakers better understand the region's subsurface geology. This work also shows that reliable geologic models can be made even in areas with limited data, using a repeatable method that can be applied in other underexplored areas.

Introduction

The northern Great Plains physiographic province spans more than 776,996 square kilometers (km^2) in the north-central United States, encompassing eastern Montana and Wyoming and western North Dakota and South Dakota (Downey and Dinwiddie, 1988). The region is characterized by a predominantly flat landscape of plains and grasslands, interrupted locally by high-relief features, such as the Bighorn Mountains, Laramie Mountains, and the Black Hills (fig. 1). Major waterbodies, such as Fort Peck Lake, Lake Sakakawea, and reaches of the Missouri River, and the Yellowstone River drain the northern extent of the study area to the southwest and southeast.

The geology of the northern Great Plains province has significant societal and economic value. It is the subject of six natural areas within the National Park Service system (fig. 1), contains more than 23.8 percent of United States farmland (U.S. Department of Agriculture, 2018), is a significant source of domestic energy resources (U.S. Energy Information Administration, undated), is a primary source of economic and industrial minerals (DeWitt and others, 1986; Harris and King, 1989), and hosts large volumes of groundwater essential for consistent water supply to the region (Thamke and others, 2014). Exploration, development, and management of these resources necessitate a comprehensive understanding of the geologic systems present in the region, which in turn requires an accurate and quantitative geologic framework that underpins these systems. Previous studies of northern Great Plains geology have largely focused on specific resources or individual stratigraphic units (for example, Downey and Dinwiddie, 1988; Fox and Higley, 1996; Thamke and others, 2014; Gelman, 2023), however a full three-dimensional (3D) geologic framework model (GFM) of the region has not been constructed prior to this study.

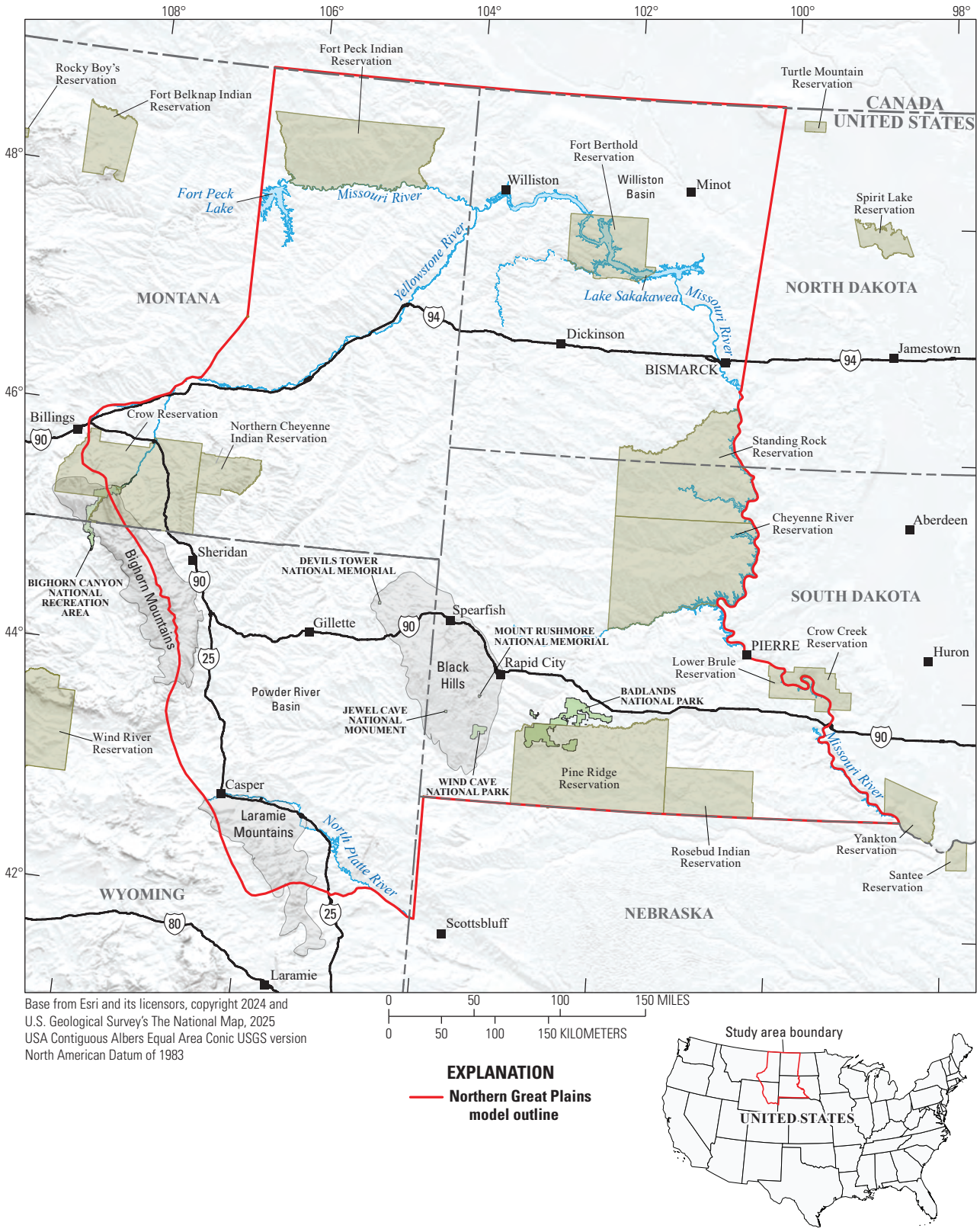

Figure 1. Map showing the three-dimensional geologic model outline for the northern Great Plains region of Montana, North Dakota, South Dakota, and Wyoming. The study area includes locations of geologic interest managed by the National Park Service, federally recognized Native American reservations, major waterbodies, mountain ranges, and U.S highways.

Geologic framework models are volumetric interpretations of the subsurface, which map the elevation, extent, and geometry of stratigraphic units, faults, and structural features in three dimensions (Turner and others, 2021). These models function similarly to two-dimensional (2D) geologic maps in that they provide foundational context for more detailed studies, provide boundary conditions for distributed properties modeling, and are critical tools for geological survey organizations (GSOs) to systematically document, analyze, and communicate subsurface geology across jurisdictional boundaries (MacCormack and others, 2019; Sweetkind and others, 2019; Thorliefson and others, 2019). In response to national priorities to develop a consistent subsurface geologic framework, the U.S. Geological Survey's (USGS) National Cooperative Geologic Mapping Program has emphasized basin-scale 3D GFMs as core components of potential future mapping work (U.S. Congress, 2019; Brock and others, 2021; Shelton and others, 2022; Sweetkind and Zellman, 2022, 2023). This study contributes to this broader national effort by demonstrating an efficient, scalable, and quantitative methodology for constructing large-area 3D GFMs across a combination of well-defined sedimentary basins, geologically complex uplifts, and data sparse regions of the subsurface.

Purpose and Scope

This report describes the development of a 3D GFM of the northern Great Plains region of the United States. The purpose of the model is to provide a regionally consistent, geographic information system (GIS)-ready representation of Phanerozoic sedimentary strata and major structural features within the study area. The modeling workflow presented here demonstrates a flexible and scalable approach that can be transferred to other data-limited areas where accurate geologic frameworks are needed to support USGS groundwater, energy, or mineral assessments. This work highlights the value of rapid, regional-scale subsurface mapping in areas that have received limited modern geologic exploration but where decision making increasingly relies on high-quality, integrated interpretations of the subsurface.

The scope of this report includes a summary of the geologic and physiographic setting, the types and sources of data compiled for the model, and the methods used to construct the 3D geologic framework. The report includes a discussion that highlights key aspects of the subsurface that may be important to users of this work, and of model limitations where additional data may improve interpretations. Incongruencies in stratigraphic nomenclature were not rectified in this study. Supporting data from this investigation are available as geospatial databases published as USGS data releases (Spangler, 2024a, b).

Geographic and Geologic Setting of the Study Area

The northern Great Plains 3D GFM encompasses a 381,000 km^2 region of eastern Montana, western North Dakota and South Dakota, and northeastern Wyoming (fig. 1). The boundary for this study was drawn along geopolitical lines, down the traces of mountain range divides, and through regions of thin sedimentary sections near structural uplifts. Boundaries were established to include the entirety of the Powder River Basin and Williston Basin, and to incorporate a wide periphery around the uplifted regions that define the basin margins.

The northern boundary of the model follows the United States–Canada border (fig. 1). The western boundary of the model extends southward from the border near Fort Peck Lake, Montana, toward Casper, Wyoming, and along the divide of the Bighorn Mountains and the western flank of the Laramie Mountains. The southern boundary of the model extends eastward along the southern border of South Dakota to where it intersects with the Missouri River near the Yankton Sioux Tribe of South Dakota Reservation. The eastern boundary of the model follows the Missouri River northward into North Dakota, at which point it extends back to the United States–Canada border along an arbitrary line intended to capture the eastern margin of the Williston Basin. Vertically, the top of the model is the modern-day land surface, and the base of the model is an arbitrary depth into crystalline Precambrian rock (−10,100 vertical meters below sea level) that is intended to represent a depth below the deepest sedimentary section within the model.

Land surface elevation within the study area slopes downward to the east, ranging from a maximum of 4,014.5 meters (m) at Cloud Peak in the Bighorn Mountains of Wyoming to 381.6 m in south-central South Dakota near the Missouri River. Much of the region consists of gently rolling plains underlain by Late Cretaceous and Cenozoic, sedimentary rocks, with prominent bedrock exposures in areas such as Badlands National Park (fig. 2). In the northern part of the study area, bedrock is locally obscured by glacial erosion and deposition associated with the Laurentide Ice Sheet, which covered approximately 15 percent of the study area during the Last Glacial Maximum (fig. 2).

In contrast to the low-relief plains, several tectonically uplifted regions expose crystalline Precambrian basement at the surface, including the Bighorn Mountains, Laramie Mountains, and the Black Hills (figs. 1 and 2). These uplifts are flanked by steeply dipping, folded, and locally faulted Phanerozoic sedimentary rocks that form prominent canyon systems, such as those at Bighorn Canyon National Recreation Area, and extensive karst terrains, including Jewel Cave National Monument and Wind Cave National Park. Isolated igneous intrusions, such as Devils Tower National Monument, occur primarily near uplifted regions where sedimentary cover is thin (fig. 2).

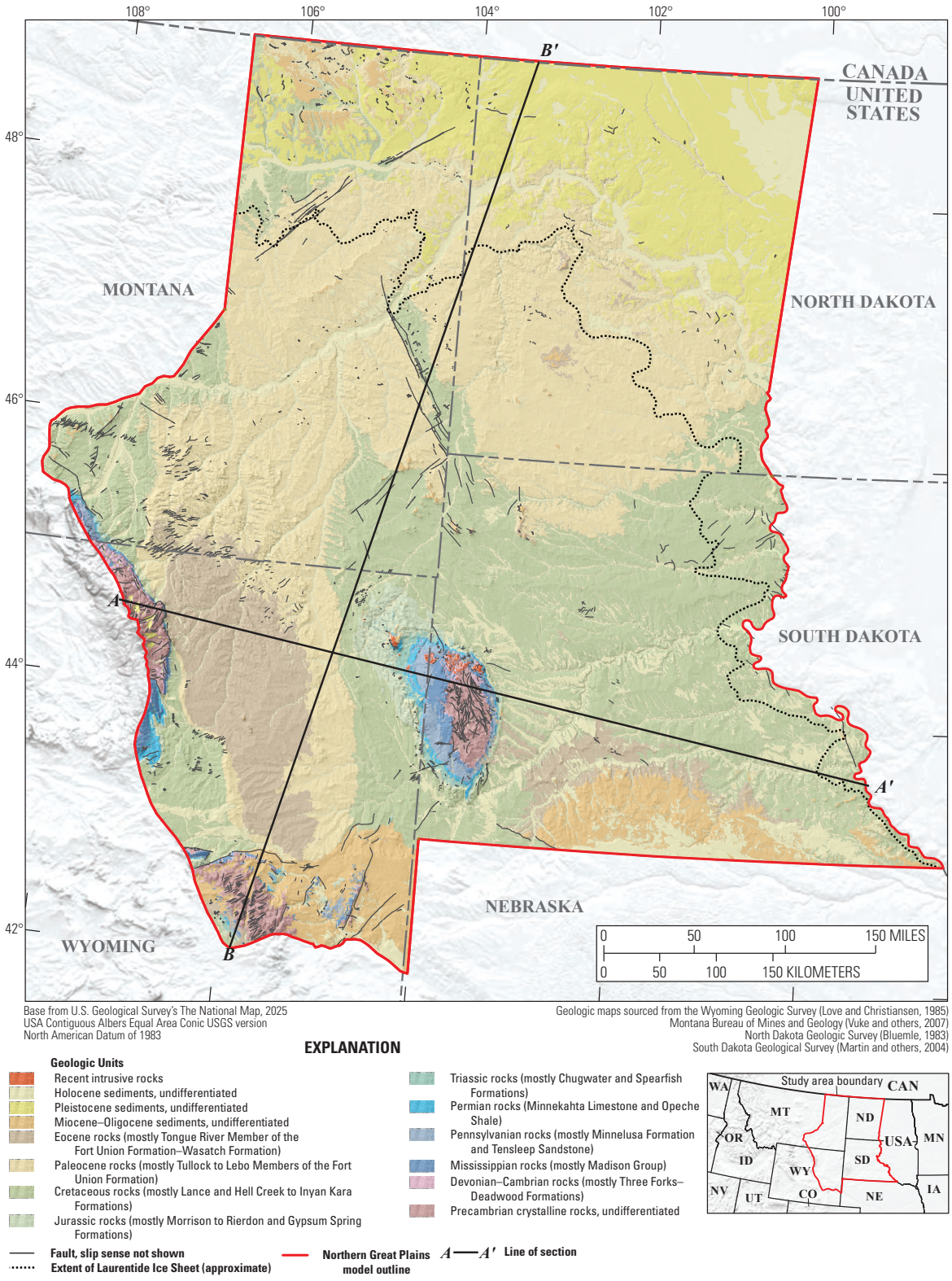

Figure 2. Generalized geologic map of the northern Great Plains study area in North Dakota (data from the North Dakota Geologic Survey [Bluemle, 1988]), South Dakota (data from the South Dakota Geological Survey [Martin and others, 2004]), Wyoming (data from the Wyoming Geologic Survey [Love and Christiansen, 1985]), and Montana (data from the Montana Bureau of Mines and Geology [Vuke and others, 2007]); geologic units are grouped approximately by geologic age. Simplified surface expressions of faults and the extent of the Laurentide Ice Sheet are approximate. Cross sections *A*–*A*′ and *B*–*B*′ are simplified profiles cut through the three-dimensional geologic framework model in this study (refer to fig. 4).

Structural Setting

The northern Great Plains encompasses two prominent sedimentary basins with contrasting structural styles: the Powder River Basin of Wyoming and Montana, and the Williston Basin which spans South Dakota, North Dakota, and Montana and extends northward into Canada (fig. 3). Although geographically proximate, these basins and the uplifts defining their margins are associated with distinct orogenic events, subsidence histories, and structural styles, which are crucial to consider prior to model construction.

The Williston Basin is a nearly symmetrical intracratonic basin characterized by a thick and nearly continuous record of Phanerozoic sedimentation (Gerhard and others, 1990; fig. 4*A*, *B*). The total maximum thickness of the sedimentary package in the Williston Basin is approximately 4,611-m thick, and the maximum depth of the basin reaches approximately 4,200 m below sea level near Williston, North Dakota. Structural dips of the basin limbs are continuous and shallow (less than 2 degrees of dip), making the southern and eastern boundaries of the basin challenging to distinctly define to the south and east, where the crystalline Precambrian rocks rise toward modern-day land surface from the South Dakota Plains onto the Transcontinental Arch (Carlson, 1999; fig. 3).

Subsidence of the Williston Basin occurred episodically from the Middle Ordovician through the Late Mississippian, producing long-wavelength structural relief that is subtle in magnitude but regionally persistent (Crowley and others, 1985; Bader, 2019a). The few structural features in the basin formed during this time, such as the Nesson Anticline, which bisects the center of the basin, and Cedar Creek Anticline, which bounds the basin to the southwest (Gerhard and Anderson, 1988; Kent and Christopher, 2007). Notably, the fault controlling the Cedar Creek Anticline is one of the longest-lived structures in the northern Great Plains, having experienced multiple phases of normal and reverse motion since the Devonian (Clement, 1986).

Pennsylvanian through Late Cretaceous strata show broadly uniform thicknesses across the Williston, indicating relative tectonic stability during much of the Late Paleozoic and Mesozoic (Peterson, 1984; Smith and others, 2004). Far-field Laramide-derived strain is believed to be the penultimate phase of deformation and inversion of the Williston Basin from the Late Cretaceous to the late Paleogene, resulting in reactivation of major structural features to their modern-day configuration (Gelman, 2023). Modern strain is accommodated through structural lineaments, such as the Weldon and Brockton-Froid Fault Zones, which outcrop at the surface and offset Quaternary tills yet remain enigmatic in their origin (Wheeler, 1999). From a modeling perspective, the primary challenge in the Williston Basin is its low structural relief, where shallow dips and unconformities allow even minor geometric errors to propagate through the stratigraphic sequence over long distances.

In contrast to the structural symmetry of the Williston Basin, the Powder River Basin is classified as an "asymmetric broken foreland basin" formed during the Laramide orogeny (DeCelles, 2004; Yonkee and Weil, 2015; Horton and others, 2022; fig. 3). Sedimentary fill within the Powder River Basin spans the entire Phanerozoic but features a thin Paleozoic section relative to thick overlying Cretaceous and early Cenozoic strata (Glass, 1993; fig. 4*A*). The basin axis trends south–southeast and is flanked by a steep western limb defined by the Bighorn Uplift, Casper Arch, and Piney Creek Thrust Fault (fig. 3). The eastern limb of the basin shallows eastward at approximately 1 degree of dip until it meets the Black Hills Monocline and Miles City Arch. Stratal thicknesses exceeding 5,182 m are recorded along the basin axis, which reaches a maximum depth of approximately 4,177 m below sea level to the north of Casper, Wyoming (Blackstone, 1993). A subtle northeast-trending upwarp known as the Belle Fourche Arch bisects the basin axis (Blackstone, 1993).

Flexural subsidence of the Powder River Basin likely initiated due east–northeast oriented shortening in the Late Cretaceous (Yonkee and Weil, 2015; Carrapa and others, 2019). Continued northeast-directed shortening through the Paleocene and early Eocene activated low-angle, basement-involved fault networks and resulted in a series of basement uplifts and arches that define the western and southern margins of the Powder River Basin (Stone, 1993; DeCelles, 2004; fig. 3). The Piney Creek Thrust Fault is a classic example of Laramide basement faulting, exposing Precambrian crystalline rocks at the land surface due to as much as 4,100 m of vertical displacement along the Bighorn Uplift (Stone, 1993, 2003).

Despite the general east–northeast shortening trend, a series of en-echelon thrust faults bound the southern extent of the Powder River Basin against the Laramie Mountains and Hartville Uplift (Blackstone, 1988; Stone, 2002; fig. 3). The geometry of the faulted basin margin can be complex; local nuances in the geology result in an anastomosing network of subsurface faults and folds, transferring displacement along strike of the uplift (Hoy and Ridgway, 1997). Many of these features (such as the Northern Bounding Fault) are obscured by late Cenozoic basin fill and do not outcrop directly at the surface, but can be inferred from the geometry of preorogenic sedimentary units and seismic survey lines (Stone 1993; Blackstone, 1996; Hoy and Ridgway, 1997; Caylor and others, 2023). From a modeling perspective, the primary structural consideration in the Powder River Basin is accurately representing fault geometry and displacement while honoring detailed surface mapping in areas where subsurface data are sparse, legacy, or unevenly distributed.

Laramide intraplate stress activated low-angle basement-cored thrust faults as far east as the Black Hills Uplift, which is the eastern limit of the Cordilleran strain front (DeCelles, 2004). The Black Hills Uplift is a shallow broken foreland-type uplift that forms an elongate basement-cored antiform, exposing crystalline Precambrian rocks at the surface (Erslev and others, 2001; Erslev, 2005; Horton and others, 2022; fig. 2). Numerous north–south trending faults have been

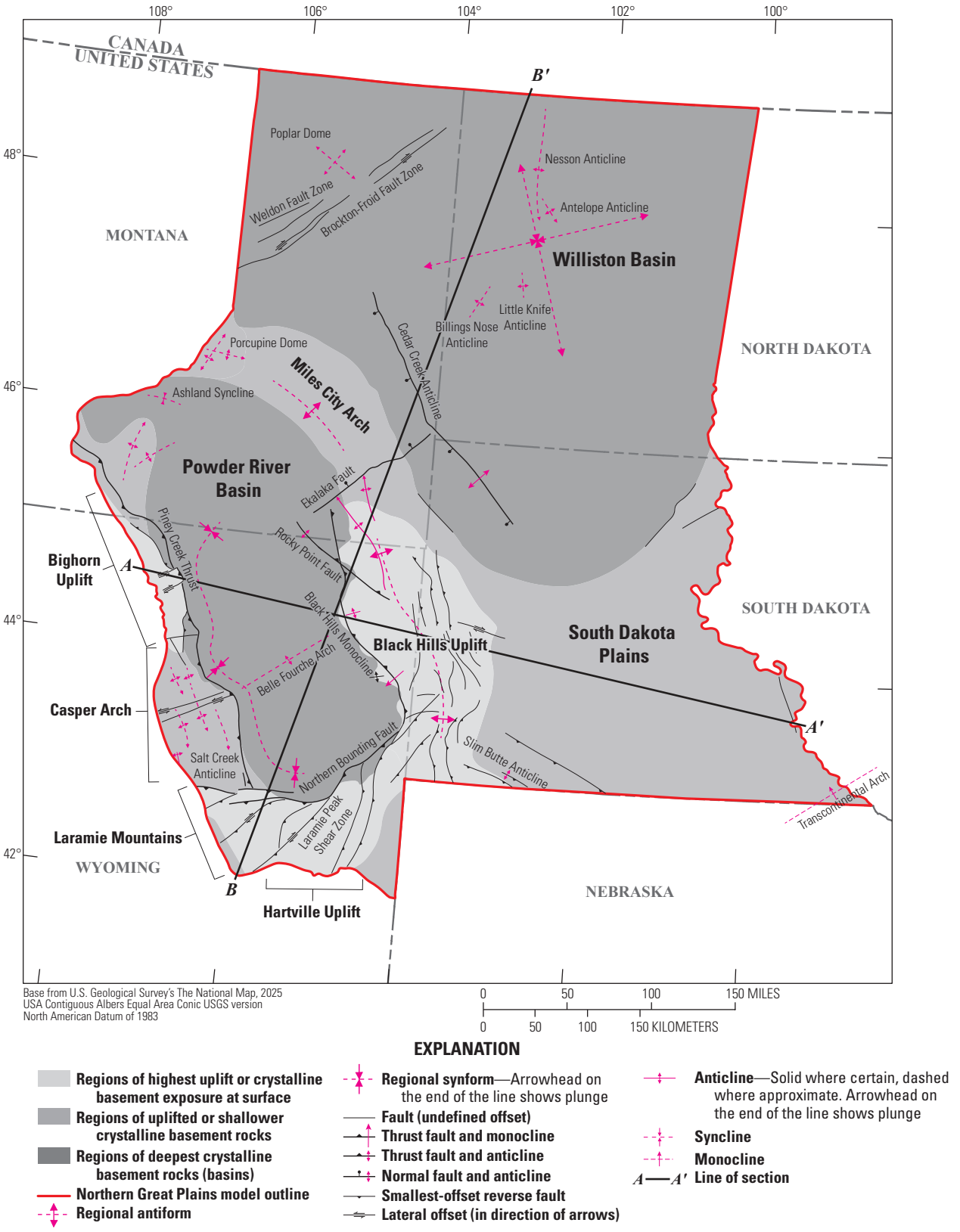

Figure 3. Map of the northern Great Plains region of Montana, North Dakota, South Dakota, and Wyoming, showing major structural and tectonic features of the study area. Cross sections *A*–*A*′ and *B*–*B*′ are simplified profiles cut through the three-dimensional geologic framework model in this study (refer to fig. 4). Faults and folds occupy the same structure at this map scale.

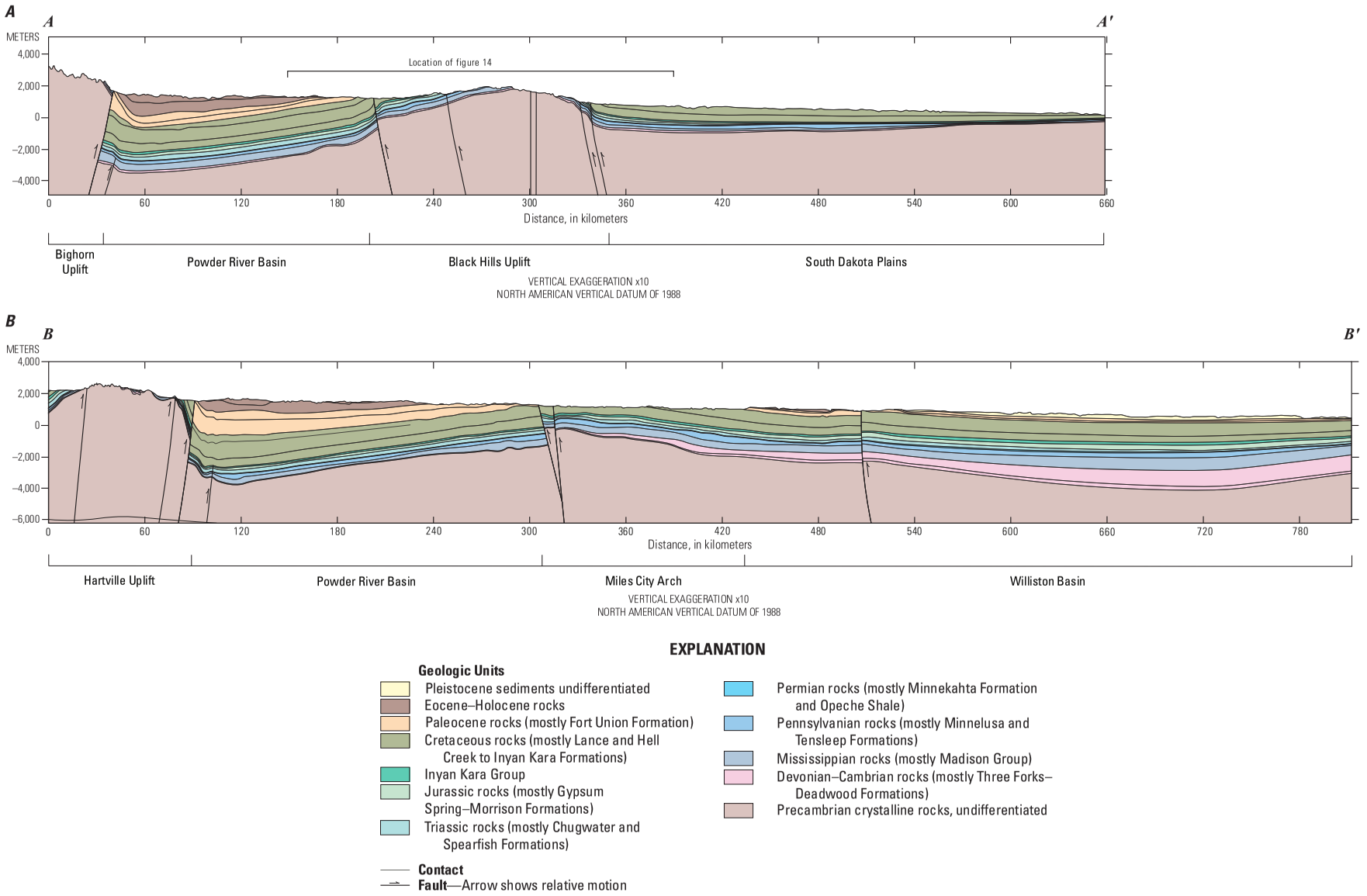

Figure 4. General geologic *A*, cross sections *A–A′* and *B*, cross sections *B–B* through the northern Great Plains three-dimensional geologic framework model described in this study; model units are combined by geologic age and modeled faults are shown as planes. Refer to figure 2 for the location of sections and grouping of units.

mapped through the Black Hills at the surface (for example, Redden and DeWitt, 2008) and in the subsurface (for example, Lisenbee, 1978), which offset the crystalline Precambrian basement (fig. 3). These faults lose displacement vertically up section and form structural folds in more ductile Cretaceous strata evident in surface outcrop patterns. These outcrop patterns present a unique opportunity to asses how effectively surface mapping can produce accurate geologic structure in the 3D GFM. Eastward of the Black Hills, strata gently dip to the east where structural complexity decreases across the South Dakota plains.

Temporally related to uplift of the Black Hills, a northwest-striking trend of alkalic and carbonatite intrusive rocks were emplaced through the crystalline Precambrian rocks and the overlying sedimentary succession as dikes, sills, laccoliths, and small stocks (Redden and DeWitt, 2008; fig. 2). Intrusives occasionally form prominent topographic features where they crop out at surface, such as Devils Tower National Monument, Sundance Mountain, or Tinton Dome (DeWitt and others, 1986). Intrusive activity began between 62 and 50 mega-annum (Ma), followed by a second magmatic pulse around 39 Ma (Lisenbee and DeWitt, 1993).

Stratigraphic Setting

Phanerozoic sedimentary rocks in the northern Great Plains range in age from Cambrian to Holocene, and unconformably overlie Precambrian crystalline basement rock throughout the study area (Anna, 1986). Stratigraphic relations are summarized in figure 5, relative to a generalized Phanerozoic sea-level curve, which represents the primary allogenic control on basin-scale sedimentation trends in conjunction with regional tectonic (Sloss, 1963; Algeo and others, 2014; Marcilly and others, 2022). A strong understanding of these allogenic controls is crucial for appropriately capturing stratigraphic thickness trends, lateral extents, and unconformities within the 3D GFM.

Cambrian sandstones of the Deadwood Formation form the basal sedimentary unit of the GFM and are overlain by laterally extensive Ordovician carbonate and shale units, including the Winnipeg Group and Red River Formation. These laterally continuous units were deposited across the entire study area during a period of rising global sea level and relative tectonic quiescence (Martin and others, 2004; fig. 5). From a modeling perspective, these units can be treated as regionally conformable layers that largely follow basement structure because most deformation affecting their geometry postdates deposition.

Elevated sea levels and episodic subsidence in the Williston Basin from the Late Ordovician through Early Mississippian restricted sedimentary units, such as the Interlake Dolomite, Three Forks Shale, and Bakken Formation, to the north of the study area (Gerhard and Anderson, 1988; fig. 4*B*). Nondeposition or erosion to the south and west resulted in regional pinch-out of these units. Accurate modeling of this interval needs careful representation of low-angle unconformities and subtle thickness variations, which exert strong control on stratigraphic architecture over long distances.

Falling sea level during the Mississippian was accompanied by widespread carbonate deposition across much of the study area, recorded by units, such as the Madison and Big Snowy Groups (Sonnenfeld, 1996; fig. 5). Mississippian carbonates thin southward and crop out along major uplifts, which requires careful integration of subsurface and surface constraints to retain lateral continuity in structurally deformed areas (Kent and Christopher, 2007; Anna, Pollastro, and Gaswirth, 2013).

Upper Paleozoic and early Mesozoic strata, including the Minnelusa and Spearfish Formations, lie unconformably on the Mississippian section and thin northward and eastward across the study area (Downey, 1986). These rocks show pronounced lateral and vertical lithologic heterogeneity due to deposition in restricted marine, sabkha, lacustrine, and eolian environments during prolonged global sea-level lowstand and relative tectonic quiescence (Carr-Crabaugh and Dunn, 1995; Anna, 2010; Fryberger and Hern, 2014; fig. 5).

Overlying Triassic and Jurassic units, including the Sundance, Gypsum Spring, and Morrison Formations, are internally heterogeneous and less laterally continuous than older Paleozoic units. (Vuke and others, 2007; Syzdek and others, 2019). These strata are bound by widespread unconformities and are locally truncated or entirely absent beneath the Cretaceous Inyan Kara Group (Anna 1986; Downey, 1986; fig. 5). Modeling of Triassic–Jurassic units needs to account for highly variable thicknesses, local nondeposition, and incision from overlying units.

Lower Cretaceous shales and fine sandstones blanket much of the post-Jurassic northern Great Plains and record a deepening-upward sequence from the predominantly nonmarine Inyan Kara Group to the open marine Mowry Shale (Anna, 1986, 2010; Vuke and others, 2007). This deepening-upward sequence records episodic sea level rise and transgression of the Western Interior Seaway during global greenhouse climate conditions (Anna and Cook, 2008; Marcilly and others, 2022; fig. 5). These units are laterally continuous across the study area and can be modeled in a layer-cake fashion, with attention to subtle subsidence-related thickness changes in the Powder River Basin.

Upper Cretaceous strata consist predominantly of shales and sandstones, including the Niobrara Formation and Pierre Shale, which span much of the study area and record low-amplitude transgressive–regressive cycles during global sea-level high stand (Love and others, 1993; Farenbach and others, 2007; Lynds and Slattery, 2017; fig. 5). Locally developed sandstone bodies, such as the informal Turner and Teckla sandstones, are confined to the southwestern Powder River Basin and are most appropriately modeled as eastward-thinning clastic wedges encased within regionally extensive shale units (Lichtner and others, 2020; fig. 4*A*).

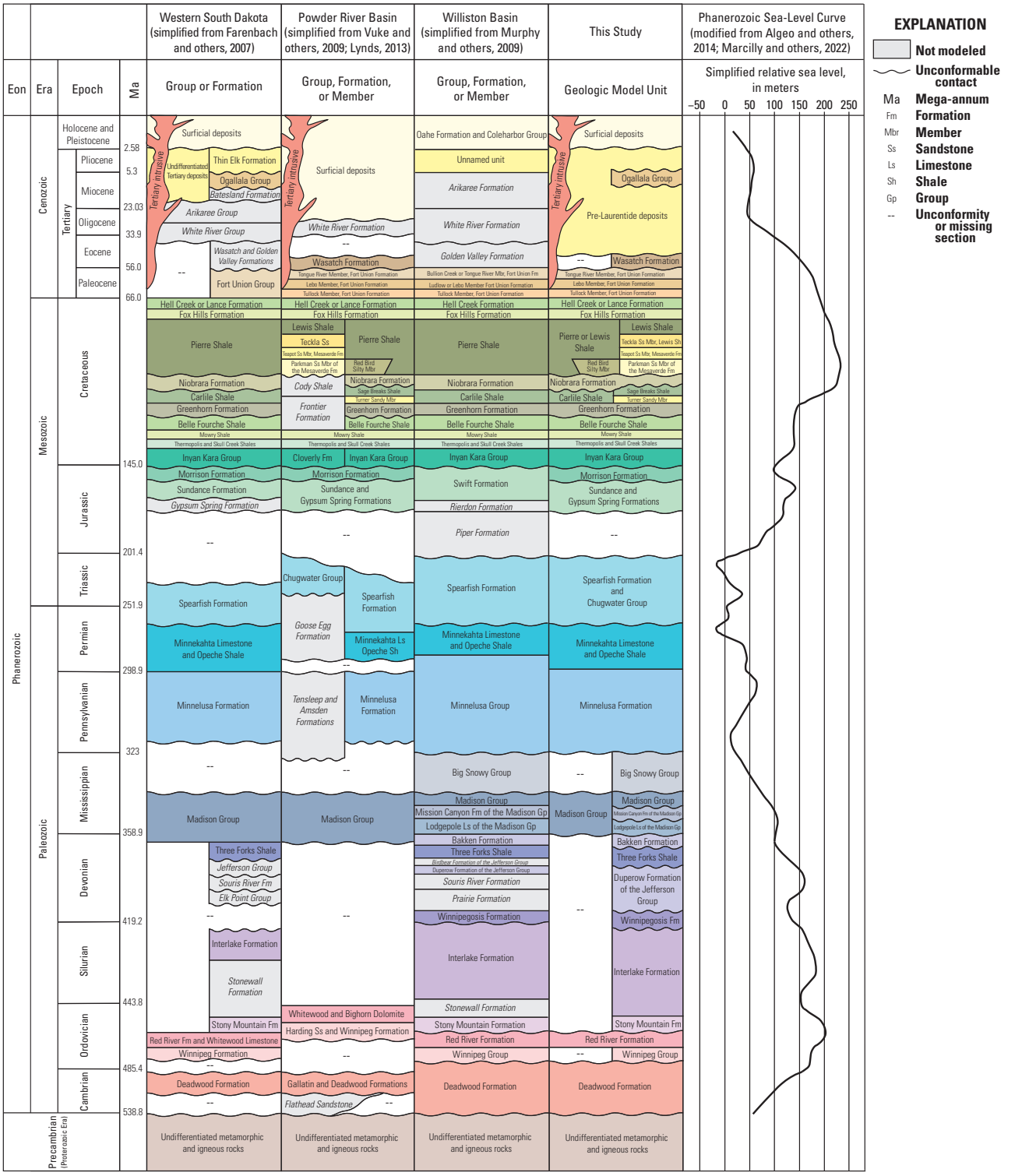

Figure 5. Simplified stratigraphic columns from South Dakota (data from Farenbach and others, 2007 [South Dakota Geological Survey]), the Powder River Basin (data from Love and others, 1993 [Wyoming State Geological Survey]), and the Williston Basin (data from Murphy and others 2009 [North Dakota State Geological Survey]) compared to model units included in the northern Great Plains three-dimensional geologic framework model. Unit color corresponds to units that correlate across regions. The colors are used in the geologic model so one could more quickly identify units when looking at an image of the model. Stratigraphy shown in comparison to a simplified Phanerozoic relative sea level curve modified from Algeo and others (2014) and Marcilly and others (2022). Ma, mega-annum; m, meters; Mbr., Member; Fm., Formation; Ss., Sandstone; Sh., Shale.

The latest Cretaceous Fox Hills, Lance, and Hell Creek Formations, which cap the Mesozoic section record a fall from sea-level high stand, and regression of the Western Interior Seaway (Lynds and Slattery, 2017; Marcilly and others, 2022; fig.5). Late Cretaceous sandstone intervals additionally record incipient tectonic activity in the northern Great Plains, including elevated clastic sediment supply from the advancing Sevier fold-thrust belt, and increased accommodation space from early subsidence of the Powder River Basin (Yonkee and Weil, 2015; fig. 5). The primary consideration for modeling these units is accurately capturing their subsurface geometry in the west of the model in the Powder River Basin while seamlessly transitioning northeastward to discontinuous outcrop and subcrop in the South Dakota plains and Williston Basin.

Consolidated Cenozoic sedimentary rocks from the Fort Union Group at the base through the Thin Elk Formation at the top (undifferentiated in this study) exceed 1,500 m in thickness in the western Powder River Basin and thin eastward across the South Dakota plains (Love and others, 1993; Martin and others, 2004; Murphy and others; 2009; fig. 5). These strata include sandstones, claystones, conglomerates, lignite, and coal deposited in fluvial, lacustrine, alluvial-plain, and swamp environments (Vuke and others, 2007; Murphy and others 2009; Osmonson and others, 2011). Westward thickening reflects increased sediment supply from Laramide uplifts and rapid flexural subsidence along the basin axis into the Eocene (Fan and Carrapa, 2014; fig. 4*A*). In contrast, these consolidated units are thin or absent in the Williston Basin and eastern plains, likely owing to early Eocene basin inversion and erosion, with subsequent removal of section during later Cenozoic drainage reorganization (Caylor and others, 2023; Gelman, 2023; fig. 4*B*).

Poorly or unconsolidated Cenozoic deposits consist of gravels, silts, and muds that overlie a deeply incised unconformity cut into consolidated bedrock, particularly in the northern and eastern parts of the study area (Soller and Garrity, 2018). These deposits record glaciofluvial, lacustrine, and alluvial sedimentation during advance of the Laurentide Ice Sheet in the Pleistocene (Murphy and others, 2009; Naylor and others, 2021; fig. 5). These deposits are not a primary focus of the model and remain undifferentiated in this study.

Previous Subsurface Investigations

The northern Great Plains has a longstanding history of subsurface investigations, primarily driven by assessments of mineral, energy, and groundwater resources. Initial subsurface studies in the northern Great Plains were motivated by exploration of paleoplacer and strataform iron-formation hosted gold deposits in the northern Black Hills, particularly around the Homestake Mine, which has produced as much as 43.9 million ounces of gold since the 1870s (Caddey and others, 1991). These early investigations included detailed drawings and Anaconda-style mapping, which were pivotal for understanding subtle stratigraphic relations between Precambrian basement rocks, the Cambrian Deadwood Formation, and intrusive bodies (Caddey and others, 1991). Although gold production has declined in recent years, exploration attention has shifted toward other mineral resources, such as thorium, uranium, and rare-earth elements. Each of these resource types have contributed valuable insights into the structural configuration of Paleozoic units and the timing of intrusive events in the western Black Hills (Staatz, 1983; DeWitt and others, 1986; Moore and others, 2015).

Hydrocarbon exploration has been the dominant driver of geologic framework studies in the Williston and Powder River Basins since the discovery of oil at the Salt Creek Field near Casper, Wyoming, in 1889 (Baker, 1957). This initial discovery catalyzed the development of an extensive body of literature pertinent to geologic framework modeling, including structure contour maps, model grids, and cross-sections. Early hydrocarbon studies focused on delineating structural traps with structure contours in Cretaceous sandstones, which were accessible and conventionally producible with vertical wells (Baker, 1957). As the availability of well and seismic data increased, the focus expanded to regional syntheses that highlighted complex faulted structural traps, stratigraphic accumulations, and alternative hydrocarbon plays, such as coal bed methane (for example, Blackstone, 1988; Fox and Higley, 1996; Flores, 2004; Sonnenberg and Pramudito, 2009; Anna, Pollastro, and Gaswirth, 2013).

The advent of horizontal drilling and hydraulic fracturing prompted a renewed focus on regional stratigraphic mapping and modeling of previously uneconomic source-rock reservoirs. In the Powder River Basin, this work has primarily concentrated on the Late Cretaceous Mowry Shale and Niobrara Formation, which are thermally mature enough for economic production across much of the basin (for example, Anna and Cook, 2008; Sonnenberg, 2018; Lichtner and others, 2020). Similarly, in the Williston Basin the Late Devonian to Early Mississippian Bakken Formation and the Early to Middle Mississippian Three Forks Shale have become the subject of intense study as one of the leading tight oil plays in the United States (for example, Webster, 1984; LeFever, 2007; Sarg, 2011; Sonnenberg, 2012; Pollastro and others, 2013; Marra and others, 2021; Gelman, 2023). Explorers of these unconventional hydrocarbon plays have constructed numerous contour maps and model grids using picks from wireline logs that add significant value to geologic framework studies because the geographic footprint of these studies is generally much larger than comparable work in conventional plays.

Similar subsurface mapping in the region has been motivated by exploration of other unconventional targets, such as the Late Permian to Triassic Spearfish Formation (LeFever, 2011), or as wastewater disposal units, such as the Early Cretaceous Inyan Kara Group (Bader, 2017). Using similar methods as oil explorers, assessments of carbon dioxide storage potential or geothermal resources have been conducted

in the Powder River and Williston Basins, resulting in maps and model grids of strata and basement structure that may have otherwise only been a tangential focus of hydrocarbon producers (for example, Craddock and others, 2012; Lynds, 2013; Melick, 2013; Gelman and Burns, 2025).

Expansive subsurface investigations have also focused on water resources and major hydrogeologic units in the northern Great Plains. Multiple USGS hydrogeologic studies have characterized bedrock aquifers over a footprint similar to this study, delineating unit extent, thickness, and structure in a series of structure contour and isopach maps (Anna, 1986; Downey and Dinwiddie, 1988; Whitehead, 1996; Stanton, 2015). In more localized studies, structure-contour maps helped estimate that 256 million acre-feet of water is contained in bedrock aquifers in the South Dakota part of the Black Hills alone, where water well yields are as high as 1,000 gallons per minute (Driscoll and others, 2002; Carter and others, 2003; Hocking, 2013a, b, c, d). Additional hydrogeologic studies have focused on thick synorogenic to postorogenic sedimentary sequences that form the most voluminous bedrock aquifers in the Powder River and Williston Basins (Thamke and others, 2014). In these regions, Paleogene units, such as the Fort Union and Wasatch Formations, have been studied for their dual significance as groundwater sources and coal resource plays. The Wyodak-Anderson coal zone in the Powder River Basin, in particular, contains the most productive coal deposits in the United States (with as much as 162 billion tons considered technically recoverable) while also hosting substantial groundwater resources that intermingle with the coal beds (Flores and others, 2010; Osmonson and others, 2011; Taboga and others, 2015). To the southeast of the study area, the northern extent of the economically vital High Plains aquifer has been rigorously delineated for similar groundwater modeling purposes (Peterson, 2016). In the northern parts of the study area, subsurface topography related to the advance of the Laurentide Ice Sheet during the Quaternary has been investigated and mapped because of the importance of postglacial sediment as a groundwater aquifer, source of industrial materials, and common geotechnical substrate (Tomhave and Schulz, 2004; Soller and Garrity, 2018; Naylor and others, 2021).

Given the abundant and diverse natural resources of the northern Great Plains, considerable effort has been made by various GSOs to publish fundamental geologic framework studies, including surficial geologic maps, stratigraphic cross sections, and structure contour maps. These studies provide a critical foundation of work and standardization that public and private subsurface explorers rely on. Pertinent examples of this work produced by State organizations include geologic mapping, stratigraphic measured sections and type logs, and subsurface horizon maps by the South Dakota Geological Survey (for example, Farenbach and others, 2007; Fox and others, 2009), the Wyoming Geological Survey (for example, Love and Christiansen, 1985; Glass, 1993; Snoke and others, 1993; Lynds and Slattery, 2017), the Montana Bureau of Mines and Geology (for example, Vuke and others 2007, 2009), and the North Dakota Geological Survey (for example, Anderson, 2007, 2009, 2012; LeFever, 2007, 2011; Murphy and others, 2009; Nesheim, 2016; Bader 2017, 2019a, b). Framework studies by Federal agencies and other GSOs include the Alberta Geological Survey (2021), U.S. Department of Energy (Perry, 2019), and USGS (for example, Redden and DeWitt, 2008; Soller and Garrity, 2018). A more detailed record of data and studies that contributed to this work is included in the “Model Input Data” section of this report.

Stratigraphy, Model Units, and Stacking Order

The 3D GFM includes 41 stratigraphic model units and 47 interpreted faults. For the purposes of this study, model units are defined as sealed 3D volumes bounded by stratigraphic horizons or, for igneous intrusions, the volume enclosed within an intrusive body. Faults are defined as planar features that represent zones of structural offset or deformation affecting one or more model units. At the scale of the 3D GFM, simplification of the geology is necessary to facilitate data collection, compilation, synthesis, and postconstruction analysis. To accomplish this task in a consistent manner, selection criteria were developed for stratigraphic units of interest and faults of significance. Selection criteria for model units include the following:

1. Formations with broad lateral continuity that can be correlated throughout the spatial extent of the model and into adjacent regions,
2. Stratal horizons with sufficient data density to create a useful product with a high degree of confidence,
3. Stratal horizons or intrusive bodies describing geologic units with economic or scientific significance,
4. Horizons that represent major discontinuities or structural and stratigraphic discordance that directly affect subsurface geometries, and
5. Horizons that preserve the upper extent of a geologic age (for example, the top of Mississippian rocks), which can be easily correlated with adjacent geologic models.

The 41 model units span a generalized geologic column that includes: 1 undifferentiated Precambrian basement unit, 18 Paleozoic units, 14 Mesozoic units, 6 consolidated Cenozoic units, 1 unconsolidated Cenozoic unit, and 1 intrusive suite. Stratigraphic units were generalized by grouping thin, laterally discontinuous, or locally named formations into broader composite units to ensure regional continuity across heterogeneous datasets. Where possible, stratigraphic nomenclature was aligned with regional stratigraphic columns published by State geological surveys

(for example, Martin and others, 2004; Farenbach and others, 2007; Murphy and others, 2009; Vuke and others, 2009; Lynds, 2013; Lynds and Slattery, 2017; Lichtner and others, 2020) and supplemented by the Correlation of Stratigraphic Units of North America (COSUNA) charts (Childs, 1985). Nonetheless, many model units retain generalized or informal names to preserve continuity within the model domain and facilitate efficient regional-scale mapping. Table 1.1 (app. 1) summarizes the modeled stratigraphic units, including abbreviations, geologic age, and brief descriptions with key references. Detailed model unit descriptions and input datasets used to define these units are available in Spangler (2024a, b).

A similar approach was applied to the selection of faults, which were included to represent first-order structural features and simplify the fault-related deformation framework of the northern Great Plains. Faults were selected if they met one or more of the following criteria:

1. Faults documented in 1:500,000-scale surface mapping with a kilometer-scale strike length;
2. Subsurface expression supported by stratigraphic, geophysical, or borehole data;
3. Faults with enough available input data to infer a likely geometry; and
4. Apparent structural offset indicated by a combination of stratigraphic offsets and geophysical anomalies (for example, gravity or magnetic data) even when dip is uncertain.

Table 1 tabulates the data for faults included in this study, including characteristics such as strike length, average dip, average dip direction, interpreted kinematics, and maximum vertical offset.

Model Input Data

Constructing geologic models that are internally consistent across large regions presents several challenges, primarily because of variability in the type, quantity, spatial distribution, and quality of available data. These factors vary in three dimensions and between horizons, complicating efforts to maintain internal consistency. Furthermore, high-quality observations in published papers or figures have considerable value for the modeling process and may need to be applied even if they cannot be incorporated as discrete inputs for grid calculations (Caumon and others, 2016; de la Varga and Wellmann, 2016; Burt and others, 2021).

For the purposes of this study, modeling inputs are broadly categorized as either "explicit" or "implicit." Explicit inputs refer to geologic features that are represented as discrete lines, points, polygons, or surfaces with defined spatial attributes that can be directly used in grid-based model calculations. Examples include polylines with X, Y, and Z coordinates representing mapped geologic contacts, stratigraphic formation tops identified in well logs, or comma-delimited American Standard Code for Information Interchange (ASCII) arrays that define surface elevations on a regularly spaced grid. In contrast, implicit inputs consist of supplementary information that may affect the interpretation or preparation of explicit data, inform boundary conditions and modeling rules, or serve as a basis for quality control during model construction. These may include interpretive cross sections, illustrative figures, or explicit data of insufficient quality to be used in the gridded model itself. Table 2 defines key model-specific terms used throughout this report to clarify the framework used to prepare and interpret the geologic model presented herein.

Topographic and Geopolitical Data

Digital elevation data for this study were extracted from the USGS 3D Elevation Program (3DEP) 1/3 arc-second Digital Elevation Model (DEM; USGS, 2021a) into an ASCII elevation grid. The 1-arc-second grid was resampled to 100 m to remain within software memory limits for the regional mesh. The ASCII file was then gridded using a standard triangular mesh routine in the Leapfrog Geo 2021.2 (Seequent, 2021) 3D modeling software. The DEM data were used to define land surface elevation and to add elevation values to 2D surficial data used as model inputs (fig. 6*A–E*).

Surficial Geologic Map Data

Surficial geologic contacts and structural surface exposures were compiled across the study area from a combination of digital vector data and scanned images. A generalized digital geologic map was compiled in a GIS by merging the following four datasets:

1. Digital vectors of the South Dakota Geological Survey's 1:500,000-scale geologic map of South Dakota (Martin and others, 2004),
2. Digital vectors of the Wyoming Geological Survey's 1:500,000-scale geologic map of Wyoming (Love and Christiansen, 1985),
3. Digital vectors of the Montana Bureau of Mines and Geology's 1:500,000-scale geologic map of Montana (Vuke and others, 2007), and
4. Digital vectors of the North Dakota Geological Survey's 1:670,000-scale geologic and topographic bedrock map of North Dakota (Bluemle, 1988).

Source data were given a common map projection (North American Datum of 1983; Contiguous USA Albers, EPSG 5070), and correlative geologic units from each source map were merged in a GIS. Several inconsistencies exist in mapped contacts and stratigraphic nomenclature across State boundaries, but mapping discrepancies were not rectified

Table 1. Tabulation of faults and their characteristics as modeled within the three-dimensional geologic framework model, consisting of the fault name, fault strike length, average fault dip and dip direction, interpreted fault kinematics, and maximum vertical offset.

[Refer to figure 8 for location information. ?, high degree of uncertainty; —, no data or interpretation]

Modeled fault name	Modeled strike length (in kilometers)	Modeled average dip direction (in degrees)	Modeled average dip (in degrees)	Interpreted kinematics	Modeled maximum vertical offset (in meters)
Western South Dakota					
Slim Butte Anticline	51.5	190	35	Reverse	318
Cold Brook Anticline	52.5	106	31	Reverse	324
Horse Trip Anticline	44.1	089	38	Reverse	257
Whitewood Anticline	74.6	078	30	Reverse	175
Pine Ridge Anticline	26.6	217	89	—	—
Fairburn Anticline	45.1	140	69	Reverse	370
Spring Creek Anticline	51.0	073	30	Reverse	51
Spearfish Anticline	25.5	061	30	Reverse	142
Edgemont Anticline	46.9	123	35	Reverse	—
Hell Canyon Fault System	39.4	159	70	Reverse	90
Teepee Canyon Fault	18.1	182	70	Reverse?	156
Pringle-Reno Fault Zone	48.0	084	67	Transpressional?	—
Pactola Fault Zone	42.9	054	65	Transpressional?	—
Murphy Anticline	13.7	246	70	Reverse	40
Boxelder Creek Anticline	11.0	230	75	Reverse	58
Pedimont Anticline	19.6	248	68	Reverse	68
Alkali Creek Fault	47.6	024	89	—	—
Crow Creek Fault	86.2	067	89	—	—
Mobridge Fault	57.4	149	89	—	—
Slim Butte Anticline	42.7	203	35	Reverse	289
Little Eagle Fault	78.7	132	89	—	—
Unknown fault	11.0	031	89	Reverse?	748
Moreau River Anticline	38.9	049	89	—	—
Powder River Basin					
Piney Creek Thrust	376.1	254	32	Reverse	4,133
Ekalaka Fault	142.3	142	43	Reverse	43
Piney Creek Backthrust	202.3	054	50	Reverse	1,718
Shell Lineament	29.8	168	64	Transpressional	485
Granite Ridge Tear Fault	26.4	333	65	Transpressional	296
Clear Creek Thrust	50.6	062	31	Reverse	563
Florence Pass Lineament	41.8	157	47	Transtensional?	281
North Sisters Hill Fault	75.6	159	70	Transtenstional?	53
South Sisters Hill Fault	78.6	336	70	Transtenstional?	45
Tisdale Fault	70.1	072	30	Reverse	—
Salt Creek Fault	57.1	074	33	Reverse	—
Casper Mountain Fault	38.8	194	35	Reverse	1520
Deer Creek Fault	54.8	157	30	Reverse	1945
Northern Bounding Fault	184.6	143	35	Reverse	1976
Sheep Mountain Thrust	32.1	044	29	Reverse	—

Table 1. Tabulation of faults and their characteristics as modeled within the three-dimensional geologic framework model, consisting of the fault name, fault strike length, average fault dip and dip direction, interpreted fault kinematics, and maximum vertical offset.—Continued

[Refer to figure 8 for location information. ?, high degree of uncertainty; —, no data or interpretation]

Modeled fault name	Modeled strike length (in kilometers)	Modeled average dip direction (in degrees)	Modeled average dip (in degrees)	Interpreted kinematics	Modeled maximum vertical offset (in meters)
Powder River Basin—Continued					
Laramie Peak Shear Zone	113.9	136	34	Transpressional?	858
Orin Junction Fault	81.1	310	55	Transpressional?	—
Fanny Peak Monocline	170.7	097	40	Reverse	—
Wheatland Fault System	101.1	119	44	Reverse	486
Black Hills Monocline	133.4	079	35	Reverse	894
Hartville Fault	113.6	282	35	Transpressional?	296
Monument Hill Fault	71.4	034	34	Reverse?	659
Williston Basin					
Cedar Creek Anticline	69.0	044	89	Normal?	126
Weldon Fault Zone	218.0	327	89	—	—
Brockton-Froid Fault Zone	85.9	142	89	—	—

in this study. Vector polylines delineating stratigraphic contacts of interest and surface expressions of structural features were isolated from the generalized geologic map, resulting in a dataset of 6,834 vectors, which were then draped on the DEM or top bedrock surface as explicit inputs for modeling stratigraphic horizons and structural planes (fig. 6*B*). Sometimes, minor mapped details or intricate contact polylines were manually simplified to eliminate conflicts between the true ground surface and lower-resolution DEM used in this model. This conflict is a known source of error that may deviate from true ground conditions.

Mapping at a 1:500,000 scale was locally supplemented by scanned and vector 1:100,000-scale geologic maps in the Black Hills (McLaughlin and Ver Ploeg, 2006; Sutherland, 2007, 2008; Johnson and Micale, 2008; Redden and DeWitt, 2008), eastern Montana (Vuke and others, 2001, 2003), the Bighorn Mountains (Lopez, 2000; Vuke and others, 2000; Ver Ploeg and Boyd, 2002, 2003; Ver Ploeg and others, 2004; Wittke, 2007) and the southern Powder River Basin (Hallberg and Case, 2001; Hunter and others, 2005; McLaughlin and Harris, 2005; McLaughlin and Ver Ploeg, 2008; McLaughlin and others, 2011) among others. In GIS software, 1:100,000-scale geologic maps were manually georeferenced and draped on the topographic surface as images. These maps served as general guides and provided implicit information about local portions of the model (for example, local strike and dip values).

Previously Published Model Grids

Incorporating previously published geological models into regional subsurface compilations is an efficient way of adding local expertise and potentially higher-quality data and presents an opportunity for immediate comparison with model outputs constructed by this study.

Fourteen stratigraphic horizons in the northwestern part of the model were derived from a USGS petroleum systems model of the Williston Basin (Gelman and Johnson, 2023; fig. 6*E*); associated descriptions of modeled stratigraphic horizons, 148,000 formation top picks, and notes on horizon creation are in Gelman (2023). Additionally, horizon grids of six stratigraphic horizons were constructed from 28,000 wells and their associated logs as part of a dissertation examining geologic heterogeneity related to carbon sequestration in the Powder River Basin (Melick, 2013). Grids were extracted, converted to a standardized format, reprojected, and released as a USGS data release for use in this study (Spangler and others, 2023). Grids of Lower Cretaceous aquifers (Stanton, 2015) were used for comparison, but were not applied in this study.

Table 2. Definitions of three-dimensional geological modeling terms used in this study.

[DEM, digital elevation model]

Term	Definition
Anchor surface	A model surface with high confidence used to infer characteristics of overlying or underlying surfaces.
Boundary filter	A setting that restricts data points outside a predefined boundary from being used in grid calculations.
Delaunay triangulation	A method of mesh generation that divides a set of input points into triangles, ensuring no point lies within the circumcircle of any triangle.
Depositional surface	A stratigraphic surface that only onlaps underlying surfaces.
Draped	The process of assigning elevation values from a surface (for example, DEM) to data, such as maps or lines.
Erosional surface	A stratigraphic surface that can incise or erode into underlying surfaces.
Explicit model	A model derived from interpolating between a regularly spaced grid of cross sections.
Fault block	A subdivision of a geological model, defined by faults and (or) topography, functioning as an independent unit within a broader framework.
Implicit model	A model generated algorithmically from input data and user-defined constraints.
Offset surface	A stratigraphic surface created as a forward or backward offset of an anchor surface, either by a specific distance or within defined bounds.
Point	A finite X, Y, or Z coordinate in space, associated with a model-relevant attribute.
Polyline	A georeferenced line representing a model-relevant attribute.
Radial basis function	An interpolation method that assigns weights to data points based on their distance from a centroid, fitting a smooth curve through or near the points.
Residual	The vertical difference between input data and model grid results.
Stratigraphic horizon	A grid or surface delineating the upper or lower boundary of a stratigraphic unit.
Snap tolerance	Snap tolerance dictates how far the radial basis function may search in the Z direction for additional data inputs and forces interpolations to exactly match all data inputs in XYZ space.
Synthetic control point	A theoretical point that is added to grid calculations to adjust the attitude of a surface by ensuring the surface passes through this point.

Oil and Gas Wells

The location of 146,904 hydrocarbon well collars were compiled from tabular databases provided by the South Dakota Geological Survey's Oil and Gas Permits Digital Database (South Dakota Geological Survey, undated), Wyoming Oil and Gas Conservation Commission (WYOGCC; WYOGCC, undated), North Dakota Department of Mineral Resources (North Dakota Department of Mineral Resources, undated), and Montana Board of Oil and Gas Conservation (MBOGC; MBOGC, undated). Ground elevation data were extracted from the USGS 3DEP 1m dataset (USGS, 2021b) to all wells missing collar or kelly bushing elevations. Such extracted elevation data deviated from provided collar values by a mean of 0.7 m, which was deemed acceptable for this application.

Throughout the northern Great Plains, historical oil and gas fields are delineated by high-density well placement (160-acre spacing) along linear structural and stratigraphic hydrocarbon accumulations, such as the Cedar Creek Anticline, whereas modern well collars for unconventional development follow a broader grid-defined spacing (1,150-acre spacing), such as in northwestern North Dakota. Exploratory and wildcat wells drilled away from known oil and gas fields are spaced widely and irregularly, which provides particular value to this study as datapoints in poorly tested parts of the study area (fig. 6*C*).

Borehole deviation surveys or telemetry data were incorporated into this study where available. Boreholes lacking this information were assumed to be vertical with a dip of 90 degrees and a dip direction of 180 degrees.

A total of 288,892 stratigraphic formation tops of interest were selected from the four State databases. After compiling and standardizing names for this study, stratigraphic tops were plotted in 3D space by correlating unit American Petroleum Institute (API) number with well collar, survey, and stratigraphic top. Each data point was plotted on the respective borehole trace at the given depth (in meters) for use as explicit model inputs (fig. 6*C*).

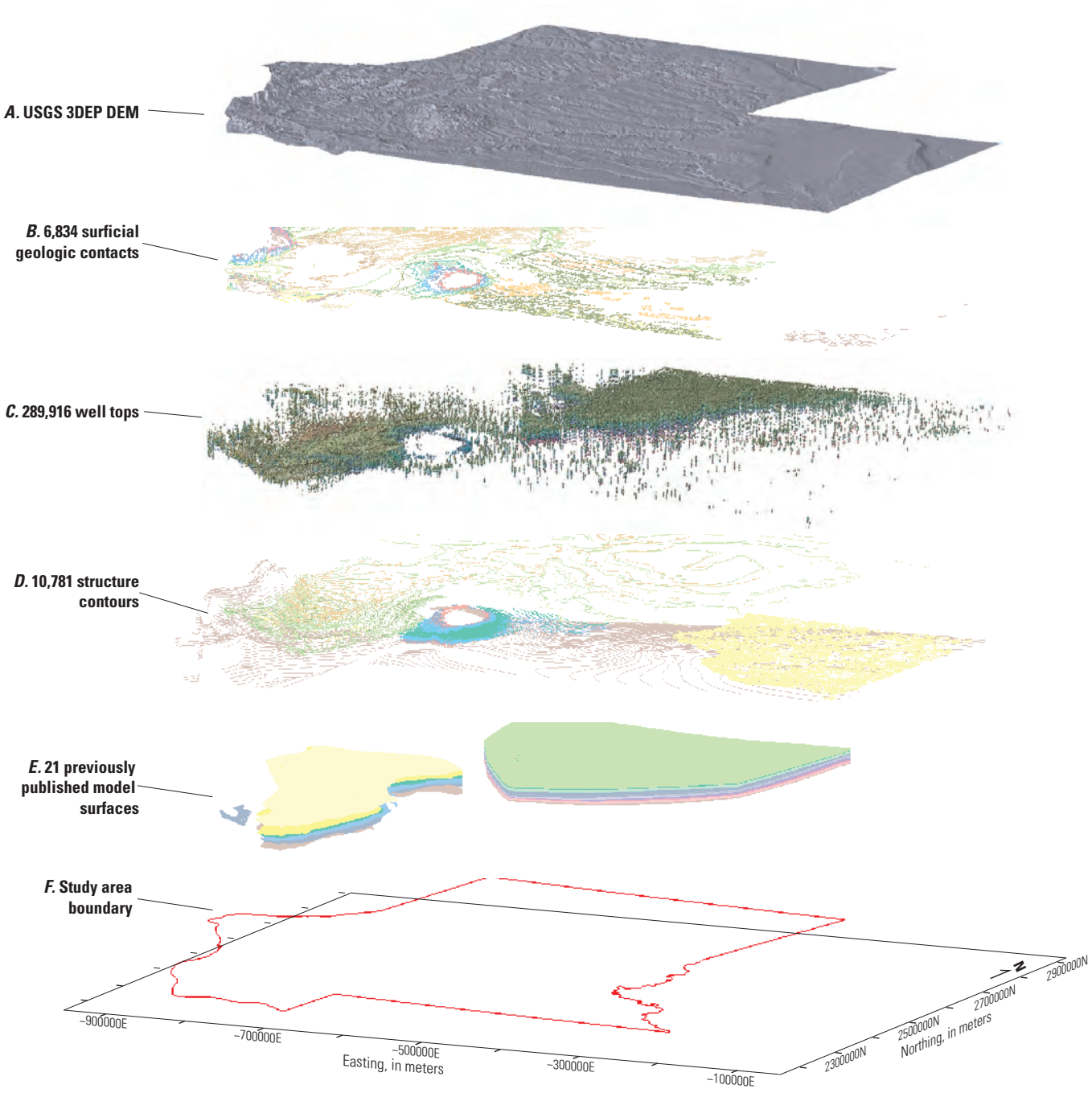

Figure 6. Visualization of explicit input data types used in the northern Great Plains three-dimensional geologic framework model, including *A*, topography from the U.S. Geological Survey 3D Elevation Program (3DEP); *B*, 6,834 surficial geologic contacts with elevation values derived from 3DEP Digital Elevation Model (DEM) data; *C*, 289,916 oil and gas and water well tops; *D*, 10,781 individual structure contours; *E*, grids of 21 stratigraphic surfaces from previously published models (Spangler and Sweetkind, 2022; Gelman and Johnson, 2023; Spangler and others, 2023); *F*, the study area outline.

Water Wells

The locations of 1,024 water wells in the eastern Black Hills were re-released as digital point data (Spangler and Sweetkind, 2022) after Carter (1999) compiled data from water well scout tickets. Collar elevation information was not provided; therefore, elevation data were extracted from the USGS 3DEP 1m dataset (USGS, 2021b) to all wells. Wells were assumed to be entirely vertical with a dip of 90 degrees and a dip direction of 180 degrees because well deviation data were not provided. Collar elevations and well deviations are known sources of error deemed acceptable for this modeling application because stratigraphic horizon elevations from water well information were consistent with nearby oil and gas tops. Data were displayed along proper borehole traces by correlating unique well identification numbers and depth along the borehole survey. Water well data were used as an explicit input for gridding.

Structure Contour Datasets

Structure contours are lines of constant elevation of a geologic surface. They are interpretive products that interpolate between discrete data points, such as stratigraphic formation tops in wells. The 3D GFM incorporates 10,781 individual structure contour lines from several maps of local and regional extent to define stratigraphic horizons and the subsurface expression of faults (fig. 6*D*).

In the South Dakota region, vector-format structure contours of the Precambrian basement (McCormick, 2010) served as the primary reference for the geometry of the basement horizon. Structure contours of the Cambrian Deadwood Formation, Mississippian Madison Limestone, Pennsylvanian-Permain Minnelusa Formation, Permian Minnekahta Limestone, and Early Cretaceous Inyan Kara Group in the Black Hills by Williamson and others (2000) were digitized and re-released by Spangler and Sweetkind (2022) for use in this study. Contours on the top of bedrock in eastern South Dakota (Tomhave and Schulz, 2004); the tops of the Late Cretaceous Fox Hills, Hell Creek, and Paleocene Fort Union Formations near the South Dakota border (Thamke and others, 2014); and the base of the Miocene Ogallala Group in southern South Dakota (Peterson, 2016) were imported into GIS software, reprojected, and converted to meters. Scanned Portable Document Format (PDF) contours of the top Deadwood Formation, Madison Group, Minnelusa Formation, and Inyan Kara Group were digitized and applied to areas northeast of the Black Hills (Hocking, 2013a, b, c, d).

Contours for the top of the Precambrian basement horizon provided by the Wyoming State Geological Survey (2022) were foundational for establishing a structural framework of the Powder River Basin margin. In the Williston Basin, contours on the top basement horizon were sourced from Anderson (2009). A set of 825 structure contours mapping Cretaceous strata in the Wyoming part of the Powder River Basin by Lichtner and others (2020) were applied to the top Lower Cretaceous Mowry Shale, Upper Cretaceous Belle Fourche Shale, Greenhorn Formation, Turner Sandy Member of the Carlile Shale, Carlile Shale, Niobrara Formation, Red Bird Silty Member of Pierre Shale and Parkman Sandstone Member of the Mesaverde Formation, Teapot Member of Mesaverde Formation, Tekla Sandstone Member of Lewis Shale, and Fox Hills Formation horizons. These contours cover a substantial part of the Powder River Basin study area and were generally regarded as high-quality data inputs because they were generated using hand-picked formation tops from geophysical logs in more than 2,200 wells. Contours depicting the complex structure of the eastern Black Hills provided valuable detail where well data are sparse (Lisenbee, 1985). Contours mapping the top of the Minnelusa Formation, Minnekahta Limestone, Goose Egg Formation, and Fox Hills Formation by Fox and Higley (1996) were digitized and released by Goldberg and Sweetkind (2022). However, the level of detail of these contours was insufficient for use in the 3D GFM. Thamke and others (2014) released a series of structure contours that define a 3D GFM of the uppermost principal aquifer system in the Williston and Powder River Basins. These contours delineate the top of the Fox Hills Formation, upper and lower parts of the Hell Creek Formation, and three members of the Fort Union Formation. This dataset was essential in the Powder River and Williston Basins and was enhanced with local detail from additional contours delineating the top of the Fort Union Formation in the coal-rich parts of the Powder River Basin (Jones and others, 2003). Finally, contours of the upper bedrock horizon from Soller and Garrity (2018) and Naylor and others (2021) were used to construct an upper bedrock horizon in the glaciated parts of Montana, North Dakota, and South Dakota.

Contour datasets were manually preprocessed by removing redundant data or contours that ignored fault offset. Datasets were then uploaded to 3D modeling software for use as explicit inputs for constraining the geometry of horizons defining the upper boundary of stratigraphic model units.

Geologic Cross Sections and Geophysical Data

Published cross sections, depth-converted 2D seismic lines, gravity, and aeromagnetic maps were used to serve as guidelines in areas where drilling is sparse, and better constrain mesoscale structural features not evident in other data types.

Sixteen stratigraphic cross sections from wireline geophysical well logs in South Dakota by Fox and others (2009) were consulted to constrain regional stratigraphic architecture and provided evidence of key stratigraphic pinch-outs and unconformities not immediately evident in the explicit input data. Additional stratigraphic cross sections consulted for this study include Gregory (1997), De Bruin (1998), Anderson (2012), and Nesheim (2016).

Three 2D depth-converted seismic lines were published by Stone (2003) which run approximately west-southwest–east-northeast from the Bighorn Mountains to the axis of the Powder River Basin. These data and their accompanying interpretations were incorporated to constrain the geometry of the Piney Creek Thrust and Granite Ridge tear faults along the western margin of the Powder River Basin. Tagged Imaged File Format (TIFF) images of seismic sections were adjusted to a one-to-one aspect ratio, georeferenced in a GIS, and imported to the modeling software as planar surfaces on which control points were added. Geologic context was added to these lines by three Wyoming Geological Survey cross sections by Wendell and others (1976) and Stone (1987), which were added to the modeling software using a similar method. Additional cross sections were consulted for individual 1:250,000- and 1:100,000-scale quadrangles around the margin of the Powder River Basin and in the Black Hills, but not used as explicit input data given that these were drafted by extrapolating surface mapping into the subsurface using geological first principles (for example, law of superposition, lateral continuity, and so forth) and professional expertise instead of subsurface data (Lopez, 2000; Vuke and others, 2000, 2003; Redden and DeWitt, 2008).

Georeferenced gravity and aeromagnetic maps were used as implicit data. Interpretations of these data by Redden and DeWitt (2008) and McCormick (2010) in South Dakota, Robbins (1994) and Anna (2010) in the Powder River Basin, and Bader (2019a) in the Williston Basin region were applied to identify deep-rooted faults that penetrate the Precambrian basement. Isostatic and Bouguer gravity anomaly data, as well as magnetic anomaly maps, for the conterminous United States were sourced from the USGS Mineral Resources Online Spatial Database (Phillips and others, 1993; Bankey and others, 2002). Subsurface geometries of igneous intrusions were interpreted directly from cross sections, gravity, and magnetic maps where available.

Modeling Methodology

Selection of a subsurface modeling approach depends on the geologic setting of the study area, the availability and type of input data, and the intended application of the model. Based on these considerations, this study used a hybrid-implicit modeling approach in which algorithmically interpolated surfaces are locally refined using traditional explicit techniques (for example, wireframing). Similar approaches have been applied in studies characterized by sparse data (Caumon and others, 2016; de Kemp and others, 2016), complex faulting or stratigraphy inferred from surface mapping (Sweetkind and others, 2013; Collon and others, 2016; Burt and others, 2021; Siler and others, 2023), and heterogeneous data types (Sweetkind, 2017; Cikoski and others, 2020).

Following compilation and standardization of input data within a centralized geodatabase, model construction proceeded independently for three subregions: western South Dakota, the Williston Basin region, and the Powder River Basin region. Initial construction consisted of (1) building independent implicit stratigraphic and fault frameworks for each region; (2) merging these frameworks into a unified 3D GFM parsed into fault-bounded blocks; and (3) iteratively refining the combined interpretation by removing erroneous inputs, adjusting algorithmic parameters, or introducing synthetic control points using wireframe patterns until geologically acceptable results were achieved (fig. 7*A–C*). Final model outputs were exported as raster grids and point datasets, and visualizations were generated as images and animations.

Although many commercially available and open-source geological modeling software packages are used by the USGS, this study primarily used commercial implicit modeling software Leapfrog Geo 2023.1 (Seequent, 2021), which interpolates grids using either a radial basis function (RBF; Leapfrog's FastRBF) or Delaunay triangulation. Leapfrog Geo's algorithms have the option to incorporate geologic rules in implicit gridding calculations, such as fault hierarchy, erosional horizons, and intrusive geometries, a feature of this software program that is particularly valuable when modeling at the basin scale. However, other commercially available software packages are capable of achieving similar results.

Implicit Stratigraphic Framework Interpolation

Selected stratigraphic horizons were interpolated using input data from well tops, structure contours, and surface contacts, among other data types mentioned in this study. These surfaces are composed of triangular elements with a resolution of 250 square meters that are calculated using Leapfrog's FastRBF. Gridding resolution does not necessarily convey model confidence.

Initial grid construction involved simple triangulation among all available explicit inputs for each stratigraphic horizon. Following this initial calculation, horizons were then ordered chronologically to enforce the law of superposition and establish relative timing relations. Further refinement involved classifying horizons as either "depositional" or "erosional," which governs their crosscutting relations within the modeling software. Depositional horizons are truncated by younger units, whereas erosional horizons may incise both underlying and overlying strata. This configuration allows regional unconformities, such as the base of the Inyan Kara Group, to bevel underlying stratigraphy where appropriate. Intrusive bodies were included within the stratigraphic framework because they crosscut and deform older sedimentary units into which they intrude.

Substantial variation in data density among stratigraphic horizons resulted in locally inconsistent geometries where poorly constrained surfaces deviated unrealistically from

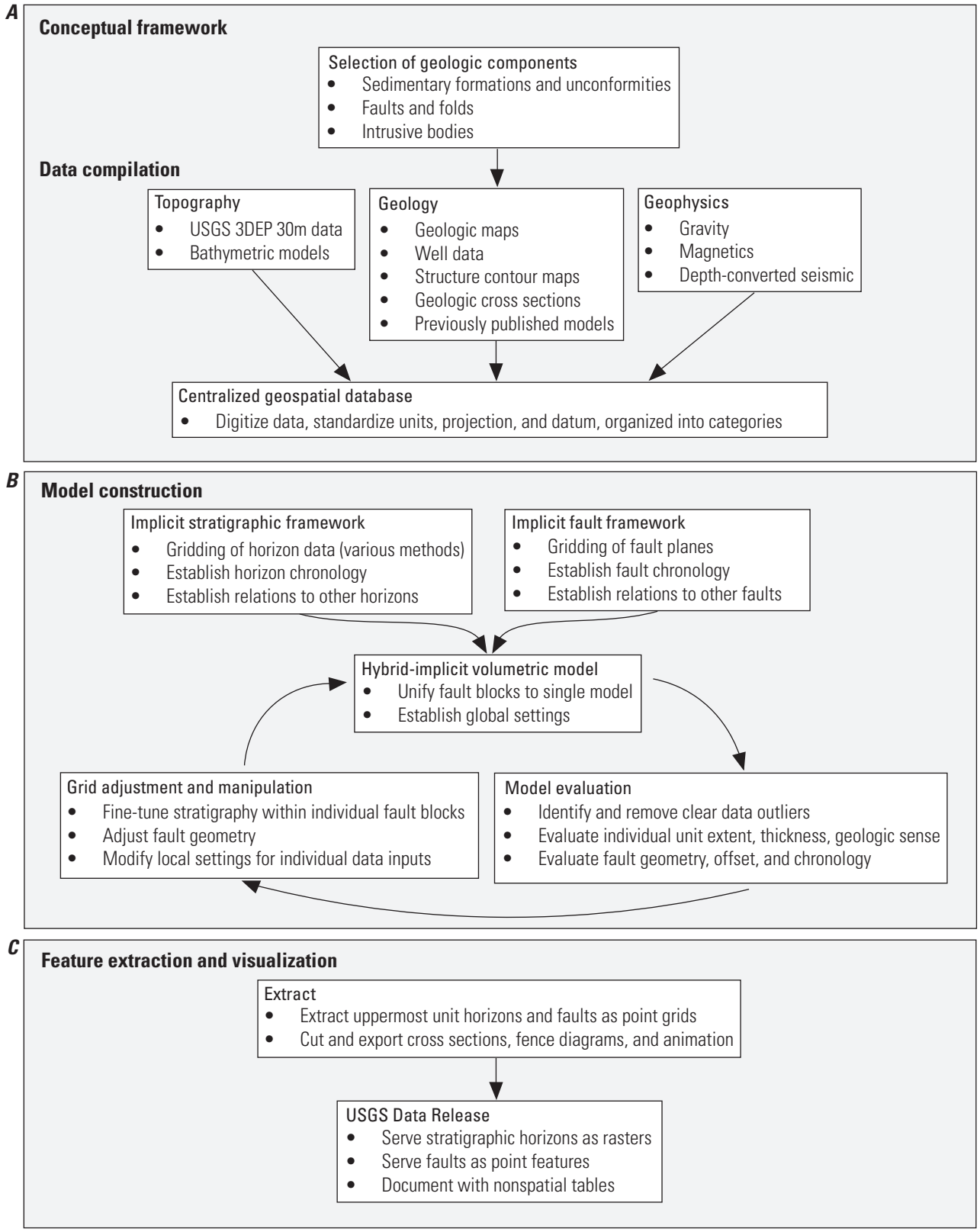

Figure 7. Flowchart showing the process of development of digital data through *A*, conceptual framework and data compilation, *B*, model construction, and *C*, feature extraction and visualization for the three-dimensional geologic framework model.
USGS, U.S. Geological Survey; 3DEP, 3D Elevation Program; m, meter.

adjacent units. To address this issue, horizons with sparse input data were reconstructed as offset surfaces derived from better-constrained "anchor surfaces." Anchor surfaces were defined as horizons with the highest data density and most reliable subsurface control, such as the Interlake Dolomite horizon, Madison Group horizon, Minnelusa Formation horizon, Inyan Kara Group horizon, Greenhorn Formation horizon, and Pierre Shale horizon. Adjacent low-data horizons were regenerated as offset facsimiles of anchor surfaces using minimum and maximum vertical offset constraints. Available data for low-data horizons were still honored where present. Offset surfaces are considered more uncertain than anchor surfaces.

Implicit Fault Framework Interpolation

Forty-seven faults were modeled as planar surfaces that offset stratigraphy and subdivide the 3D GFM into computational fault blocks. Surface traces of selected faults were identified from 1:500,000-scale geologic mapping draped over a DEM and served as primary inputs for constructing fault surfaces (Horton and others, 2017). Complex fault zones or swarms were simplified into representative master faults where appropriate, such as in the Brockton–Froid Fault Zone of Montana and North Dakota (fig. 8*A*).

For concealed faults that do not propagate to the surface but were identifiable in other data types, representative synthetic control points containing basic structural orientations (for example, dip and dip direction) were placed in space as the primary input. Georeferenced one-to-one geologic cross sections, depth-converted seismic lines, and gravity or magnetics maps served as guides for placing synthetic control points and modifying fault attitudes. Faults with unspecified orientations were modeled with a 90-degree dip, representing structures with a high degree of positional uncertainty. These faults were included because they likely exist, but their orientation, slip sense, and timing of deformation are not well understood.

Fault chronology was defined manually to establish crosscutting relations among intersecting faults. This process required interpretation of relative fault timing, including whether one fault truncates or offsets another, or whether faults intersect with minimal interaction. The resulting fault network was interpolated using Delaunay triangulation at a resolution of 500 m (fig. 8*A*).

Hybrid-Implicit Volumetric Geologic Model

Refined stratigraphic and fault frameworks were combined into a single 3D GFM subdivided into fault-bounded volumes, referred to here as "fault blocks" (fig. 8*B*). Global modeling parameters, such as grid resolution, were applied consistently across all fault blocks, whereas region-specific settings were applied selectively. For example, in the hanging wall of the Piney Creek Thrust (fault block named "PRB 13"; fig. 8*B*), well data were filtered to exclude footwall wells from RBF interpolation. In this same fault block, stratigraphic horizons were forced to honor mapped surface contacts, which represent the most reliable and abundant data type in that area.

To ensure that model grids reflect geologically plausible geometries, additional adjustments were made using 2,803 synthetic control points. In the Black Hills region, synthetic points were placed hundreds of meters above the modern land surface to reconstruct pre-erosional stratigraphic configurations, resulting in more realistic dips and surface contacts around the uplift (fig. 9*A*). Moreover, additional synthetic control points were added when RBF-interpolated horizons "warp" in a sinusoidal pattern where data are sparse (fig. 9*B*). These artifacts were mitigated using wireframe control points to stabilize surface curvature.

Detailed documentation of stratigraphic hierarchy and horizon-specific modeling parameters is provided in the data releases accompanying this report (Spangler, 2024a, b). Plates showing the elevation from sea level for the uppermost horizon of the Precambrian rock (pl. 1), Interlake Dolomite (pl. 2), Madison Group (pl. 3), Minnelusa Formation and Tensleep Sandstone (pl. 4), Inya Kara Group (pl. 5), Greenhorn Formation (pl. 6), and Pierre Shale (pl. 7) that served as anchor surfaces in this study are available at http://doi.org/10.3133/sir20265127.

Input Data Hygiene

Given the regional scale and heterogeneity of input datasets, this study applied a systematic and conservative data-screening workflow to identify and remove anomalous values while preserving genuine geologic variability. This approach balances model fidelity with realistic representation of the subsurface, particularly in data-poor areas where overcorrection could obscure meaningful structural or stratigraphic features.

In well data, inaccuracies were most apparent when erroneous stratigraphic picks resulted in a "spike" that conflicted with surrounding data (fig. 9*C*). Smoothing functions were avoided so that legitimate geologic variability was not removed; only clear outliers were excluded. A conservative approach to eliminating well data is especially important in areas where well data density is low because isolated data points exert a much stronger control and bear higher relative importance on the shape of a mesh than points in high-density areas.

Interpretive datasets incorporated into this study, such as structure contour maps or model grids, may not always represent the best possible interpretation. Because structure-contour maps may conflict with well data or adjacent horizons, contours were clipped where inconsistent with better-constrained inputs (fig. 9*C*). Similarly, model grids

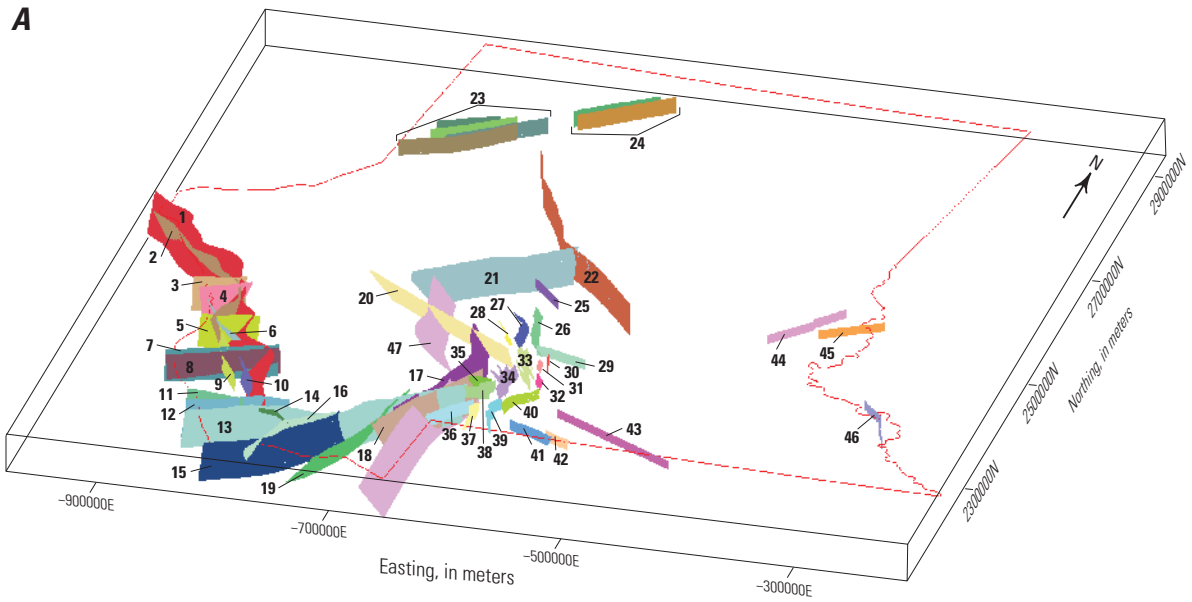

EXPLANATION

Study area boundary

Fault zone or swarm identifiers

1	Piney Creek Thrust	11	Casper Mountain Fault	21	Ekalaka Fault	31	Boxelder Creek Anticline	41	Slim Butte Anticline
2	Piney Creek Backthrust	12	Deer Creek Fault	22	Cedar Creek Anticline	32	Murphy Anticline	42	Pine Ridge Anticline
3	Shell Lineament	13	Northern Bounding Fault	23	Weldon Fault Zone	33	Pactola Fault Zone	43	Unknown Fault
4	Granite Ridge Tear Fault	14	Sheep Mountain Thrust	24	Brockton Froid Fault Zone	34	Pringle-Reno Fault Zone	44	Little Eagle Fault
5	Florence Pass Lineament	15	Laramie Peak Shear Zone	25	Moreau River Anticline	35	Teepee Canyon Fault	45	Mobridge Fault
6	Clear Creek Thrust	16	Orin Junction Fault	26	Whitewood Anticline	36	Edgemont Anticline	46	Crow Creek Fault
7	North Sisters Hill Fault	17	Fanny Peak Monocline	27	Spring Creek Anticline	37	Horse Trip Anticline	47	Black Hills Monocline
8	South Sisters Hill Fault	18	Wheatland Fault System	28	Spearfish Anticline	38	Hell Canyon Fault System		
9	Tisdale Fault	19	Hartville Fault	29	Alkali Creek Fault	39	Cold Brook Anticline		
10	Salt Creek Fault	20	Monument Hill Fault	30	Pedimont Anticline	40	Fairburn Anticline		

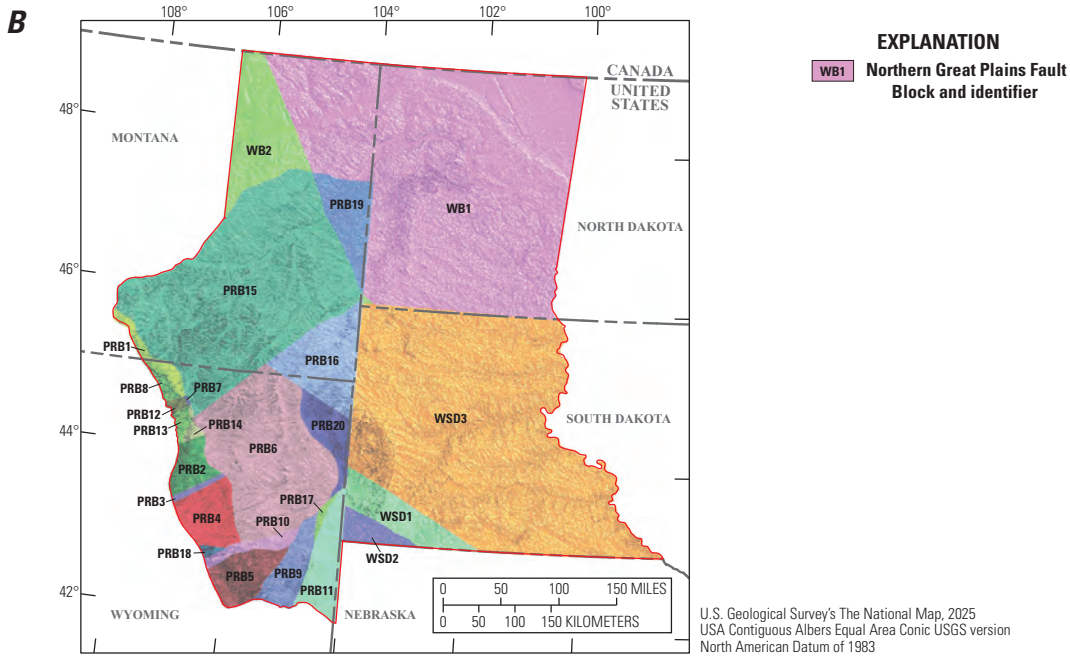

EXPLANATION

WB1 Northern Great Plains Fault Block and identifier

U.S. Geological Survey's The National Map, 2025
USA Contiguous Albers Equal Area Conic USGS version
North American Datum of 1983

Figure 8. *A,* Three-dimensional geologic framework model of the northern Great Plains, naming specific faults included in this study. All faults and their relevant references are named and captured in Spangler (2024a, b). *B*, Map showing the subdivisions or "fault blocks" used in the northern Great Plains region three-dimensional geologic framework model.

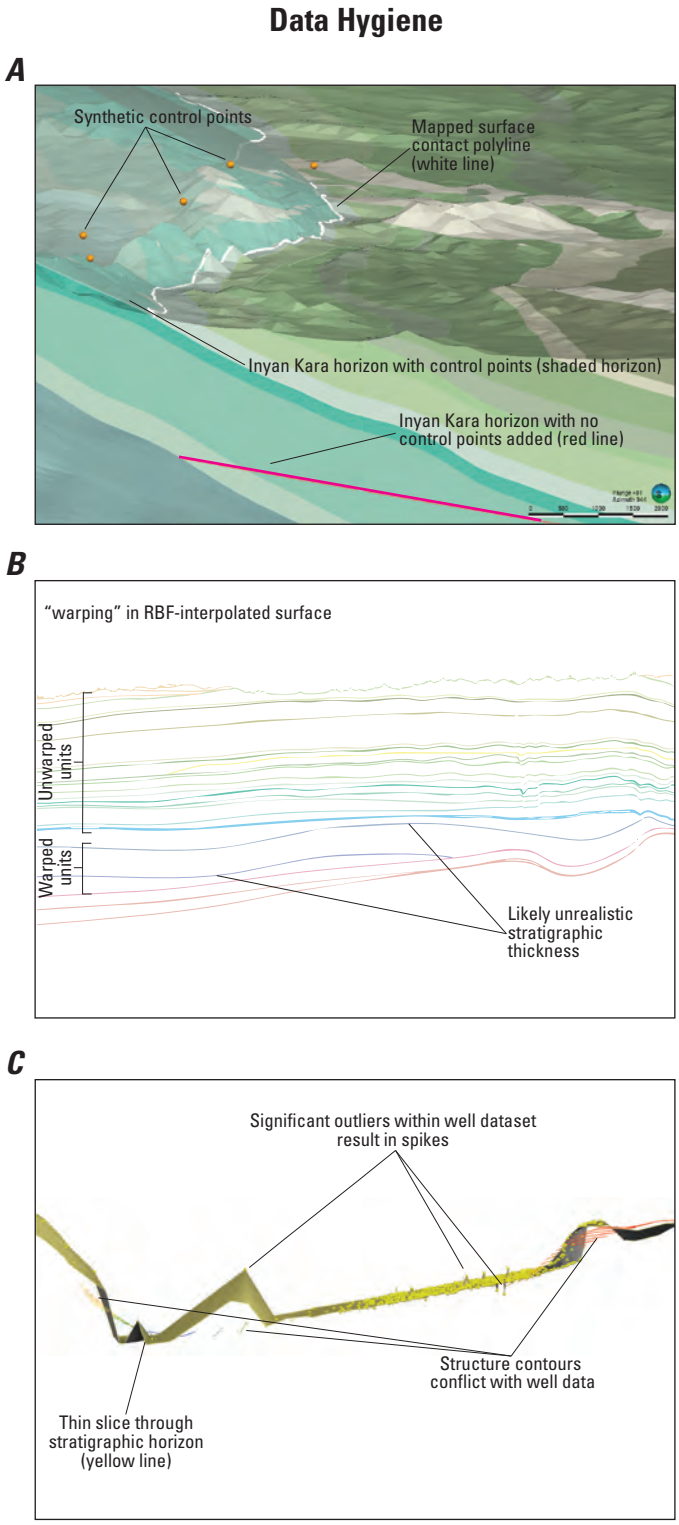

Figure 9. *A*, Example of synthetic control points improving model realism at the surface near the Black Hills. The points are forcing the top Inyan Kara horizon to extend above the modern-day land surface, similar to pre-erosional topography. The horizon with no control points is unrealistic. *B*, Example of radial basis function (RBF) interpolant producing unrealistic stratigraphic geometries in lower Paleozoic units with poor well control. *C*, Examples of outliers within a single well dataset causing spikes in RBF-interpolated horizon. A structure contour dataset from the same stratigraphic horizon is shown to illustrate how well and structure contour datasets may significantly conflict.

that conflicted with other data inputs were eliminated where significant discrepancies made subsurface geometries highly unrealistic.

Model Evaluation

Six horizons spanning shallow to deep stratigraphy were evaluated to quantify model fit across the section: the Top Lance and Hell Creek Formations horizon (fig. 10*A*), Top Mowry Shale horizon (fig. 10*B*), Top Inyan Kara Group horizon (fig. 10*C*), Top Minnekahta Limestone horizon (fig. 10*D*), Top Madison Group horizon (fig. 10*E*), and Top Precambrian basement horizon (fig. 10*F*). The elevation (Z) values of the modeled horizons were sampled at 133,109 X and Y locations of well formation tops or mapped geologic contacts that were used to calculate the surface. At each location, the Z value of the model was subtracted from the Z value of the input data, resulting in a Z-residual value that can be plotted in graphical space and on a base map (fig. 10). Only well data and geologic contacts were chosen for evaluation because they are considered the highest confidence data.

In each surface, Z-residual values are generally less than ±20 m. Population means range from −0.5 m of offset (top Minnekahta horizon) to 31.7 m of offset (top Madison horizon; table 3). However, each surface contains a few extreme outliers that skew the population standard deviation and mean, including an extreme 4,758-m outlier in the top Madison horizon near the Piney Creek Thrust that likely occurred because of wells that intercepted the unit multiple times in the overthrust. Median Z-residual values are therefore a better estimation of model fit and range from ±0.4 m (top Minnekahta horizon) to ±3.1 m (top Precambrian basement horizon; table 3).

Uncertainty

Z-residual values were plotted within the study area and on top of the surfaces they were derived from to visualize their spatial distribution. This visualization serves as a qualitative proxy to communicate uncertainty to the end user. Where dense clusters of low Z-residual values exist, interpretation uncertainty is low. Where clusters of high Z-residual values exist, interpretation uncertainty is high.

When examining the Z-residual distribution of the upper Madison horizon, model results closely honor tightly spaced wells in the eastern Powder River Basin, Cedar Creek Anticline, and Williston Basin (fig. 10*E*). Isolated outliers in these low Z-residual regions likely indicate issues with input data, such as a bad pick or a wellbore lacking deviation information. Similarly, sporadic well picks in the Lance and Hell Creek horizons led to high Z-residual values because well data for this unit conflicted significantly with structure contour datasets used in grid calculations (fig. 10*A*).

Clusters of high Z-residuals convey high uncertainty. For example, in the upper Mowry horizon (fig. 10*B*), high Z-residual clusters near the Black Hills Monocline indicate the presence of small structural features that were not adequately captured by this study. Similar trends occur in the southwestern Powder River Basin near the Hartville Uplift (fig. 10*B*), where complex fault relations unresolved in this model result in high Z-residual values and uncertainty. Regions with interspersed high and low Z-residual values additionally convey relatively high uncertainty, although the source of uncertainty may be a combination of complex subsurface geology, uncertain input data, and (or) other factors leading to a mismatch between inputs and outputs. This pattern is exemplified by the interspersed high and low Z-residuals for the Mowry Shale near the Casper Arch (fig. 10*B*).

Z-residuals are not a perfect proxy for uncertainty. For example, many subsurface modeling packages have the capability to match grids exactly to all inputs, which would result in Z-residuals of zero even where obvious outliers exist (for example, fig. 9*C*). Another factor that affects an uncertainty metric is the data density. It is reasonable to assume that regions with few inputs, or isolated clusters of data, such as the top Precambrian basement horizon (fig. 10*F*), have an inherently elevated uncertainty even if the Z-residuals are low.

Discussion of Model Results and Limitations

A series of perspective views shows the upper crystalline Precambrian basement volume of the model, and a series of fence diagrams to illustrate the Phanerozoic basin fill throughout these regions (figs. 11–13). Various aspects of the model relevant to its applicability and limitations are discussed to communicate the level of detail captured throughout the 3D GFM, explain characteristic geologic features found within the study area, discuss caveats in regions of high uncertainty, and identify anomalies that warrant further investigation.

Powder River Basin Region

From a perspective view of the Powder River Basin part of the northern Great Plains, the shape of the basin itself and the surrounding uplifts are clearly defined (fig. 11). The northern extent of the model contains relatively flat-lying strata, gently deformed by broad folds and upwarps in the crystalline basement, such as Porcupine Dome and the Ashland Syncline (fig. 3; Vuke and others, 2009). Silurian–Mississippian strata are thickest to the northeast, and thin on top of more isopachous and regionally continuous Cambrian–Ordovician strata to the southwest in the core of the Powder River Basin (Peterson, 1988). The basin axis is modeled in the footwall of the Piney Creek Thrust, which was simplified in

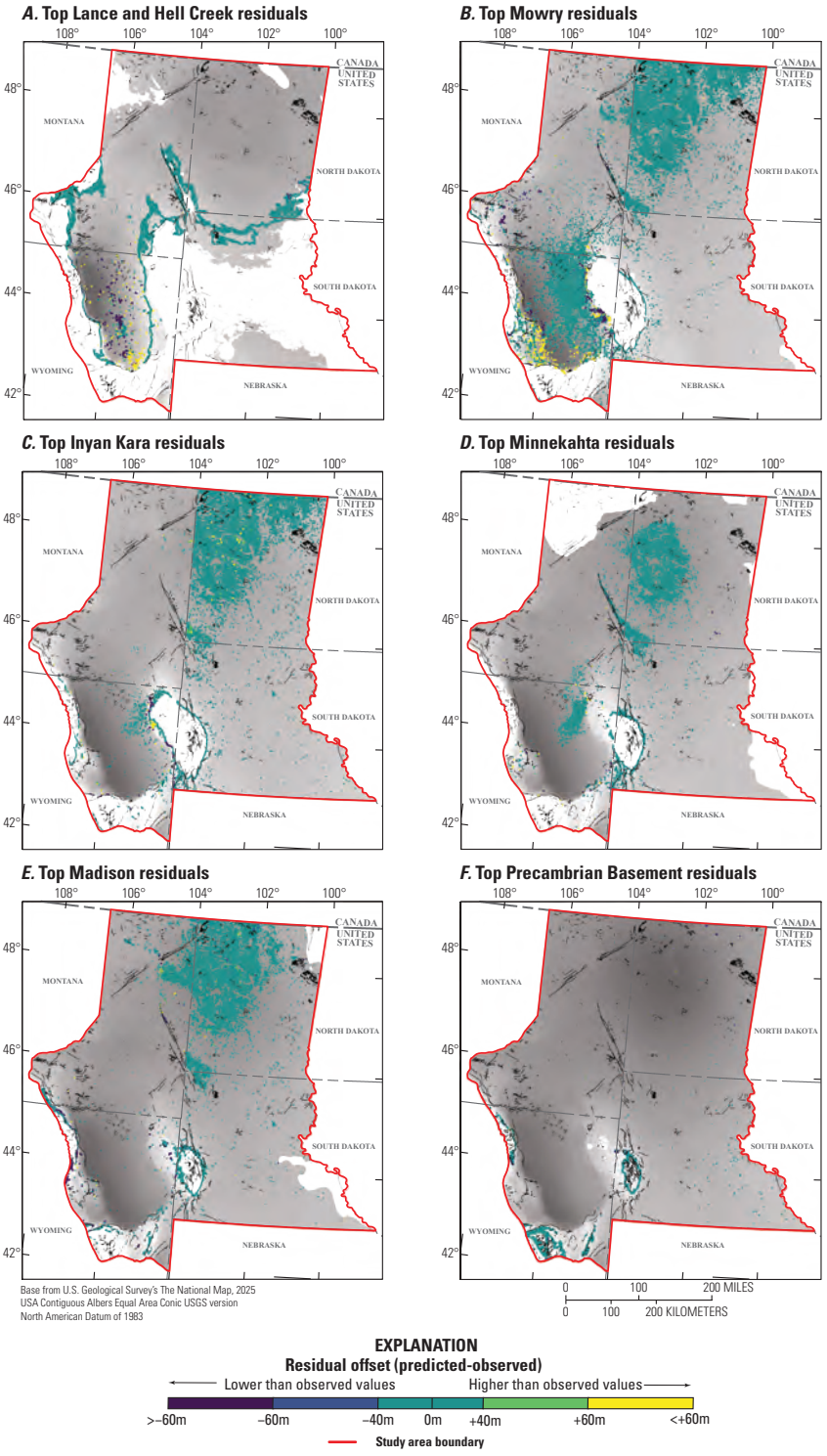

Figure 10. Z-residual maps illustrating the upper surface elevation of select model units (gray), location of mapped faults from the State Geologic Map Compilation (Horton and others, 2017), and input data points from well data and surface outcrops. Dense clusters of low Z-residual values indicate low uncertainty, whereas clusters of high Z-residual values indicate high uncertainty. Points are colored by the residual difference between input data elevation value and predicted elevation value from the northern Great Plains three-dimensional geologic framework model. Surfaces include the *A*, Uppermost part of the Lance and Hell Creek Formations model unit, *B*, Uppermost part of the Mowry Shale model unit, *C*, Uppermost part of the Inyan Kara Group model unit, *D*, Uppermost part of the Minnekahta Limestone model unit, *E*, Uppermost part of the Madison Group model unit, and *F*, Uppermost part of the Precambrian basement model unit. >, less than; m, meters.

Table 3. Summary statistics for northern Great Plains three-dimensional geologic framework model residuals.

Model unit name	Number of inputs	Maximum outlier residual (in meters)	Mean residual (in meters)	Median residual (in meters)	Standard deviation
Uppermost part of the Lance and Hell Creek model unit	29,102	1,833	3.7	1.9	57
Uppermost part of the Mowry model unit	36,019	3,299	2.7	1.2	101
Uppermost part of the Inyan Kara model unit	25,460	1,964	10.9	3	123
Uppermost part of the Minnekahta model unit	14,038	1,174	0.5	0.4	29
Uppermost part of the Madison model unit	23,338	4,758	31.7	1.9	241
Uppermost part of the Precambrian basement model unit	5,152	1,832	9.6	3.1	69

this study as a single low-angle master thrust with a shallow back-thrust dipping to the east (fig. 11*A*; Erslev, 1993; Stone, 1993, 2003). The east–west oriented strike-slip faults referred to as the "Shell Lineament and Granite Ridge Tear Faults" (fig. 8*A*) probably occurred synchronously with major slip of the Piney Creek Thrust and resulted in a small laterally offset anomaly of exposed Precambrian rocks near Granite Ridge (fig. 11*A*; Hoy and Ridgway, 1997; Stone, 2003). Seismic, surface mapping, and wells that drilled through the overthrust Precambrian hangingwall into the underlying Paleozoic sedimentary footwall (for example, Gulf Granite Ridge 9–1–2D) were used to constrain the geometry of this part of the Powder River Basin; however, more detailed interpretations of Stone (2003) may be more appropriate for subregional investigations in this area.

Thick accumulations of Fort Union Formation rocks are modeled clearly in the footwall of the Piney Creek Thrust, although the calculated geometry of each individual member within the Fort Union is speculative in this area (Love and Christiansen, 1985). The modeled Tullock Member of the Fort Union Formation is shown to drastically thicken directly adjacent to Granite Ridge; however, the model may overstate the thickness of the Tullock and understate the thickness of the overlying Lebo and Tongue River Members in the footwall syncline, which is truncated by the thrust system in its current configuration (fig. 11*A*). Furthermore, structural overthickening of these units could have occurred due to propagation of local lower-angle or blind thrust splays in the footwall growth syncline not recognized for more than a few kilometers of strike length. Fort Union rocks are overlain by the Wasatch Formation, which is another synorogenic deposit situated in the footwall syncline of the Piney Creek Thrust that records peak Laramide contraction along the system in the Eocene (Fan and Carrapa, 2014). Roll-front uranium deposits have been identified in Forth Union and Wasatch strata from the Piney Creek Thrust to the Casper Arch, which are possibly related to the weathering of uplifted granites proximal to reducing groundwater in the greater Tullock or Tongue River aquifers.

Eastward-thinning Upper Cretaceous sand bodies, such as the Turner, Teapot, and Tekla sandstone model units, are shown within a thick section of shales near the basin axis (fig. 11*A*; Lynds and Slattery, 2017). However, the thickness of these units is highly variable in the 3D GFM because of conflict between publicly available well data and published contour maps of these units (Merewether, 1996). Detailed modeling of these sandstones would be more appropriately conducted using original picks from wireline logs and a sequence stratigraphic modelling approach.

A simplified representation of the eastern Powder River Basin and Black Hills Monocline is shown in figure 11*B*. Many interpretations have been made in this region to define the structure of the uplift (for example, Lisenbee, 1978, 1988; Lisenbee and DeWitt, 1993; Fox and Higley, 1996; Driscoll and others, 2002). This study simplified the uplift to a single eastward-dipping master fault with maximum displacement to the north of the Black Hills Uplift, similar to Marshak and others (2000). However, many small but densely drilled oil fields in the downthrown side of the structure (with significant residual offset in the 3D GFM) indicate more structural complexity. It is likely that a single fault is a significant oversimplification of this region which is better represented by many small-offset faults and "in-line lenses" or "terraces" of Lisenbee (1988). Low-angle faults that were not explicitly modeled may be expressed in the 3D GFM as small undulations in stratigraphic horizons instead of with proper stratigraphic offset (fig. 11*B;* table 1.1). A highly interpretive rendering of the Bear Lodge intrusive complex and other intrusive bodies in this region were constructed using surface mapping, published cross sections, gravity and magnetic anomalies, and by interpreting intrusives to have uplifted Paleozoic sedimentary rocks where they outcrop at surface outside of the regional structural trend. Although these features have received considerable attention from geologists as natural attractions and a possible source of rare-earth elements, limited subsurface data on these intrusives have been made public (DeWitt and others, 1986; Moore and others, 2015). Additional publicly available data, including high-resolution gravity and magnetic anomaly surveys, geochemical sampling,

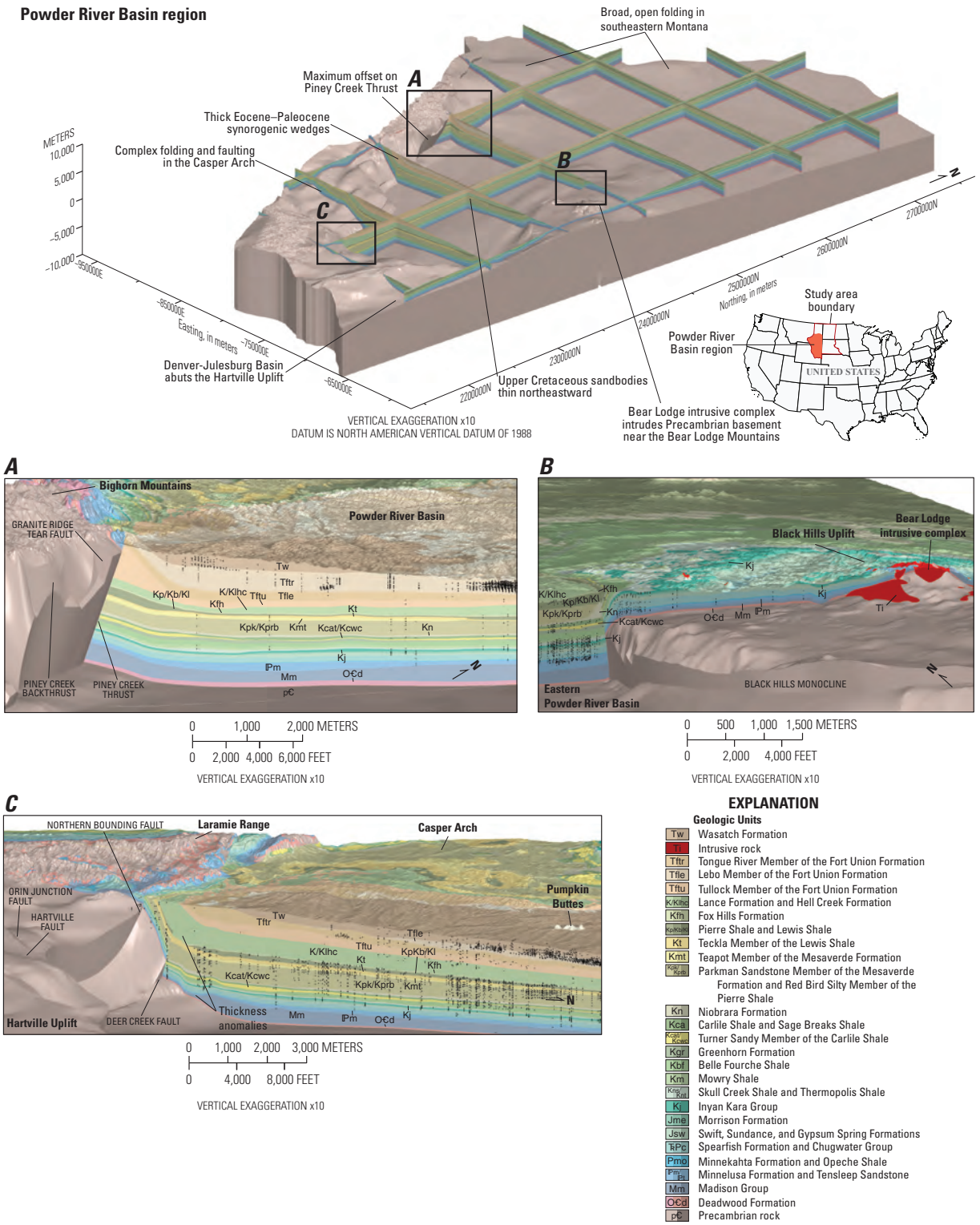

Figure 11. Perspective view of the Powder River Basin part of the three-dimensional (3D) geologic framework model (GFM), showing serial cross sections through the Phanerozoic section resting on top of the crystalline Precambrian basement model volume. Black dots in detail views are stratigraphic well picks projected 1,000 meters from the line of the slice. *A*, A west–east detail view of the 3D GFM showing the sedimentary section adjacent to the Piney Creek Thrust and Bighorn Mountains. *B*, A west–east detail view of the 3D GFM showing the interpreted subsurface geometry near the Black Hills Monocline and Bear Lodge Mountains. *C*, A north–south detail view of the 3D GFM showing the sedimentary section adjacent to the Northern Bounding Fault, Laramie Range, and Hartville Uplift.

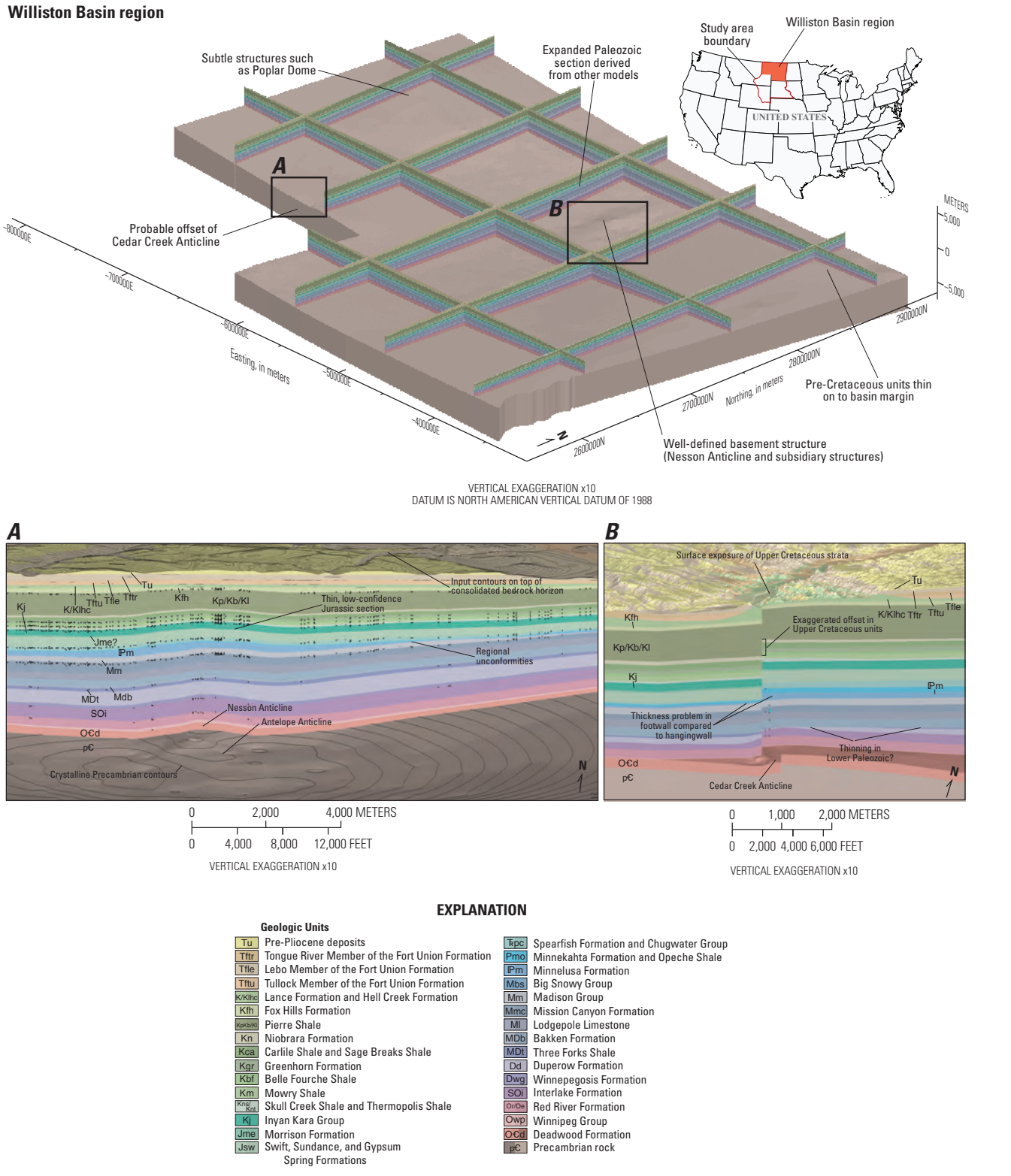

Figure 12. Perspective view of the Williston Basin part of the three-dimensional (3D) geologic framework model (GFM), showing serial cross sections through the Phanerozoic section resting on top of the crystalline Precambrian basement model volume. *A*, A west–east detail cutaway of the Phanerozoic sedimentary section near Nesson Anticline. The upper surface in this cutaway shows the top of consolidated bedrock with most recent glacial till stripped away. Contours used to construct this surface are from Soller and Garrity (2018). *B*, A detail view of the 3D GFM near the Cedar Creek Anticline, illustrating challenges associated with detailed fault offset modeling in this study.

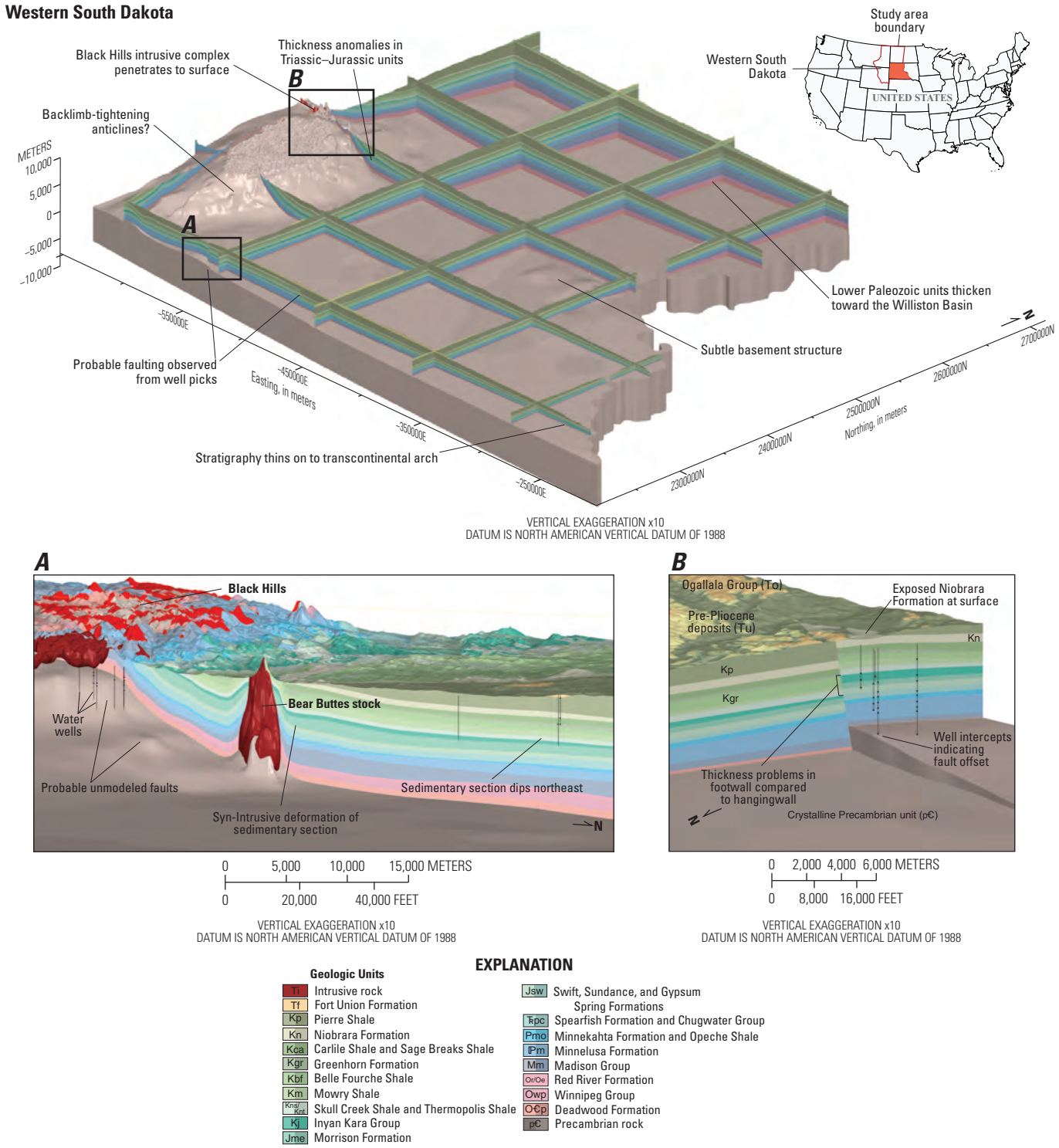

Figure 13. Perspective view of the western South Dakota part of the three-dimensional geologic framework model, showing serial cross sections through the Phanerozoic section resting on top of the crystalline Precambrian basement model volume. *A*, A north–south detail cutaway of the Slim Butte Anticline in southern South Dakota. This view shows the clear surface expression of the fault, well intercepts indicating its presence, and stratal thickness problems in the three-dimensional geologic framework model resulting in potentially unrealistic offset. *B*, A south–north perspective cutaway of the Black Hills near Bear Buttes. The cutaway displays the interpreted geometry of the intrusive stock, associated deformation in the surrounding sedimentary section, and warping of the Precambrian basement that may be small faults beneath the level of detail of this study.

and drilling, could better constrain interpretations beyond surface mapping and conceptual hand-drawn sketches of these complex but increasingly relevant intrusives.

Complex folding and faulting in the Casper Arch is well documented and evident in well picks and outcrop patterns (for example, Baker, 1957; Love and Christiansen, 1985; Melick, 2013). Major structures, such as the Salt Creek Anticline and Teapot Dome, are shown in the perspective view of the 3D GFM, in addition to smaller faults and folds that crosscut the uplift (fig. 11). The vintage of wells and lack of publicly available seismic data in this region contribute significantly to the level of uncertainty in the Casper Arch despite a well distributed well dataset. Although modeled as throughgoing fault planes in the 3D GFM, it is more probable that faults lose displacement in ductile strata overlying the Madison Group and tip out up section as folds, such as in the fold of Teapot Dome (Baker, 1957; Roberts and others, 2022). Faults bounding the southern margin of the Powder River Basin and Casper Arch, such as the Deer Creek, Casper Mountain, and Northern Bounding Faults, were modeled as en-echelon, low-angle thrust faults similar to interpretations of Blackstone (1996; 1988), Stone (2002), and Bader (2021; fig. 11*C*). Slip on these faults likely occurred into the Eocene and truncate older faults exposed at surface in the Hartville Uplift and Laramie Mountains, such as the Laramie Peak Shear Zone and Orin Junction Fault. In the footwall of the Deer Creek and Northern Bounding Faults, stratal thicknesses became challenging to rectify, resulting in thickness anomalies in Paleozoic strata, such as the Madison Group, or overthickening in the Fox Hills Formation (fig. 11*C*). Notable in this area is an overthickened Lance and Hell Creek model unit, the geometry of which is supported by WOGCC well picks and structure contours from wireline log interpretation (Thamke and others, 2014). Relevant to subsurface workers in this region, anomalously high heat flow is observed in Upper Cretaceous strata near the Salt Creek Anticline (150 milliwatts per square meter [mW/m^2]) and Teapot Dome (225 mW/m^2) (McPherson and Chapman, 1996). Anomalous heat flow values could be attributed to advection by a regional-scale groundwater system, which charges in the Black Hills, sweeps heat from the deeper parts of the basin, and discharges near the fracture-porosity enhanced anticlines of the Casper Arch (McPherson and Cole, 2000; fig. 11*C*). This thermal regime, coupled with numerous interlayered reservoir and seal intervals and a well-established hydrocarbon industry, could make the southern Powder River Basin an attractive locality for potential future enhanced geothermal exploration or carbon capture use and storage infrastructure development.

Williston Basin Region

A perspective view of the Williston Basin region of the 3D GFM illustrates the subtlety of structural features in the northern extent of the northern Great Plains, such as Nesson Anticline and Poplar Dome (fig. 12; Nesheim, 2016). However, the most important consideration in this part of the 3D GFM was the numerous unconformities between sedimentary units, such as the erosional unconformity at the base of the Cretaceous Inyan Kara Group (Gerhard and Anderson, 1988). Occasionally, attempts to model these unconformities using Leapfrog's RBF results in thin slivers of sedimentary section (less than 5–10 meters) that may not actually exist in the subsurface. An example of this phenomenon is the Jurassic Morrison Formation, which is shown in the 3D GFM as a thin remnant unit at the base of the Cretaceous unconformity despite the Morrison not generally being recognized in the Williston Basin (Murphy and others, 2009). Similarly, the true extents of units may not be appropriately captured in the GFM, but were left as is to ensure stratal horizons were fully interlocking. For example, the true limits of the Bakken Formation may be improved by eliminating any section in the 3D GFM with a vertical thickness under 2 m because the vertical resolution of this work is not fine enough to capture such granular detail.

Near the top of the sedimentary basin fill, an erosional unconformity at the top of consolidated bedrock is shown scouring into sediments as old as the Late Cretaceous, forming significant relief between channels and ridges in the subglacial till topography (fig. 12*A*; Soller and Garrity, 2018; Naylor and others, 2021). In this view, as much as 90 m of undifferentiated sedimentary deposits (mostly consisting of glacial till) have been stripped away for illustrative purposes. Details of the shallow bedrock and glacial geology most applicable to groundwater resources or contaminant assessments are likely lost because of the scale of the 3D GFM cannot capture geologic heterogeneity at this scale. A framework model focused exclusively on the uppermost Cretaceous and Cenozoic sedimentary section similar to Thamke and others (2014) or Peterson (2016) could be most appropriate to improve on the synthesis presented in this report.

The Cedar Creek Anticline is one of the most prominent structural features in the Williston Basin region and has long been a focus of hydrocarbon producers with more than 100 wells delineating the structure along strike. High subsurface data density, combined with interpretations from Gelman and Johnson (2023) could make rigorous modeling of the structure relatively straightforward, however geologic problems at the field-scale are still observed on the 3D GFM results (fig. 12*B*). In lower Paleozoic strata, such as the Interlake Dolomite or Winnipegosis Formations, potentially unrealistic thickening and thinning are observed directly adjacent to the structure. Because the Cedar Creek Anticline has been active since the Late Devonian (Clement, 1986), these relations could certainly be real. However, even slight errors in input data or interpolation settings could dramatically affect the thickness of these units. Similarly, thickness variations in Mississippian and Permian units across the fault are corroborated by well data compiled for this study; however, it would be challenging to identify a convincing natural mechanism for this observation. These thickness issues

compound up section, leading to potentially exaggerated vertical offset on the structure in Upper Cretaceous units, such as the Pierre Shale (fig. 12*B*). Outcropping Upper Cretaceous units are mapped along the strike of the Cedar Creek Anticline (Vuke and others, 2009) and are shown to outcrop correspondingly in the 3D GFM.

Western South Dakota

A perspective view of the western South Dakota part of the 3D GFM captures the major structural elements in the region, including the Transcontinental Arch, southern margin of the Williston Basin, and Black Hills Uplift (fig. 13). Lower Paleozoic rocks, such as the Deadwood Formation and Red River Formation, are preserved in the southern extent of South Dakota; however, these units thicken to the northeast where they dip into the Williston Basin (fig. 13*A*; Peterson, 1988). Mesozoic rocks are relatively isopachous compared to the lower Paleozoic section, which corroborates the hypothesis that the Williston Basin was tectonically quiescent (inactive) throughout much of this period (Kent and Christopher, 2007; Gelman, 2023). Multiple unconformity surfaces, such as at the top of the Madison Group, base of the Sundance Formation, or base of the Inyan Kara Group, intersect near the southeastern extent of the northern Great Plains and create a complex and challenging to parse stratigraphic framework near the South Dakota–Nebraska border. These relations were approximated using stratigraphic sections of Fox and others (2009). Similarly, unconformity surfaces resulted in apparent thickness anomalies in the Sundance Formation and Morrison Formation on the eastern margins of the Black Hills Uplift (Anna, 1986; Williamson and others, 2000). Although these thickness anomalies are supported by well data and theoretical knowledge of the region, further explanation is needed to confirm the existence of excess thickness in Jurassic units (fig. 13).

Faults below the scale of this model unit are on the margin of the Black Hills as small linear undulations in the crystalline Precambrian basement model unit (fig. 13*A*). These faults deform the overlying sedimentary rocks in the 3D GFM, which is corroborated by water well data and structure contour mapping by Carter (1999) and Carter and others (2003). It is probable that these faults offset the crystalline Precambrian basement and lose displacement up section in more ductile sediments, which causes these structures to crop out at the surface as folds. Intrusion of laccoliths and small stocks, such as the Bear Buttes stock postdate layered bedrock, and deformation associated with their intrusion is captured in the 3D GFM (fig. 13*A*). The geometry of the Bear Buttes stock was interpreted from cross sections by Redden and DeWitt (2008), however the geometry is only slightly less speculative than other intrusive bodies in this study.

In addition to challenges with unconformity relations, faults in southern South Dakota near the Nebraska border were noted in this study. Well intercepts of basement rock indicate the presence of some structural features where the Slim Butte Anticline, Pine Ridge Anticline, and an unknown fault are modeled in the 3D GFM. Linear gravity anomalies with a similar west–northwest orientation were noted by McCormick (2010) and could possibly be the northern extent of the Chadron Arch, which predominantly underlies Nebraska. The Slim Butte Anticline is the most prominent of these features, which is modeled in the 3D GFM with basement offset down to the northeast approximately 289 m inferred from wells Amerada #1 Red Eagle and Integrity #1 Pine Ridge. Dip on the fault associated with the Slim Butte Anticline is modeled as a reverse fault of 35 degrees; however, this structure could be high angle with a complex fault history similar to the Cedar Creek Anticline, with phases of normal and reverse activation. Notably, Cambrian Deadwood Formation is not explicitly picked in the public well records on the upthrown side of this fault. While modeled as a thin remnant unit in the 3D GFM, it is possible that this structure was active as early as the Cambrian or was activated shortly thereafter, eroding Deadwood strata from the hangingwall. Up section, a similar challenge to the stratal thickness problems encountered near the Cedar Creek Anticline was observed, where a lack of well picks on the footwall side of the structure results in stratal modeled thickness problems across the fault. As these stratal thickness changes compound up section, the vertical displacement of the fault might become exaggerated in the 3D GFM (fig. 13*B*). The Niobrara Formation is mapped at the surface of the Slim Butte Anticline and does appropriately crop out in the 3D GFM (fig. 13*B*); however, these interpretations only provide one rendering of the geology in a region of sparse drilling. The Pine Ridge Anticline and Unknown fault were included in this model because of strong linear magnetic anomalies adjacent to wells English #1 Eucks and KG&S #1 Farley, which required some structural discordance to exist to maintain probable Cretaceous stratigraphic thicknesses. Remarkably low magnetic anomalies are observed on the southwest sides of the structures; and regional values increase gradually to the northeast. These structures were modeled with basement offset down to the northeast at 90 degrees of dip because their slip history is likely similar to the kinematics of the Slim Butte Anticline, but remains uncertain.

National-scale maps of geothermal potential have shown that the region southeast of the Black Hills near the Slim Butte and Pine Ridge faults is highly prospective for hidden sedimentary geothermal resources (Roberts, 2018) Local thermal gradients are as high as 127 degrees Celsius per kilometer (Schoon and McGregor, 1974), which could make characterization of these faults significantly more relevant to subsurface explorers, local communities, and land managers than they historically have been. The Slim Butte, Pine Ridge, and “unknown” faults included in this study are a starting point; however, 4–5 colinear magnetic anomalies trending northwest–southeast may be the source or conduit

for anomalously hot fluids in southern South Dakota and have even been postulated to be related to a series of deeply buried volcanic centers (McCormick, 2010).

Fault modeling in the Black Hills region of the northern Great Plains 3D GFM is shown to have been highly simplified on the western margin near the Black Hills Monocline and to the east, where the uplift transitions to the South Dakota plains (figs. 11*B* and 13*A*). The geometry of basement-cored faults in this model is similar to large offset, range-bounding Laramide faults, such as the Piney Creek Thrust on the western margin of the Powder River Basin (Lisenbee and DeWitt, 1993). However, many subtle anticlines and probable faults are in the sedimentary units in cross section view through the Black Hills region of the 3D GFM, which are not accounted for by this structural model (fig. 14). Although the results presented in this report are likely adequate for many 3D modeling applications, a significantly more complex fault geometry similar to a shallow broken foreland-type uplift of Erslev (2005) or Horton and others (2022) may be more appropriate in this region. The inline lenses and terraces of Lisenbee (1988) to the west of the Black Hills Monocline corroborated by drilling and modeling in this study would likely be accounted for by nearly horizontal subthrust splay anticlines (fig. 14). Contractional structures in the Wyoming part (or forelimb) of the Black Hills Uplift could be accounted for by west-dipping backthrust-tip anticlines, and small-scale faulting on the east side of the Back Hills (backlimb) would likely be caused by backlimb-tightening anticlines (figs. 13 and 14; Horton and others, 2022).

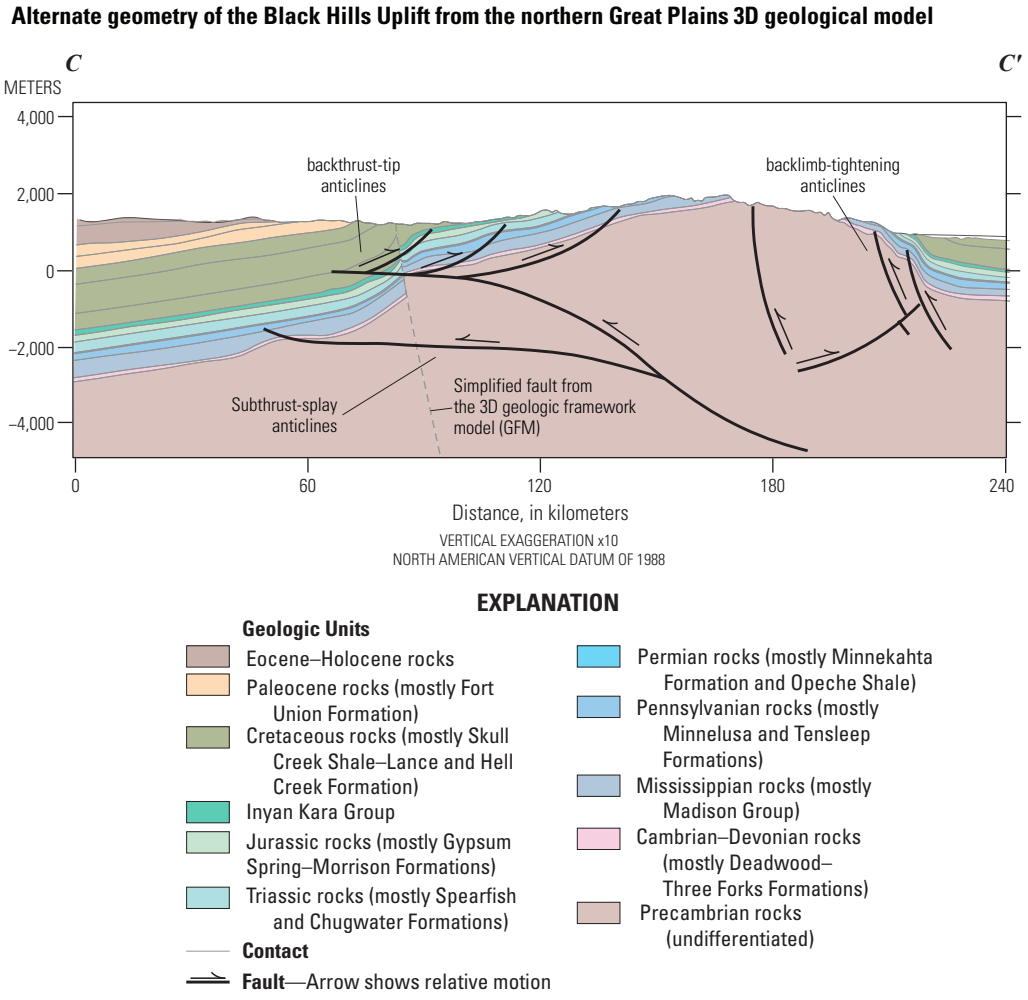

Figure 14. A subset of figure 4*A* (cross section *A*–*A*′) showing a simplified cut through the Black Hills Uplift section of the three-dimensional (3D) geologic framework model presented in this study. A schematic of a significantly more complex fault geometry than the three-dimensional geologic framework model is shown, similar to a shallow broken foreland-type uplift from Erslev (2005) and Horton and others (2022).

Summary

A digital, deterministic three-dimensional (3D) geologic framework model (GFM) of the northern Great Plains, including the Powder River Basin of Wyoming and Montana and the Williston Basin of North Dakota and South Dakota, was developed from a variety of publicly available geologic data. A total of 41 stratigraphic horizons and 47 faults were combined to construct a solid-volume 3D GFM. The 3D GFM is internally consistent with no gaps or undefined space between model elements. Outcrop patterns displayed by this model, including major structure and unit outcrops, are broadly consistent with published surface geologic mapping at a 1:500,000 scale.

The model depicts the overall geometry of the westward-deepening Powder River Basin and the complex basement uplifts that encircle it to the east, south, and west, including the Black Hills, Hartville Uplift, and Bighorn Mountains. The model additionally depicts how these Laramide deformation-related crustal features link with major crustal structures that have ancestry as early as the Paleozoic, including the Transcontinental Arch and Williston Basin. The model illustrates the spatial extent, elevation, and thickness of Phanerozoic sedimentary rocks as well as a simple interpretation of the elevation and geometry of major intrusive features to the northwest of the Black Hills. A simplified interpretation of major faults is included with this study that offset stratigraphic units.

This 3D GFM is intended to provide a foundational interpretive geologic framework from well-studied basins to underexplored regions with little subsurface interpretation. Metaevaluation of this study serves to emphasize the need for data collection and focused subsurface analyses outside of traditional hydrocarbon-producing fairways, such as the western and northwestern Black Hills, southern Casper Arch, southern Powder River Basin, and southwestern South Dakota.

References Cited

Alberta Geological Survey, 2021, Geologic framework of Alberta, version 3 (interactive app and map, methodology, model, dataset, storymaps, webmaps): Alberta Geological Survey, Alberta Energy Regulator, AER/AGS interactive application, accessed March 5, 2023, at https://ags.aer.ca/publication/iam-012.

Algeo, T.J., Meyers, P.A., Robinson, R.S., Rowe, H., and Jiang, G.Q., 2014, Icehouse–greenhouse variations in marine denitrification: Biogeosciences, v. 11, no. 4, p. 1273–1295, accessed October 20, 2023, at https://doi.org/10.5194/bg-11-1273-2014.

Anderson, F.J., 2007, Precambrian basement drillhole map of North Dakota: North Dakota Geological Survey Geologic Investigations no. 43, scale 1:750,000 and 1:250,000, accessed May 19, 2023, at https://www.dmr.nd.gov/ndgs/documents/Publication_List/pdf/geoinv/GI_43.pdf.

Anderson, F.J., 2009, Depth to Precambrian basement rock in North Dakota: North Dakota Geological Survey Geologic Investigations no. 85, scale 1:750,000, accessed March 5, 2023, at https://www.dmr.nd.gov/ndgs/documents/Publication_List/pdf/geoinv/GI_85_web.pdf.

Anderson, F.J., 2012, Generalized geologic cross-section in southeastern North Dakota: North Dakota Geological Survey Geologic Investigations no. 152, accessed May 28, 2023, at https://www.dmr.nd.gov/ndgs/documents/Publication_List/pdf/geoinv/GI_152.pdf.

Anna, L.O., 1986, Geologic framework of the ground-water system in Jurassic and Cretaceous rocks in the northern Great Plains, in parts of Montana, North Dakota, South Dakota, and Wyoming: U.S. Geological Survey Professional Paper 1402–B, 36 p., 18 pls., accessed May 28, 2023, at https://doi.org/10.3133/pp1402B.

Anna, L.O., comp., 2010, Geologic assessment of undiscovered oil and gas in the Powder River Basin province, Wyoming and Montana (revised April 2010), *in* Total petroleum systems and geologic assessment of oil and gas resources in the Powder River Basin province, Wyoming and Montana: U.S. Geological Survey Digital Data Series DDS–69–U, chap. 1, 97 p., accessed November 11, 2023, at https://pubs.usgs.gov/dds/dds-069/dds-069-u/REPORTS/69_U_CH_1.pdf.

Anna, L.O., and Cook, T.A., 2008, Assessment of the Mowry Shale and Niobrara Formation as continuous hydrocarbon systems, Powder River Basin, Montana and Wyoming: U.S. Geological Survey Open-File Report 2008–1367, 1 sheet, accessed October 20, 2023, at http://pubsdata.usgs.gov/pubs/of/2008/1367/index.html.

Anna, L.O., Pollastro, R., and Gaswirth, S.B., 2013, Williston Basin Province—Stratigraphic and structural framework to a geologic assessment of undiscovered oil and gas resources, chap. 2 *of* Assessment of undiscovered oil and gas resources of the Williston Basin Province of North Dakota, Montana, and South Dakota, 2010 (ver. 1.1, November 2013): U.S. Geological Survey Digital Data Series 69–W, 17 p., accessed May 28, 2023, at https://pubs.usgs.gov/dds/dds-069/dds-069-w/.

Bader, J.W., 2017, Mapping sandstones of the Inyan Kara Formation for saltwater disposal in North Dakota: North Dakota Department of Mineral Resources, Geo News, North Dakota Geological Survey Investigations, v. 44, no. 1, p. 6–9, accessed March 5, 2023, at https://www.dmr.nd.gov/ndgs/documents/newsletter/2017Winter/Mapping%20Sandstones%20of%20the%20Inyan%20Kara%20Formation%20for%20Saltwater%20Disposal%20in%20North%20Dakota.pdf.

Bader, J.W., 2019a, An ancient Everest—Precambrian basement terranes of the Williston Basin: North Dakota Department of Mineral Resources, Geo News, v. 46, no. 1, p. 30–34, accessed May 19, 2023, at https://www.dmr.nd.gov/ndgs/documents/newsletter/2019Winter/An_Ancient_Everest_Precambrian_Basement_Terranes_of_the_Williston_Basin.pdf.

Bader, J.W., 2019b, Structural inheritance for the Laramide, Central Montana Uplift—A wrench-fault tectonic model related to Proterozoic orogenesis in the foreland of the North American Cordillera: Northwest Geology, v. 46, p. 21–39, accessed May 28, 2023, at https://www.researchgate.net/publication/334431998_Structural_inheritance_for_the_Laramide_Central_Montana_Uplift_A_wrench-fault_tectonic_model_related_to_Proterozoic_orogenesis_in_the_foreland_of_the_North_American_Cordillera.

Bader, J.W., 2021, Structural analysis of the Casper Mountain fault zone and surrounding area, Wyoming—Implications for Laramide kinematics and structural inheritance across the Wyoming Province: The Mountain Geologist, v. 58, no. 4, p. 433–452, accessed May 19, 2023, at https://doi.org/10.31582/rmag.mg.58.4.433.

Baker, F.E., 1957, History of the Salt Creek Oil Field, *in* Wyoming Geological Association, Wyoming Oil and Gas Fields Symposium (Includes 1961 Supplement), 1957: The AAPG/Datapages Combined Publications Database, p. 388, accessed November 11, 2023, at https://archives.datapages.com/data/wga/data/013/013001/388_wga0130388.htm.

Bankey, V., Cuevas, A., Daniels, D., Finn, C.A., Hernandez, I., Hill, P., Kucks, R., Miles, W., Pilkington, M., Roberts, C., Roest, W., Rystrom, V., Shearer, S., Snyder, S., Sweeney, R.E., Velez, J., Phillips, J.D., and Ravat, D.K.A., 2002, Digital data grids for the magnetic anomaly map of North America: U.S. Geological Survey Open-File Report 2002–414, [variously paged], accessed May 28, 2023, at https://doi.org/10.3133/ofr02414.

Blackstone, D.L., Jr., 1988, Thrust faulting—Southern margin Powder River Basin, Wyoming, *in* Diedrich, R.P., Dyka, M.A.K., and Miller, W.R., eds., Eastern Powder River Basin—Black Hills, Wyoming Geological Association 39th Field Conference, Casper, Wyoming, September 9–11, 1988, Guidebook: Wyoming Geological Association, p. 35–44, accessed May 19, 2023, at https://archives.datapages.com/data/wga/data/046/046001/pdfs/35.pdf.

Blackstone, D.L., Jr., 1993, Precambrian basement map of Wyoming—Outcrop and structural configuration: Geological Survey of Wyoming [Wyoming State Geological Survey] Map Series 43, scale 1:1,000,000, accessed May 19, 2023, at https://www.wsgs.wyo.gov/products/wsgs-1993-ms-43.pdf.

Blackstone, D.L., Jr., 1996, Structural geology of the Laramie Mountains, southeastern Wyoming and northeastern Colorado: Wyoming State Geological Survey Report of Investigations 51, 28 p., 3 pls., scale 1:500,000, accessed May 19, 2023, at https://sales.wsgs.wyo.gov/structural-geology-of-the-laramie-mountains-southeastern-wyoming-and-northeastern-colorado-1996/.

Bluemle, J.P., 1988, Generalized bedrock geologic map of North Dakota: North Dakota Geological Survey, Miscellaneous Map 28, scale 1:500,000, accessed May 19, 2023 at https://www.dmr.nd.gov/ndgs/documents/Publication_List/pdf/MisMaps/MM-28.pdf.

Brock, J., Berry, K., Faulds, J., Berg, R., House, K., Marketti, M., McPhee, D., Schmidt, K., Schmitt, J., Soller, D., Spears, D., Thompson, R., Thorleifson, H., and Walsh, G., 2021, Renewing the National Cooperative Geologic Mapping Program as the Nation's authoritative source for modern geologic knowledge: U.S. Geological Survey Open-File Report 2021–1013, 10 p., accessed May 19, 2023, at https://doi.org/10.3133/ofr20211013.

Burt, A.K., Sirles, P., and Turner, A.K., 2021, Data sources for building geological models, chap. 7 *of* Turner, A.K., Kessler, H., and van der Meulen, M., eds., Applied multidimensional geological modeling—Informing sustainable human interactions with the shallow subsurface: John Wiley & Sons Ltd, p. 133–182. [Also available at https://doi.org/10.1002/9781119163091.ch7.]

Caddey, S.W., Bachman, R.L., Campbell, T.J., Rolland, R.R., and Otto, R.P., 1991, The Homestake gold mine, an early Proterozoic iron-formation-hosted gold deposit, Lawrence County, South Dakota: U.S. Geological Survey Bulletin 1857–J, 67 p., accessed March 5, 2023, at https://doi.org/10.3133/b1857J.

Carlson, M.P., 1999, Transcontinental Arch—A pattern formed by rejuvenation of local features across Central North America: Tectonophysics, v. 305, no. 1–3, p. 225–233, accessed March 5, 2023, at https://doi.org/10.1016/S0040-1951(99)00005-0.

Carr-Crabaugh, M., and Dunn, T.L., 1995, Reservoir heterogeneity as a function of accumulation and preservation dynamics, Tensleep Sandstone, Bighorn and Wind River Basin, Wyoming, *in* M.W. Longman and M.D. Sonnenfeld, eds., Paleozoic systems of the Rocky Mountain region: Denver, Colo., Rocky Mountain Section, SEPM (Society for Sedimentary Geology), p. 305–320, accessed November 11, 2023, at https://archives.datapages.com/data/rocky_sepm/data/034/034001/305_rocky_mount340305.html.

Carrapa, B., DeCelles, P.G., and Romero, M., 2019, Early inception of the Laramide orogeny in southwestern Montana and northern Wyoming—Implications for models of flat-slab subduction: Journal of Geophysical Research Solid Earth, v. 124, no. 2, p. 2102–2123, accessed May 19, 2023, at https://doi.org/10.1029/2018JB016888.

Carter, J.M., 1999, Selected data for wells and test holes used in structure-contour maps of the Inyan Kara Group, Minnekahta Limestone, Minnelusa Formation, Madison Limestone, and Deadwood Formation in the Black Hills area, South Dakota: U.S. Geological Survey Open-File Report 99–260, 51 p., accessed May 28, 2023, at https://doi.org/10.3133/ofr99260.

Carter, J.M., Driscoll, D.G., and Sawyer, J.F., 2003, Groundwater resources in the Black Hills area, South Dakota: U.S. Geological Survey Water-Resources Investigations Report 03–4049, 36 p., accessed May 19, 2023, at https://pubs.usgs.gov/wri/wri034049/.

Caumon, G., Jessell, M., de Kemp, E., Nemeth, B., Peron, G., and Schetselaar, E., 2016, Introduction to special section—Building complex and realistic geological models from sparse data: Interpretation, v. 4, no. 3, art. SMi, 1 p., accessed May 19, 2023, at https://doi.org/10.1190/INT-2016-0614-SPSEINTRO.1.

Caylor, E., Carrapa, B., Jepson, G., Sherpa, T.Z.L., and DeCelles, P.G., 2023, The rise and fall of Laramide topography and the sediment evacuation from Wyoming: Geophysical Research Letters, v. 50, no. 14, art. e2023GL103218, 10 p., accessed May 28, 2023, at https://doi.org/10.1029/2023GL103218.

Childs, O.E., 1985, Correlation of stratigraphic units of North America—COSUNA: The American Association of Petroleum Geologists Bulletin, v. 69, no. 2, p. 173–180, accessed October 20, 2023, at https://doi.org/10.1306/AD461C73-16F7-11D7-8645000102C1865D.

Cikoski, C., Fichera, M., Mamer, E., and Sturgis, L., 2020, A three-dimensional hydrogeologic model from the Pecos Slope, the Southern High Plains, southeastern New Mexico: New Mexico Bureau of Geology and Mineral Resources Open-File Report 614, 136 p., accessed March 5, 2023, at https://catalog.newmexicowaterdata.org/dataset/a-three-dimensional-hydrogeologic-model-from-the-pecos-slope-to-the-southern-high-plains.

Clement, J.H., 1986, Cedar Creek—A significant paleotectonic feature of the Williston Basin, *in* Peterson, J.A., ed., Paleotectonics and sedimentation in the Rocky Mountain region, United States: The American Association of Petroleum Geologists Memoir, v. 41, p. 213–240, accessed May 19, 2024, at https://doi.org/10.1306/M41456C11.

Collon, P., Pichat, A., Kergaravat, C., Botella, A., Caumon, G., Ringenbach, J.-C., and Callot, J.-P., 2016, 3D modeling from outcrop data in a salt tectonic context—Example from the Inceyol minibasin, Sivas Basin, Turkey: Interpretation, v. 4, no. 3, p. SM17–SM31, accessed May 19, 2023, at https://doi.org/10.1190/INT-2015-0178.1.

Craddock, W.H., Drake, R.M., II, Mars, J.C., Merrill, M.D., Warwick, P.D., Blondes, M.S., Gosai, M.A., Freeman, P.A., Cahan, S.M., DeVera, C.A., and Lohr, C.D., 2012, Geologic framework for the national assessment of carbon dioxide storage resources—Powder River Basin, Wyoming, Montana, South Dakota, and Nebraska, chap. B *of* Warwick, P.D., and Corum, M.D., eds., Geologic framework for the national assessment of carbon dioxide storage resources: U.S. Geological Survey Open-File Report 2012–1024–B, 30 p., accessed May 28, 2023, at https://doi.org/10.3133/ofr20121024B.

Crowley, K.D., Ahern, J.L., and Naeser, C.W., 1985, Origin and epeirogenic history of the Williston Basin—Evidence from fission-track analysis of apatite: Geology, v. 13, no. 9, p. 620–623, accessed March 5, 2023, at https://pubs.geoscienceworld.org/gsa/geology/article-abstract/13/9/620/189561/Origin-and-epeirogenic-history-of-the-Williston.

De Bruin, R.H., 1998, Subsurface correlation of selected Late Cretaceous and older formations along the eastern Powder River Basin, Wyoming (cross section B-B'): Wyoming State Geological Survey, Geophysical Log Cross Section 98–1, accessed May 19, 2023, at https://sales.wsgs.wyo.gov/subsurface-correlation-of-selected-late-cretaceous-and-older-formations-along-the-eastern-powder-river-basin-wyoming-cross-section-b-b-1998/.

DeCelles, P.G., 2004, Late Jurassic to Eocene evolution of the Cordilleran thrust belt and foreland basin system, Western U.S.A.: American Journal of Science, v. 304, no. 2, p. 105–168, accessed November 11, 2023, at https://doi.org/10.2475/ajs.304.2.105.

DeWitt, E., Redden, J.A., Wilson, A.B., and Buscher, D., 1986, Mineral resource potential and geology of the Black Hills National Forest, South Dakota and Wyoming: U.S. Geological Survey Bulletin 1580, 135 p., accessed May 19, 2023, at https://pubs.usgs.gov/bul/1580/report.pdf.

Downey, J.S., 1986, Geohydrology of bedrock aquifers in the northern Great Plains in parts of Montana, North Dakota, South Dakota, and Wyoming: U.S. Geological Survey Professional Paper 1402–E, 87 p., accessed May 28, 2023, at https://pubs.usgs.gov/pp/1402e/report.pdf.

Downey, J.S., and Dinwiddie, G.A., 1988, The regional aquifer system underlying the northern Great Plains in parts of Montana, North Dakota, South Dakota, and Wyoming—Summary: U.S. Geological Survey Professional Paper 1402–A, 64 p., accessed May 19, 2023, at https://pubs.usgs.gov/pp/1402a/report.pdf.

Driscoll, D.G., Carter, J.M., Williamson, J.E., and Putnam, L.D., 2002, Hydrology of the Black Hills area, South Dakota: U.S. Geological Survey Water-Resources Investigations Report 2002–4094, 150 p., accessed May 28, 2023, at https://doi.org/10.3133/wri024094.

Erslev, E.A., 1993, Thrusts, back-thrusts, and detachment of Rocky Mountain foreland arches, *in* Schmidt, C.J., Chase, R.B., and Erslev, E.A., eds., Laramide Basement Deformation in the Rocky Mountain Foreland of the Western United States: Boulder, Colo., The Geological Society of America [GSA], GSA Special Paper 280, 339–358 p. [Also available at https://doi.org/10.1130/SPE280-p339.]

Erslev, E.A., 2005, 2D Laramide geometries and kinematics of the Rocky Mountains, Western USA, *in* Karlstrom, K.E., and Keller, G.R., eds., The Rocky Mountain region—An evolving lithosphere: American Geophysical Union, Geophysical Monographs, v. 154, p. 7–20, accessed May 19, 2024, at https://doi.org/10.1029/154GM02.

Erslev, E.A., Hennings, P.H., and Zahm, C.K., 2001, Kinematics and structural closure of basement-involved anticlines in the central Rocky Mountains petroleum province [abs.], *in* American Association of Petroleum Geologists (AAPG) Annual Convention, Denver, Colo., June 3–6, 2001, Abstracts: AAPG Annual Convention, vol. 85, p. A58, accessed May 28, 2023.

Fan, M., and Carrapa, B., 2014, Late Cretaceous-early Eocene Laramide uplift, exhumation, and basin subsidence in Wyoming—Crustal responses to flat slab subduction: Tectonics, v. 33, no. 4, p. 509–529, accessed March 5, 2023, at https://doi.org/10.1002/2012TC003221.

Farenbach, M.D., Steece, F.V., Sawyer, J.F., McCormick, K.A., McGillivray, G.L., Schulz, L.D., and Redden, J.A., 2007, South Dakota stratigraphic correlation chart: South Dakota Geological Survey Oil and Gas Investigation 3, accessed November 11, 2023, at http://www.sdgs.usd.edu/pubs/PDF/OGI-03.pdf.

Flores, R.M., 2004, Coalbed methane in the Powder River Basin, Wyoming and Montana—An assessment of the Tertiary-Upper Cretaceous coalbed gas in the Powder River Basin Province, Wyoming and Montana, chap. 2 *of* Total petroleum system and assessment of coalbed gas in the Powder River Basin Province, Wyoming and Montana: U.S. Geological Survey Digital Data Series DDS–69–C, 56 p., accessed May 28, 2023, at https://pubs.usgs.gov/publication/ds69C.

Flores, R.M., Spear, B.D., Kinney, S.A., Purchase, P.A., and Gallagher, C.M., 2010, After a century—Revised Paleogene coal stratigraphy, correlation, and deposition, Powder River Basin, Wyoming and Montana: U.S. Geological Survey Professional Paper 1777, 97 p., CD-ROM in pocket, accessed March 5, 2023, at https://pubs.usgs.gov/pp/1777/.

Fox, J.E., and Higley, D.K., 1996, Structure-contour maps of the Powder River Basin, Montana and Wyoming: U.S. Geological Survey Oil and Gas Investigation Chart 147–A, 10 p., 1 sheet, scale 1:630,000, accessed May 19, 2023, at http://www.mbmg.mtech.edu/mbmgcat/public/ListCitation.asp?pub_id=32414&#gsc.tab=0. [Also available at https://doi.org/10.3133/oc147A.]

Fox, J.E., McCormick, K.A., and Haggar, T.N., 2009, Cross sections showing geophysical logs of Phanerozoic rocks in South Dakota: South Dakota Geological Survey Oil and Gas Investigation 2, 16 pls., accessed March 5, 2023, at https://www.sdgs.usd.edu/pubq/ogi/. [Link is not active in 2025.]

Fryberger, S.G., and Hern, C.Y., 2014, A geometric approach to the analysis of global Eolian hydrocarbon reservoirs: American Association of Petroleum Geologists Rocky Mountain Section, American Association of Petroleum Geologists Search and Discovery Article 41478, 5 p., accessed May 19, 2023, at https://www.searchanddiscovery.com/documents/2014/41478fryberger/ndx_fryberger.pdf. [Adapted from a poster presentation given at the American Association of Petroleum Geologists Rocky Mountain Section Meeting in Denver, Colo., July 20–22, 2014.]

Gelman, S.E., 2023, Modeling the maturation history of the stacked petroleum systems of the Williston Basin, USA: Marine and Petroleum Geology, v. 155, art. 106390, 25 p., accessed October 20, 2023, at https://doi.org/10.1016/j.marpetgeo.2023.106390.

Gelman, S.E., and Burns, E.R., 2025, Three dimensional temperature maps of the Williston Basin, USA—Implications for deep hot sedimentary and enhanced geothermal resources: Geothermics, v. 125, 9 p., accessed January 14, 2025, at https://doi.org/10.1016/j.geothermics.2024.103196.

Gelman, S.E., and Johnson, B.G., 2023, Data release for the 3D petroleum systems model of the Williston Basin, USA: U.S. Geological Survey data release, accessed May 19, 2023, at https://doi.org/10.5066/P9N7O1OT.

Gerhard, L.C., and Anderson, S.B., 1988, Geology of the Williston Basin (United States portion), *in* Sloss, L.L., ed., Sedimentary cover—North American Craton—U.S.: Boulder, Colo., Geological Society of America, The Geology of North America, v. D–2, p. 221–241, accessed May 28, 2023, at https://doi.org/10.1130/DNAG-GNA-D2.221.

Gerhard, L.C., Anderson, S.B., and Fischer, D.W., 1990, Petroleum geology of the Williston Basin, chap. 29 *of* Leighton, M.W., Kolata, D.R., Oltz, D.T., and Eidel, J.J., eds., Interior Cratonic Basins: American Association of Petroleum Geologists Memoir, v. 51, p. 507–559, accessed May 19, 2023, at https://archives.datapages.com/data/specpubs/basinar3/data/a134/a134/0001/0500/0507.htm?q=%2BtextStrip%3Aoil+textStrip%3Ageneration+textStrip%3Awilliston+textStrip%3Abasin.

Glass, G.B., 1993, Geology of Wyoming, v. 1 *of* Snoke, A.W., Steidtmann, J.R., and Roberts, S.M., eds., Geological Survey of Wyoming memoir no. 5: Wyoming State Geological Survey, 937 p., accessed May 19, 2023, at https://sales.wsgs.wyo.gov/geology-of-wyoming-1993/.

Goldberg, J., and Sweetkind, D.S., 2022, Data release—Digital subsurface data from previously published contoured maps of the tops of the Mowry Shale, Morrison Formation, and Minnelusa Formation, Powder River Basin, Wyoming and Montana: U.S. Geological Survey data release, accessed October 20, 2023, at https://doi.org/10.5066/P9WG1GQ3.

Gregory, R.W., 1997, Subsurface correlation of selected Late Cretaceous and older formations along the western margin of the Powder River Basin, Wyoming (cross section A-A'): Wyoming State Geological Survey Geophysical Log Cross Section 97–5, 1 sheet, accessed May 19, 2023, at https://sales.wsgs.wyo.gov/subsurface-correlation-of-selected-late-cretaceous-and-older-formations-along-the-western-margin-of-the-powder-river-basin-wyoming-cross-section-a-a-1997/.

Hallberg, L.L., and Case, J.C., 2001, Preliminary surficial geologic map of the Sundance 30' x 60' quadrangle, Crook and Weston Counties, Wyoming, and southwestern South Dakota: Wyoming State Geological Survey Hazards Section Digital Map 01–6, 1 sheet, scale 1:100,000, accessed October 10, 2023, at https://www.wsgs.wyo.gov/pubs-maps/publication-search.aspx?PubID=HSDM-01-6.

Harris, R.E., and King, J.K., 1989, Industrial minerals and construction materials map of the Powder River Basin and adjacent uplifts, Wyoming (1989): Geological Survey of Wyoming [Wyoming Geological Survey] Map Series 30, scale 1:500,00, accessed July 22, 2024, at https://www.wsgs.wyo.gov/pubs-maps/publication-search.aspx?PubID=MS-30.

Hocking, C.M., 2013a, Elevation contour map of the Inyan Kara Group Butte, Meade, and Lawrence Counties, South Dakota: Belle Fourche River Watershed Partnership, prepared by RESPEC Consulting & Services, 1 sheet, scale 1:180,000, accessed May 19, 2023, at https://www.bellefourchewatershed.org/media/bellefourchefactor360com/documents/Groundwater%20Folder/InyanKara_Structure.pdf.

Hocking, C.M., 2013b, Elevation contour map of the Madison Limestone Butte, Meade, and Lawrence Counties, South Dakota: Belle Fourche River Watershed Partnership, prepared by RESPEC Consulting & Services, 1 sheet, scale 1:180,000, accessed March 5, 2023, at https://www.bellefourchewatershed.org/media/bellefourchefactor360com/documents/Groundwater%20Folder/Madison_Structure.pdf.

Hocking, C.M., 2013c, Elevation contour map of the Minnelusa Formation Butte, Meade, and Lawrence Counties, South Dakota: Belle Fourche River Watershed Partnership, prepared by RESPEC Consulting & Services, 1 sheet, scale 1:180,000, accessed November 11, 2023, at https://www.bellefourchewatershed.org/media/bellefourchefactor360com/documents/Groundwater%20Folder/Minnelusa_Structure.pdf.

Hocking, C.M., 2013d, Elevation contour map of the Deadwood Formation Butte, Meade, and Lawrence Counties, South Dakota: Belle Fourche River Watershed Partnership, prepared by RESPEC Consulting & Services, 1 sheet, scale 1:180,000, accessed May 19, 2023, at https://www.bellefourchewatershed.org/media/bellefourchefactor360com/documents/Groundwater%20Folder/Deadwood_Structure.pdf.

Horton, B.K., Capaldi, T.N., Mackaman-Lofland, C., Perez, N.D., Bush, M.A., Fuentes, F., and Constenius, K.N., 2022, Broken foreland basins and the influence of subduction dynamics, tectonic inheritance, and mechanical triggers: Earth-Science Reviews, v. 234, art. 104193, 28 p., accessed March 5, 2023, at https://doi.org/10.1016/j.earscirev.2022.104193.

Horton, J.D., San Juan, C.A., and Stoeser, D.B., 2017, The State Geologic Map Compilation (SGMC) geodatabase of the conterminous United States (ver. 1.1, August 2017): U.S. Geological Survey Data Series 1052, 46 p., accessed March 5, 2023, at https://doi.org/10.3133/ds1052.

Hoy, R.G., and Ridgway, K.D., 1997, Structural and sedimentological development of footwall growth synclines along an intraforeland uplift, east-central Bighorn Mountains, Wyoming: Geological Society of America Bulletin, v. 109, no. 8, p. 915–935, accessed May 19, 2023, at https://pubs.geoscienceworld.org/gsa/gsabulletin/article-abstract/109/8/915/183275/Structural-and-sedimentological-development-of.

Hunter, J., Ver Ploeg, A.J., and Boyd, C.S., 2005, Geologic map of the Casper 30' x 60' quadrangle, Natrona and Converse Counties, Wyoming: Wyoming State Geological Survey Map Series 65, 1 sheet, scale 1:100,000, accessed May 28, 2023, at https://www.wsgs.wyo.gov/products/wsgs-2005-ms-65.pdf.

Johnson, J.F., and Micale, D.C., 2008, Geologic map of the Lance Creek 30' x 60' quadrangle, Niobrara and Converse Counties, Wyoming, Fall River and Custer Counties, South Dakota, and Sioux County, Nebraska: Wyoming State Geological Survey Map Series 79, 1 sheet, scale 1:100,000, accessed March 5, 2023, at https://www.wsgs.wyo.gov/products/wsgs-2008-ms-79.pdf.

Jones, N.R., Lyman, R.M., Ver Ploeg, A.J., De Bruin, R.H., Case, J.C., and Baxter, J.C., 2003, Structure contour and isopach maps of the Fort Union Formation, northern Powder River Basin, northeastern Wyoming: Wyoming State Geological Survey Open File Report 03–4, 1 sheet, accessed May 19, 2023, at https://sales.wsgs.wyo.gov/structure-contour-and-isopach-maps-of-the-fort-union-formation-northern-powder-river-basin-northeastern-wyoming-2003/.

Kemp, E.A.de, Schetselaar, E.M., Hillier, M.J., Lydon, J.W., and Ransom, P.W., 2016, Assessing the workflow for regional-scale 3D geologic modeling—An example from the Sullivan time horizon, Purcell Anticlinorium East Kootenay region, southeastern British Columbia: Interpretation, v. 4, no. 3, p. SM33–SM50, accessed May 19, 2023, at https://doi.org/10.1190/INT-2015-0191.1.

Kent, D.M., and Christopher, J.E., 2007, Geologic history of the Williston Basin and Sweetgrass arch, chap. 27 *of* Mossop, G., and Shetsen, I., comps., Geologic atlas of the Western Canada sedimentary basin: Canadian Society of Petroleum Geologists and Alberta Research Council, p. 421–429, accessed March 5, 2023, at https://ags.aer.ca/publications/atlas-western-canada-sedimentary-basin/chapters/chapter-27-williston-basin-and.

LeFever, J.A., 2007, Exploration frontiers in the Bakken Formation, Montana and North Dakota: American Association of Petroleum Geologists Search and Discovery Article no. 90071, 1 p., accessed March 4, 2023, at https://www.searchanddiscovery.com/abstracts/html/2007/rocky_mountain/abstracts/lefever.htm.

LeFever, J.A., 2011, The Spearfish Formation—Another unconventional target: North Dakota Geological Survey Newsletter, v. 38, no. 1, p. 11–14. [Also available at https://www.dmr.nd.gov/ndgs/documents/newsletter/jan.2011/Jan2011Spearfish.pdf.]

Lichtner, D.T., Toner, R.N., Wrage, J.M., and Lynds, R.M., 2020, Upper Cretaceous strata in the Powder River Basin—Formation tops database, structure and thickness contour maps, and associated well data: Wyoming State Geological Survey Open File Report 2020–9, 50 p., accessed May 19, 2023, at https://sales.wsgs.wyo.gov/upper-cretaceous-strata-in-the-powder-river-basin-formation-tops-database-structure-and-thickness-contour-maps-and-associated-well-data-2020/.

Lisenbee, A.L., 1978, Laramide structure of the Black Hills uplift, South Dakota-Wyoming-Montana, *in* Matthews, V., ed., Laramide folding associated with basement block faulting in the Western United States: Boulder, Colo., The Geological Society of America Memoir 151, p. 165–196, accessed November 11, 2023, at https://doi.org/10.1130/MEM151-p165.

Lisenbee, A.L., 1985, Tectonic map of the Black Hills uplift, Montana, Wyoming and South Dakota: Geological Survey of Wyoming Map Series 13, 1 sheet, scale 1:250,000, accessed March 5, 2023, at https://sales.wsgs.wyo.gov/tectonic-map-of-the-black-hills-uplift-montana-wyoming-and-south-dakota-1985/.

Lisenbee, A.L., 1988, Tectonic history of the Black Hills uplift, *in* Diedrich, R.P., Dyka, M.A.K., Miller, W.R., eds., Eastern Powder River Basin—Black Hills, Wyoming Geological Association Thirty Ninth Field Conference Guidebook, Casper, Wyoming, September 9–11, 1988: Wyoming Geological Association, p. 45–52, accessed May 19, 2023, at https://pbadupws.nrc.gov/docs/ML1302/ML13023A327.pdf.

Lisenbee, A.L., and DeWitt, E., 1993, Laramide evolution of the Black Hills uplift, *in* Snoke, A.W., Steidtmann, J.R., and Roberts, S.M., eds., Geology of Wyoming: Geological Survey of Wyoming Memoirs 5, v. 1, p. 374–412, accessed November 11, 2023, at https://www.wsgs.wyo.gov/products/wsgs-1993-m-05.pdf.

Lopez, D.A., 2000, Geologic map of the Bridger 30' x 60' quadrangle, Montana: Montana Bureau of Mines and Geology Geologic Map 58, 1 sheet, scale 1:100,000, accessed March 5, 2023, at https://mbmg.mtech.edu/mbmgcat/public/ListCitation.asp?pub_id=10213&#gsc.tab=0.

Love, J.D., and Christiansen, A.C., comps., 1985, Geologic map of Wyoming: U.S. Geological Survey, 3 sheets, scale 1:500,000, accessed March 5, 2023, at https://sales.wsgs.wyo.gov/geologic-map-of-wyoming-2014/. [Rereleased in 2014 by the Wyoming State Geological Survey.]

Love, J.D., Christiansen, A.C., and Ver Ploeg, A.J., comps., 1993, Stratigraphic nomenclature chart of the Laramide Basins, Wyoming: Geological Survey of Wyoming, Wyoming State Geological Survey Map Series MS–41, 1 sheet, accessed May 28, 2023, at https://www.wsgs.wyo.gov/docs/wsgs-web-basin-stratigraphy.pdf.

Lynds, R.M., 2013, Geologic storage assessment of carbon dioxide (CO_2) in the Laramide Basins of Wyoming: Wyoming State Geological Survey Technical Memorandum 3, 200 p., 20 pls., accessed May 19, 2023, at https://sales.wsgs.wyo.gov/geologic-storage-assessment-of-carbon-dioxide-co2-in-the-laramide-basins-of-wyoming-2013/.

Lynds, R.M., and Slattery, J.S., 2017, Correlation of the Upper Cretaceous strata of Wyoming: Wyoming State Geological Survey Open File Report 2017–3, 1 sheet, accessed November 11, 2023, at https://sales.wsgs.wyo.gov/correlation-of-the-upper-cretaceous-strata-of-wyoming-2017/.

MacCormack, K.E., Rokosh, D., and Branscombe, P., 2019. The Alberta Geological Survey 3D geological modeling program, chap. 5 *of* MacKormack, K.E., Berg, R.C., Kessler, H., Russel, H.A.J., and Thorliefson, L.H., eds., 2019 Synopsis of current three-dimensional geologic mapping and modelling in geological survey organizations: Alberta Energy Regulator / Alberta Geological Survey, AER/AGS Special Report 112, p. 24–38. [Also available at https://static.ags.aer.ca/files/document/SPE/SPE_112_CH05.pdf.]

Marcilly, C.M., Torsvik, T.H., and Conrad, C.P., 2022, Global Phanerozoic sea levels from paleogeographic flooding maps: Gondwana Research, v. 110, p. 128–142, accessed March 5, 2023, at https://doi.org/10.1016/j.gr.2022.05.011.

Marra, K.R., Mercier, T.J., Gelman, S.E., Schenk, C.J., Woodall, C.A., Cicero, A.D., Drake, R.M., II., Ellis, G.S., Finn, T.M., Gardner, M.H., Hearon, J.S., Johnson, B.G., Lagesse, J.H., Le, P.A., Leathers-Miller, H.M., Timm, K.K., and Young, S.S., 2021, Assessment of undiscovered continuous oil resources in the Bakken and Three Forks Formations of the Williston Basin Province, North Dakota and Montana, 2021: U.S. Geological Survey Fact Sheet 2021–3058, 4 p., accessed May 19, 2023, at https://doi.org/10.3133/fs20213058.

Marshak, S., Karlstrom, K., and Timmons, J.M., 2000, Inversion of Proterozoic extensional faults—An explanation for the pattern of Laramide and Ancestral Rockies intracratonic deformation, United States: Geology, v. 28, no. 8, p. 735–738, accessed July 31, 2024, at https://pubs.geoscienceworld.org/gsa/geology/article-abstract/28/8/735/191901/Inversion-of-Proterozoic-extensional-faults-An.

Martin, J.E., Sawyer, J.F., Fahrenbach, M.D., Tomhave, D.W., and Schulz, L.D., 2004, Geologic map of South Dakota: South Dakota Department of Environment and Natural Resources Geological Survey General Map 10, 1 sheet, 20 p., accessed May 19, 2023, at https://sddenr.net/pubs/pdf/G-10.pdf. [Also available at https://www.sdgs.usd.edu/publications/default.aspx.]

McCormick, K.A., 2010, Precambrian basement terrane of South Dakota: South Dakota Department of Environment & Natural Resources Geological Survey Bulletin 41, 45 p., accessed November 11, 2023, at http://www.sdgs.usd.edu/pubs/pdf/b-41.pdf.

McLaughlin, J.F., and Harris, R.E., 2005, Geologic map of the Torrington 30' x 60' quadrangle, Goshen and Platte Counties, Wyoming, and Sioux and Scotts Bluff Counties, Nebraska: Wyoming State Geological Survey Map Series 66, 1 sheet, scale 1:100,000, accessed March 5, 2023, at https://sales.wsgs.wyo.gov/geologic-map-of-the-torrington-30-x-60-quadrangle-goshen-and-platte-counties-wyoming-and-sioux-and-scotts-bluff-counties-nebraska-2005/.

McLaughlin, J.F., Stafford, J.E., and Harris, R.E., 2011, Geologic map of the Lusk 30’ x 60’ quadrangle, Niobrara, Goshen, Converse, and Platte Counties, Wyoming, and Sioux County, Nebraska: Wyoming State Geological Survey Map Series 82, 1 sheet, scale 1:100,000, accessed March 5, 2023, at https://sales.wsgs.wyo.gov/geologic-map-of-the-lusk-30-x-60-quadrangle-goshen-and-niobrara-counties-wyoming-2011/.

McLaughlin, J.F., and Ver Ploeg, A.J., 2006, Geologic map of the Newcastle 30' x 60' quadrangle, Weston and Niobrara Counties, Wyoming, and Pennington and Custer Counties, South Dakota: Wyoming State Geological Survey Map Series 71, 1 sheet, scale 1:100,000, accessed March 5, 2023, at https://sales.wsgs.wyo.gov/geologic-map-of-the-newcastle-30-x-60-quadrangle-weston-and-niobrara-counties-wyoming-and-pennington-and-custer-counties-south-dakota-2006/.

McLaughlin, J.F., and Ver Ploeg, A.J., 2008, Geologic map of the Douglas 30' x 60' quadrangle, Converse and Platte Counties, Wyoming: Wyoming State Geological Survey Map Series 83, 1 sheet, scale 1:100,000, accessed March 5, 2023, at https://sales.wsgs.wyo.gov/geologic-map-of-the-douglas-30-x-60-quadrangle-converse-and-platte-counties-wyoming-2008/.

McPherson, B.J.O.L., and Chapman, D.S., 1996, Thermal analysis of the southern Powder River Basin, Wyoming: Geophysics, v. 61, no. 6, p. 1689–1701, accessed July 31, 2024, at https://doi.org/10.1190/1.1444087.

McPherson, B.J.O.L., and Cole, B.S., 2000, Multiphase CO_2 flow, transport and sequestration in the Powder River Basin, Wyoming, USA: Journal of Geochemical Exploration, v. 69–70, p. 65–69, accessed July 31, 2024, at https://doi.org/10.1016/S0375-6742(00)00046-7.

Melick, J.J., 2013, Subsurface description and modeling of geologic heterogeneity in large subsurface datasets—Using temporal and scalar hierarchies, Powder River Basin, WY and MT, U.S.A: Bozeman, Mont., Montana State University, Ph.D. dissertation, 222 p., 2 pls., accessed March 5, 2023, at https://scholarworks.montana.edu/items/78487b3b-1731-48b2-a462-3acfbb598c07.

Merewether, E.A., 1996, Stratigraphy and tectonic implications of Upper Cretaceous rocks in the Powder River Basin, northeastern Wyoming and southeastern Montana, chap. T *of* Nuccio, V.F., Hansley, P.L., Cobban, W.A., and Whitney, C.G., eds., Evolution of sedimentary basis—Powder River Basin: U.S. Geological Survey Bulletin 1917–T, 92 p., accessed March 5, 2023, at https://doi.org/10.3133/b1917T.

Montana Board of Oil and Gas Conservation [MBOGC], [undated], [MBOGC's Online Oil and Gas Information System]: Montana Board of Oil and Gas Conservation web page, accessed November 2023 at https://bogapps.dnrc.mt.gov/dataminer/Default.aspx.

Moore, M., Chakhmouradian, A.R., Mariano, A.N., and Sidhu, R., 2015, Evolution of rare-earth mineralization in the Bear Lodge carbonatite, Wyoming—Mineralogical and isotopic evidence: Ore Geology Reviews, v. 64, p. 499–521, accessed November 11, 2023, at https://doi.org/10.1016/j.oregeorev.2014.03.015.

Murphy, E.C., Nordeng, S.H., Juenker, B.J., and Hoganson, J.W., 2009, North Dakota stratigraphic column: North Dakota Geological Survey Miscellaneous Series 91, 1 sheet, accessed March 5, 2023, at https://www.dmr.nd.gov/ndgs/documents/Publication_List/pdf/Strat-column-NDGS-(2009).pdf.

Naylor, S., Wickert, A.D., Edmonds, D.A., and Yanites, B.J., 2021, Landscape evolution under the southern Laurentide Ice Sheet: Science Advances, v. 7, no. 48, art. eabj2938, 8 p., accessed November 11, 2023, at https://doi.org/10.1126/sciadv.abj2938.

Nesheim, T.O., 2016, Generalized geologic cross-sections of eastern North Dakota: North Dakota Geological Survey Geologic Investigations no. 200, 1 sheet, accessed May 28, 2023, at https://www.dmr.nd.gov/ndgs/documents/Publication_List/pdf/GEOINV/GI-200.pdf.

North Dakota Department of Mineral Resources, [undated], Premium subscription service [well data]: North Dakota Department of Mineral Resources database, accessed November 2023 at https://www.dmr.nd.gov/oilgas/subscriptionservice.asp.

Osmonson, L.M., Scott, D.C., Haacke, J.E., Luppens, J.A., and Pierce, P.E., 2011, Assessment of coal geology, resources, and reserve base in the southwestern Powder River Basin, Wyoming: U.S. Geological Survey Open-File Report 2011–1134, 135 p. [Also available at https://doi.org/10.3133/ofr20111134.]

Perry, F., 2019, Geologic Framework Model (GFM) for the Shale Reference Case [presentation], Spent Fuel & Waste Disposition Annual Working Group Meeting UNLV-SEB, Las Vegas, Nevada, May 21–23, 2019: U.S. Department of Energy Office of Scientific and Technical Information Conference SAND2019-5534PE, 12 presentation slides, accessed November 11, 2023, at https://www.osti.gov/servlets/purl/1648805. [Link is not active in 2025]

Peterson, J.A., 1984, Stratigraphy and sedimentary facies of the Madison Limestone and associated rocks in parts of Montana, Nebraska, North Dakota, South Dakota, and Wyoming: U.S. Geological Survey Professional Paper 2173–A, 34 p., 20 pls., accessed May 28, 2023, at https://doi.org/10.3133/pp1273A.

Peterson, J.A., 1988, Phanerozoic stratigraphy of the northern Rocky Mountain region, *in* Sloss, L.L., ed., Sedimentary Cover—North American Craton—U.S.: Boulder, Color., Geological Society of America, The Geology of North America, v. D–2, p. 83–107, accessed May 19, 2023, at https://doi.org/10.1130/DNAG-GNA-D2.83.

Peterson, S., 2016, Base of aquifer contours for the Northern High Plains Aquifer: U.S. Geological Survey data release, accessed May 19, 2023, at https://doi.org/10.5066/F7K072C9.

Phillips, J.D., Duval, J.S., and Ambroziak, R.A., 1993, National geophysical data grids; gamma-ray, gravity, magnetic, and topographic data for the conterminous United States: U.S. Geological Survey Digital Data Series DDS–9, accessed November 11, 2023, at https://pubs.er.usgs.gov/publication/ds9.

Pollastro, R.M., Roberts, L.N.R., and Cook, T.A., 2013, Geologic assessment of technically recoverable oil in the Devonian and Mississippian Bakken Formation, chap. 5 *of* Assessment of undiscovered oil and gas resources of the Williston Basin Province of North Dakota, Montana, and South Dakota, 2010 (ver. 1.1, November 2013): U.S. Geological Survey Digital Data Series DDS–69–W, 34 p., accessed May 19, 2023, at https://pubs.usgs.gov/dds/dds-069/dds-069-w/.

Redden, J.A., and DeWitt, E., 2008, Maps showing geology, structure, and geophysics of the central Black Hills, South Dakota: U.S. Geological Survey Scientific Investigations Map 2777, 44-p. pamphlet, 2 sheets, accessed November 11, 2023, at https://doi.org/10.3133/sim2777.

Robbins, S.L., 1994, Gravity and aeromagnetic studies of the Powder River Basin and surrounding areas, southeastern Montana, northeastern Wyoming, and western South Dakota, chap. R *of* Nuccio, V.F., Hansley, P.L., Cobban, W.A., and Whitney, C.G., eds., Evolution of sedimentary basins—Powder River Basin: U.S. Geological Survey Bulletin 1917–R, 17 p., 4 pls., accessed May 28, 2023, at https://doi.org/10.3133/b1917R.

Roberts, B.J., 2018, Geothermal resources of the United States—Identified hydrothermal sited and favorability of deep enhanced geothermal systems (EGS): National Renewable Energy Laboratory, accessed July 31, 2024, at https://www.nrel.gov/docs/libraries/gis/high-res-images/geothermal-identified-hydrothermal-and-egs.jpg?sfvrsn=94d5211_1.

Roberts, D., Luneburg, C., Jin, D., and Kato, J., 2022, Using a kinematic and mechanical modelling workflow to constrain fracture network characteristics—Application to the Teapot Dome, Wyoming, USA: Journal of Structural Geology, v. 159, art. 104596, 13 p., accessed November 11, 2023, at https://doi.org/10.1016/j.jsg.2022.104596.

Sarg, J.F., 2011, The Bakken—An unconventional petroleum and reservoir system: U.S. Department of Energy National Energy Technology Laboratory, prepared by Colorado School of Mines, under award no. DE-NT0005672, accessed November 2024 at https://netl.doe.gov/sites/default/files/2018-03/nt0005672-final-report.pdf.

Schoon, R.A., and McGregor, D.J., 1974, Geothermal potentials in South Dakota: South Dakota Geological Survey Report of Investigations 110, 76 p., accessed June 03, 2025, at https://www.sdgs.usd.edu/pubs/pdf/RI-110.pdf.

Seequent, 2021, Leapfrog Geo (ver. 2021.2): Christchurch, New Zealand, Seequent software release, accessed May 2022 at https://www.seequent.com/products-solutions/leapfrog-geo/#resources.

Shelton, J.L., Andrews, W., Colgan, J.P., Johnstone, S., Soller, D.R., Berg, R., Sweetkind, D., Zellman, K.L., Brock, J., and Ritzel, K., 2022, The National Cooperative Geologic Mapping Program's U.S. GeoFramework Initiative—Delivering a digital database of geologic map information by 2030: U.S. Geological Survey Fact Sheet 2022–3079, 2 p., accessed May 28, 2023, at https://doi.org/10.3133/fs20223079.

Siler, D.L., Witter, J.B., Craig, J.W., Earney, T.E., Schermerhorn, W.D., Fournier, D., Faulds, J.E., Glen, J.M.G., and Peacock, J.R., 2023, Three-dimensional geologic map of the southeastern Gabbs Valley geothermal area, Nevada: U.S. Geological Survey Scientific Investigations Map 3498, 1 sheet, 23 p., accessed November 11, 2023, at https://doi.org/10.3133/sim3498.

Sloss, L.L., 1963, Sequences in the cratonic interior of North America: Geological Society of America Bulletin, v. 74, no. 2, p. 93–114, accessed March 5, 2023, at https://doi.org/10.1130/0016-7606(1963)74[93:SITCIO]2.0.CO;2.

Smith, L.B., Eberli, G.P., and Sonnenfeld, M.D., 2004, Sequence-stratigraphic and paleographic distribution of reservoir-quality dolomite, Madison Formation, Wyoming and Montana, *in* Grammer, G.M., Harris, P.M., and Eberli, G.P., eds., Integration of outcrop and modern analogs in reservoir modeling: Tulsa, Okla., American Association of Petroleum Geologists Memoir 80, p. 67–92, accessed November 11, 2023, at https://doi.org/10.1306/M80924C4.

Snoke, A.W., Steidtmann, J.R., and Roberts, S.M., eds., 1993, Geology of Wyoming: Geological Survey of Wyoming [Wyoming State Geological Survey] Memoir 5, 2 v., 937 p., 10 pls., accessed March 5, 2023, at https://sales.wsgs.wyo.gov/geology-of-wyoming-1993/.

Soller, D.R., and Garrity, C.P., 2018, Quaternary sediment thickness and bedrock topography of the glaciated United States east of the Rocky Mountains: U.S. Geological Survey Scientific Investigations Map 3392, 2 sheets, scale 1:5,000,000, accessed March 5, 2023, at https://doi.org/10.3133/sim3392.

Sonnenberg, S.A., 2012, The new Bakken play in eastern Montana: American Association of Petroleum Geologists Search and Discovery Article 10424, 37 p., accessed October 10, 2023, at https://www.searchanddiscovery.com/documents/2012/10424sonnenberg/ndx_sonnenberg.pdf.

Sonnenberg, S.A., 2018, The Niobrara Formation in the southern Powder River Basin, Wyoming—An emerging giant continuous petroleum accumulation [abs.], *in* Unconventional Resources Technology Conference, Houston, Texas, July 23–25, 2018: Unconventional Resources Technology Conference, p. 3854–3868, accessed March 5, 2023, at https://doi.org/10.15530/urtec-2018-2901558.

Sonnenberg, S.A., and Pramudito, A., 2009, Petroleum geology of the giant Elm Coulee field, Williston Basin: American Association of Petroleum Geologists (AAPG) Bulletin, v. 93, no. 9, p. 1127–1153, accessed May 19, 2023, at https://doi.org/10.1306/05280909006.

Sonnenfeld, M.D., 1996, Sequence evolution and hierarchy within the Lower Mississippian Madison Limestone of Wyoming, *in* Longman, M.W., and Sonnenfeld, M.D., Paleozoic systems of the Rocky Mountain region: Rocky Mountain Section SEPM (Society for Sedimentary Geology), p. 165–192, accessed November 11, 2023, at https://archives.datapages.com/data/rocky_sepm/data/034/034001/pdfs/165.pdf.

South Dakota Geological Survey Program, [undated], Oil and gas online databases: South Dakota Department of Agriculture and Natural Resources, accessed October 2022 at http://www.sdgs.usd.edu/SDOIL/oilgas_databases.aspx.

Spangler, L.R., 2024a, Digital database for a 3D geological model of the Powder River Basin and Williston Basin regions, USA: U.S. Geological Survey data release, https://doi.org/10.5066/P13RSCBV.

Spangler, L.R., 2024b, Digital database for a 3D geological model of western South Dakota, USA: U.S. Geological Survey data release, https://doi.org/10.5066/P9LK4QHJ.

Spangler, L.R., Melick, J., and Sweetkind, D.S., 2023, Digital subsurface database of elevation point data and structure contour maps of multiple subsurface units, Powder River Basin, Wyoming and Montana, USA: U.S. Geological Survey data release, accessed March 10, 2024, at https://doi.org/10.5066/P953MC5C.

Spangler, L.R., and Sweetkind, D.S., 2022, Digital subsurface database of previously published well tops, structural features, and contour maps of the Inyan Kara Group, Minnekahta Formation, Minnelusa Formation, Madison Group, and Deadwood Formation, Black Hills region, South Dakota and Wyoming: U.S. Geological Survey data release, accessed March 5, 2023, at https://doi.org/10.5066/P90KFVPC.

Staatz, M.H., 1983, Geology and description of thorium and rare-earth deposits in the southern Bear Lodge Mountains, northeastern Wyoming: U.S. Geological Survey Professional Paper 1049–D, 52 p., 2 pls., accessed May 19, 2023, at https://doi.org/10.3133/pp1049D.

Stanton, J.S., 2015, Geodatabase of the datasets used to represent the 4 subareas of the Lower Cretaceous aquifer, Iowa, Kansas, Minnesota, Montana, Nebraska, North Dakota, South Dakota, and Wyoming: U.S. Geological Survey data release, accessed May 28, 2023, at https://doi.org/10.5066/P99NHURK.

Stone, D.S., 1987, Rocky Mountain transect—Wyoming, transect segments NE3, NE4, NE5, NE6, NE7, NE8: Littleton, Colo., Rocky Mountain Association of Geologists, 1 DVD. [Version 2.0.]

Stone, D.S., 1993, Basement-involved thrust-generated folds as seismically imaged in the subsurface of the central Rocky Mountain foreland, *in* Schmidt, C.J., Chase, R.B., and Erslev, E.A., eds., Laramide basement deformation in the Rocky Mountain foreland of the Western United States: Boulder, Colo., Geological Society of America Special Paper 280, p. 339–358, accessed March 5, 2023, at https://doi.org/10.1130/SPE280-p271.

Stone, D.S., 2002, Morphology of the Casper Mountain uplift and related, subsidiary structures, central Wyoming—Implications for Laramide kinematics, dynamics, and crustal inheritance: American Association of Petroleum Geologists (AAPG) Bulletin, v. 86, no. 8, p. 1417–1440, accessed November 11, 2023, at https://doi.org/10.1306/61EEDCBA-173E-11D7-8645000102C1865D.

Stone, D.S., 2003, New interpretations of the Piney Creek thrust and associated Granite Ridge tear fault, northeastern Bighorn Mountains, Wyoming: Rocky Mountain Geology, v. 38, no. 2, p. 205–235, accessed March 5, 2023, at https://doi.org/10.2113/gsrocky.38.2.205.

Sutherland, W.M., 2007, Geologic map of the Sundance 30' x 60' quadrangle, Crook and Weston Counties, Wyoming, and Lawrence and Pennington Counties, South Dakota: Wyoming State Geological Survey Map Series 78, 1 sheet, scale 1:100,000, accessed March 5, 2023, at https://sales.wsgs.wyo.gov/geologic-map-of-the-sundance-30-x-60-quadrangle-crook-and-weston-counties-wyoming-and-lawrence-and-pennington-counties-south-dakota-2007/.

Sutherland, W.M., 2008, Geologic map of the Devils Tower 30' x 60' quadrangle, Crook County, Wyoming, Butte and Lawrence Counties, South Dakota, and Carter County, Montana: Wyoming State Geological Survey Map Series 81, 1 sheet, scale 1:100,000, accessed March 5, 2023, at https://sales.wsgs.wyo.gov/geologic-map-of-the-devils-tower-30-x-60-quadrangle-crook-county-wyoming-butte-and-lawrence-counties-south-dakota-and-carter-county-montana/.

Sweetkind, D.S., 2017, Three-dimensional hydrogeologic framework model of the Rio Grande transboundary region of New Mexico and Texas, USA, and northern Chihuahua, Mexico: U.S. Geological Survey Scientific Investigations Report 2017–5060, 49 p., accessed March 5, 2023, at https://doi.org/10.3133/sir20175060.

Sweetkind, D.S., Faunt, C.C., and Hanson, R.T., 2013, Construction of 3-D geologic framework and textural models for Cuyama Valley groundwater basin, California: U.S. Geological Survey Scientific Investigations Report 2013–5127, 46 p., accessed March 5, 2023, at https://pubs.usgs.gov/sir/2013/5127/pdf/sir2013-5127.pdf.

Sweetkind, D.S., Graymer, R., Higley, D.K., and Boyd, O.S., 2019, Status of three-dimensional geological mapping and modelling activities in the U.S. Geological Survey, chap. 26 *of* MacKormack, K.E., Berg, R.C., Kessler, H., Russel, H.A.J., and Thorliefson, L.H., eds., Synopsis of current three-dimensional geologic mapping and modelling in geological survey organizations: Alberta Energy Regulator / Alberta Geological Survey, AER/AGS Special Report 112, p. 278–289. [Also available at https://static.ags.aer.ca/files/document/SPE/SPE_112_CH26.pdf.]

Sweetkind, D.S., and Zellman, K.L., 2022, Spatial data from an inventory of U.S. Geological Survey three-dimensional geologic models, volume 1, 2004–2022: U.S. Geological Survey data release, accessed May 19, 2023, at https://doi.org/10.5066/P9OFRNUN.

Sweetkind, D.S., and Zellman, K.L., 2023, An inventory of three-dimensional geologic models—U.S. Geological Survey, 2004–22: U.S. Geological Survey Data Report 1183, 13 p., accessed May 19, 2023, at https://doi.org/10.3133/dr1183.

Syzdek, J.C., Malone, D.H., and Craddock, J.C., 2019, Detrital zircon U-Pb geochronology and provenance of the Sundance Formation, western Powder River Basin, Wyoming: The Mountain Geologist, v. 56, no. 3, p. 295–317, accessed May 19, 2023, at https://doi.org/10.31582/rmag.mg.56.3.295.

Taboga, K.G., Stafford, J.E., Rodgers, J.R., and Carroll, C.J., 2015, Groundwater response in the Upper Wyodak coal zone, Powder River Basin, Wyoming: Wyoming State Geological Survey Report of Investigations 66, 60 p., accessed May 28, 2023, at https://www.wsgs.wyo.gov/products/wsgs-2015-ri-66.pdf.

Thamke, J.N., LeCain, G.D., Ryter, D.W., Sando, R., and Long, A.J., 2014, Hydrogeologic framework of the uppermost principal aquifer systems in the Williston and Powder River structural basins, United States and Canada (ver. 1.1, December 2014): U.S. Geological Survey Scientific Investigations Report 2014–5047, 38 p., accessed May 28, 2023, at https://doi.org/10.3133/sir20145047.

Thorliefson, L.H., MacCormack, K.E., Berg, R.C., Russel, H.A.J., and Kessler, H., 2019, Overview, chap. 1 *of* MacKormack, K.E., Berg, R.C., Kessler, H., Russel, H.A.J., and Thorliefson, L.H., eds., 2019 synopsis of current three-dimensional geologic mapping and modelling in geological survey organizations: Alberta Energy Regulator/ Alberta Geological Survey, AER/AGS Special Report 112, p. 1–2. [Also available at https://ags.aer.ca/publications/all-publications/spe-112.]

Tomhave, D.W., and Schulz, L.D., 2004, Bedrock geologic map showing configuration of the bedrock surface in South Dakota east of the Missouri River: South Dakota Geological Survey General Map 9, 1 sheet, scale 1:500,000, accessed March 5, 2023, at https://sddenr.net/pubs/pdf/G-09.pdf.

Turner, A.K., Kessler, H., and Meulen, M.J. van der, 2021, Applied multidimensional geological modeling—Informing sustainable human interactions with the shallow subsurface: John Wiley & Sons, Ltd., 672 p., accessed January 01, 2023, at https://doi.org/10.1002/9781119163091

U.S. Congress, 2019, Department of the Interior, Environment, and related agencies appropriations bill, 2020: U.S. Congress H.R. 116–100, 237 p., accessed May 23, 2022, at https://www.congress.gov/congressional-report/116th-congress/house-report/100/1.

U.S. Department of Agriculture, 2018, State level data, chap. 2 *of* Census of Agriculture 2012: Washington D.C., U.S. Department of Agriculture Census Volume 1, National Agricultural Statistics Service, p. 245–261, accessed May 22, 2023, at [Link is not active in 2025. Also available at https://agcensus.library.cornell.edu/census_year/2012-census/.]

U.S. Energy Information Administration, [undated], U.S. States—State profiles and energy estimates—U.S. overview: Washington D.C., U.S. Energy Information Administration, State Energy Data System, accessed November 11, 2023, at https://www.eia.gov/state/.

U.S. Geological Survey, 2021a, USGS 1/3 arc-second digital elevation model: OpenTopography, accessed May 28, 2023, at https://doi.org/10.5069/G98K778D.

U.S. Geological Survey, 2021b, USGS 1 arc-second digital elevation model: OpenTopography, accessed March 2, 2023, at https://doi.org/10.5069/G9HX19WN.

Varga, M. de la, and Wellmann, J.F., 2016, Structural geologic modeling as an inference problem—A Bayesian perspective: Interpretation, v. 4, no. 3, p. SM1–SM16, accessed March 5, 2023, at https://doi.org/10.1190/INT-2015-0188.1.

Ver Ploeg, A.J., and Boyd, C.S., 2002, Geologic map of the Buffalo 30' x 60' quadrangle, Johnson and Campbell Counties, Wyoming: Wyoming State Geological Survey Map Series 59, 1 sheet, scale 1:100,000, accessed October 20, 2023, at https://sales.wsgs.wyo.gov/geologic-map-of-the-buffalo-30-x-60-quadrangle-johnson-and-campbell-counties-wyoming-2002/.

Ver Ploeg, A.J., and Boyd, C.S., 2003, Geologic map of the Sheridan 30' x 60' quadrangle, Sheridan, Johnson, and Campbell Counties, Wyoming, and southeastern Montana: Wyoming State Geological Survey Map Series 64, 1 sheet, scale 1:100,000, accessed October 20, 2023, at https://sales.wsgs.wyo.gov/geologic-map-of-the-sheridan-30-x-60-quadrangle-sheridan-johnson-and-campbell-counties-wyoming-and-southeastern-montana-2003/.

Ver Ploeg, A.J., Boyd, C.S., and Mulbay, J.M., 2004, Geologic map of the Kaycee 30' x 60' quadrangle, Johnson, and Campbell Counties, Wyoming: Wyoming State Geological Survey Map Series 63, 1 sheet, scale 1:100,000, accessed November 21, 2023, at https://portal.wsgs.wyo.gov/arcgis/apps/webappviewer/index.html?id=dff082d2d86145fc888aa7cbe3d06a2a.

Vuke, S.M., Porter, K.W., Lonn, J.D., and Lopez, D.A., 2007, Geologic map of Montana: Montana Bureau of Mines and Geology Geologic Map 62–A, 2 sheets, 75 p., scale 1:500,000. [Also available at https://mbmg.mtech.edu/Pubs/SpecialInterest.asp#gsc.tab=0.]

Vuke, S.M., Porter, K.W., Lonn, J.D., and Lopez, D.A., 2009, Geologic map of Montana field notebook: Montana Bureau of Mines and Geology Geologic Map 62–E, 59 p., scale 1:500,000, accessed May 19, 2023, at https://www.mbmg.mtech.edu/mbmgcat/public/ListCitation.asp?pub_id=31205&#gsc.tab=0.

Vuke, S.M., Wilde, E.M., Bergantino, R.N., and Colton, R.B., 2001, Geologic map of the Ekalaka 30' x 60' quadrangle, eastern Montana and adjacent North and South Dakota: Montana Bureau of Mines and Geology Open-File Report 430, 11 p., 1 sheet, scale 1:100,000, accessed June 20, 2023, at https://mbmg.mtech.edu/mbmgcat/public/ListCitation.asp?pub_id=11301&#gsc.tab=0.

Vuke, S.M., Wilde, E.M., Colton, R.B., and Stickney, M.C., 2003, Geologic map of the Wibaux 30' x 60' quadrangle, eastern Montana and adjacent North Dakota: Montana Bureau of Mines and Geology Open-File Report 465, 11 p., 1 sheet, scale 1:100,000, accessed January 15, 2023, at https://mbmg.mtech.edu/mbmgcat/public/ListCitation.asp?pub_id=11336&#gsc.tab=0.

Vuke, S.M., Wilde, E.M., Lopez, D.A., and Bergantino, R.N., 2000, Geologic map of the Lodge Grass 30' x 60' quadrangle, Montana: Montana Bureau of Mines and Geology Geologic Map 56, 1 sheet, scale 1:100,000, accessed September 06, 2024, at https://mbmg.mtech.edu/mbmgcat/public/ListCitation.asp?pub_id=10211&#gsc.tab=0.

Webster, R.L., 1984, Petroleum source rocks and stratigraphy of the Bakken Formation in North Dakota, *in* Woodward, J., Meissner, F.F., and Clayton, J.L., eds., Hydrocarbon source rocks of the greater Rocky Mountain region: Denver, Colo., Rocky Mountain Association of Geologists (Rocky Mountain Geological Association), p. 57–81, accessed November 11, 2023, at https://www.osti.gov/biblio/553627.

Wendell, W.G., Glass, G.B., Breckenridge, R.M., Root, F.K., and Lageson, D.R., 1976, Johnson County, Wyoming—Geologic map atlas and summary of land, water and mineral resources: Geological Survey of Wyoming [Wyoming State Geological Survey] County Resource Series 4, 9 pls. [Also available at https://sales.wsgs.wyo.gov/johnson-county-wyoming-geologic-map-atlas-and-summary-of-land-water-and-mineral-resources-1976/.]

Wheeler, R.L., 1999, Fault number 707, Brockton-Froid fault zone, in Quaternary fault and fold database of the United States: U.S. Geological Survey website, accessed March 5, 2023, at https://earthquake.usgs.gov/cfusion/qfault/show_report_AB_archive.cfm?fault_id=707&section_id.

Whitehead, R.L., 1996, Ground Water Atlas of the United States—Segment 8, Montana, North Dakota, South Dakota, Wyoming: U.S. Geological Survey Hydrologic Atlas 730–I, 24 p., accessed May 28, 2023, at https://doi.org/10.3133/ha730I.

Williamson, J.E., Jarrell, G.J., Clawges, R.M., Galloway, J.M., and Carter, J.M., 2000, Digital data sets for map products produced as part of the Black Hills Hydrology Study, western South Dakota: U.S. Geological Survey Open-File Report 2000–471, accessed May 28, 2023, at https://doi.org/10.3133/ofr00471.

Wittke, S.J., 2007, Geologic map of the Midwest 30' x 60' quadrangle, Natrona, Converse, Johnson, and Campbell Counties, Wyoming: Wyoming State Geological Survey Map Series 73, 1 sheet, scale 1:100,000, accessed July 22, 2024, at https://sales.wsgs.wyo.gov/geologic-map-of-the-midwest-30-x-60-quadrangle-natrona-converse-johnson-and-campbell-counties-wyoming-2007/.

Wyoming State Geological Survey, 2022, Precambrian basement map of Wyoming—Structural configuration (revised February 2023): Wyoming State Geological Survey Open File Report 2022–5, 8 p., 1 pl., scale 1:500,000, accessed November 11, 2023, at https://doi.org/10.15786/21183787.

Wyoming Oil and Gas Conservation Commission [WYOGCC], [undated], WYOGCC data: Wyoming Oil and Gas Conservation Commission database, accessed November 11, 2023, at https://pipeline.wyo.gov/.

Yonkee, W.A., and Weil, A.B., 2015, Tectonic evolution of the Sevier and Laramide belts within the North American Cordillera orogenic system: Earth-Science Reviews, v. 150, p. 531–593, accessed July 31, 2024, at https://doi.org/10.1016/j.earscirev.2015.08.001.

Appendix 1. Model Units from the Northern Great Plains Three-Dimensional Geologic Framework Model

This appendix provides a supplemental data table (table 1.1) that describes model units in the three-dimensional geologic framework model of the northern Great Plains.

Table 1.1. Model units within the northern Great Plains three-dimensional geologic framework model.

Model unit name	Model characteristics				
	Unit label	Age	Description	Reference(s)	Stacking order
Laurentide deposits	Qu	Holocene to early Pliocene	Unconsolidated sediments, including gravel, sand, silt, mud, and large cobbles or boulders. Highly variable thickness. Deposited in glaciofluvial and fluvial environments.	Murphy and others, 2009	42
Surficial undifferentiated	QT	Holocene to late Paleocene	Unconsolidated sediments including gravel, sand, silt, mud, and large cobbles or boulders. Highly variable thickness. Deposited in alluvial, fluvial, and lacustrine environments.	Martin and others, 2004; Farenbach and others, 2007; Vuke and others, 2007	41
Ogallala Group	To	Late Miocene	Well-cemented calcareous sandstone and silty limestone, along with unconsolidated fluvial siltstone, channel sandstone, and gravel. Thickness of as much as 90 meters.	Martin and others, 2004; Farenbach and others, 2007	40
Pre-Pliocene deposits	Tu	Late Miocene to early Eocene	A complex assemblage of sandstone, siltstone, claystone, mudstone, and thin tuffaceous and lignite intervals. Highly variable thickness. Deposited in lacustrine, alluvial, and fluvial environments.	Martin and others, 2004; Farenbach and others, 2007; Murphy and others, 2009	39
Wasatch Formation	Tw	Early to middle Eocene	Orangish-brown arkosic sandstone, lenticular conglomerate, siltstone, shale, coal, and varicolored claystone. Thickness of as much as 529 meters. Deposited in lacustrine, fluvial, alluvial-plain, and swamp environments.	Vuke and others, 2007	38

Table 1.1. Model units within the northern Great Plains three-dimensional geologic framework model.—Continued

Model unit name	Model characteristics				
	Unit label	Age	Description	Reference(s)	Stacking order
Intrusive rock	Ti	Eocene to Paleocene	Intrusive bodies of trachyte, phonolite, rhyolite, and monzonite. Forms dike swarms, sills, small plutons, and laccoliths. Notable carbonatite exposures.	Staatz, 1983; Martin and others, 2004; Redden and DeWitt 2008	37
Tongue River Member of the Fort Union Formation	Tftr	Late Paleocene	Sandstone, siltstone, claystone, and lignite. Thickness of as much as 663 meters. Deposited in lacustrine, fluvial, alluvial-plain, and swamp environments.	Vuke and others, 2007; Murphy and others, 2009	36
Lebo Member of the Fort Union Formation	Tfle	Middle Paleocene	Sandstone, siltstone, claystone, and lignite. Thickness of as much as 185 meters. Deposited in lacustrine, fluvial, alluvial-plain, and swamp environments.	Vuke and others, 2007; Murphy and others, 2009	35
Tullock Member of the Fort Union Formation	Tftu	Early Paleocene	Sandstone, siltstone, claystone, and lignite. Thickness of as much as 180 meters. Deposited in lacustrine, fluvial, alluvial-plain, and swamp environments.	Vuke and others, 2007; Murphy and others, 2009	34
Lance Formation and Hell Creek Formation	K/Klhc	Late Cretaceous	Tan to brown and light to dark-gray shale, interbedded with carbonaceous shale, bentonitic silty shale, and siltstone. Thickness of as much as 335 meters. Fluvial coastal and floodplain deposition.	Martin and others, 2004; Farenbach and others, 2007; Vuke and others, 2007; Murphy and others, 2009	33
Fox Hills Formation	Kfh	Late Cretaceous	Coarsening-upward packages of yellowish-orange to gray fine to medium-grained noncalcareous sandstone. Thickness of as much as 143 meters. Offshore-barrier island, foreshore, and shoreface-depositional environments.	Martin and others, 2004; Farenbach and others, 2007; Vuke and others, 2007; Lichtner and others, 2020	32
Pierre Shale and Lewis Shale	Kp/Kb/Kl	Late Cretaceous	Blue-gray to dark-gray fissile to blocky shale. Thickness of as much as 817 meters. Open-marine depositional environments.	Martin and others, 2004; Farenbach and others, 2007; Vuke and others, 2007; Murphy and others, 2009	31

Table 1.1. Model units within the northern Great Plains three-dimensional geologic framework model.—Continued

Model unit name	Model characteristics				
	Unit label	Age	Description	Reference(s)	Stacking order
Teckla Member of the Lewis Shale	Kt	Late Cretaceous	Sandstone packages are separated by bentonitic shale. Thickness of as much as 96 meters. Deposited in nearshore and deltaic-depositional environments.	Lichtner and others, 2020	30
Teapot Member of the Mesaverde Formation	Kmt	Late Cretaceous	Carbonaceous sandstone with local sandy shale and coal. Thickness of as much as 54 meters. Deposited in a progradational sequence of marine to nonmarine lithofacies.	Lichtner and others, 2020	29
Parkman Sandstone Member of the Mesaverde Formation and Red Bird Silty Member of the Pierre Shale	Kpk/Kprb	Late Cretaceous	Interbedded fine-grained sandstone and carbonaceous shale. Thickness of as much as 406 meters. Marine- to marginal-marine prodeltaic depositional environments.	Lichtner and others, 2020	28
Niobrara Formation	Kn	Late Cretaceous	White to dark-gray argillaceous chalk, marl, and shale. Thickness of as much as 284 meters. Marine depositional environment.	Martin and others, 2004; Farenbach and others, 2007; Murphy and others, 2009; Lichtner and others, 2020	27
Carlile Shale and Sage Breaks Shale	Kca	Late Cretaceous	Medium- to dark-gray noncalcareous shales, dark-gray to black silty to sandy shale, and carbonate concretions. Thickness of as much as 213 meters. Open-marine depositional environments.	Martin and others, 2004; Farenbach and others, 2007; Vuke and others, 2007; Murphy and others, 2009	26
Turner Sandy Member of the Carlile Shale	Kcat/Kcwc	Late Cretaceous	Thin- to medium-grained sandstone, interbedded noncalcareous shale, and argillaceous siltstone. Thickness of as much as 147 meters. Deposited in estuary, nearshore, and delta-front environments.	Lichtner and others, 2020	25
Greenhorn Formation	Kgr	Late Cretaceous	Dark-gray thinly bedded shaly limestone and light-blue-grey interbeds of chalky shale and bentonite. Thickness of as much as 113 meters. Marine-depositional environment.	Martin and others, 2004; Farenbach and others, 2007; Vuke and others, 2007; Murphy and others, 2009	24

Table 1.1. Model units within the northern Great Plains three-dimensional geologic framework model.—Continued

Model unit name	Model characteristics				
	Unit label	Age	Description	Reference(s)	Stacking order
Belle Fourche Shale	Kbf	Late Cretaceous	Medium- to dark-gray micaceous shales, bluish bentonites, and dark-gray to black bentonitic shale with minor limestone lenses. Thickness of as much as 282 meters. Marine-shelf depositional environment.	Martin and others, 2004; Farenbach and others, 2007; Vuke and others, 2007; Murphy and others, 2009	23
Mowry Shale	Km	Early Cretaceous	Light-gray quartzose sandstone, fissile dark shale, and dark- to medium-gray shales with bentonite layers. Thickness of as much as 181 meters. Deposited in an open-marine environment with deltaic and nearshore facies.	Martin and others, 2004; Farenbach and others, 2007; Vuke and others, 2007; Murphy and others, 2009	22
Skull Creek Shale and Thermopolis Shale	Kns/Knt	Early Cretaceous	Medium- to dark-gray micaceous shale and fine-grained glauconitic sandstone. Thickness of as much as 170 meters. Transgressive offshore open-marine depositional environment.	Martin and others, 2004; Farenbach and others, 2007; Vuke and others, 2007; Murphy and others, 2009	21
Inyan Kara Group	Kj	Early Cretaceous	Variegated brown, red, or gray to purple fine-grained sandstone, siltstone, and shale, with a thickness of as much as 200 meters. Deposited in nearshore marine, fluvial, floodplain, and terrestrial environments.	Martin and others, 2004; Farenbach and others, 2007; Murphy and others, 2009; Craddock and others, 2012	20
Morrison Formation	Jme	Late Jurassic	Light-gray to green and variegated red, brown, yellow, or lavender siliceous claystone, shale, and siltstone. Thickness of as much as 180 meters. Fluvial and paludal deposition interfingered with lacustrine environments.	Martin and others, 2004; Farenbach and others, 2007; Vuke and others, 2007	19
Swift, Sundance, and Gypsum Spring Formations	Jsw	Late to Middle Jurassic	Gypsum and anhydrite-bearing shales, multicolored calcareous shales, and interbedded fine- to coarse-grained sandstone. Thickness of as much as 251 meters. Deposited in offshore-marine, lagoonal, and restricted shallow-marine environments.	Martin and others, 2004; Farenbach and others, 2007; Vuke and others, 2007; Murphy and others, 2009	18

Table 1.1. Model units within the northern Great Plains three-dimensional geologic framework model.—Continued

Model unit name	Model characteristics				
	Unit label	Age	Description	Reference(s)	Stacking order
Spearfish Formation and Chugwater Group	TrPC	Triassic to late Permian	Siltstone, red sandy shale, sandstone, and gypsum. Thickness of as much as 229 meters. Deposited in restricted hypersaline shallow-marine, sabkha, and coastal erg environments.	Martin and others, 2004; Farenbach and others, 2007; Murphy and others, 2009	17
Minnekahta Formation and Opeche Shale	Pmo	Middle to early Permian	Purple to gray finely crystalline limestone, red shale, and interbedded siltstone and sandstone. Thickness of as much as 173 meters. Transition from open-marine to restricted-marine or lacustrine deposits.	Martin and others, 2004; Farenbach and others, 2007; Murphy and others, 2009	16
Minnelusa Formation and Tensleep Sandstone	PIPm/PIPt	Early Permian to Pennsylvanian	Variegated yellow to red sandstone, cherty limestone, dolomite, and shale. Thickness of as much as 695 meters. Deposited in mixed carbonate-siliciclastic environments, including shelfal-sabkha and coastal settings.	Martin and others, 2004; Farenbach and others, 2007; Anna, 2010; Craddock and others, 2012; Lynds, 2013	15
Big Snowy Group	Mbs	Late Mississippian	Interbedded shale, limestone, reddish-gray sandstone, and carbonaceous shale. Thickness of as much as 137 meters. Deposited in a deepening-upward trend from nearshore-intertidal to offshore-marine environments.	Murphy and others, 2009	14
Madison Group	Mm	Middle to Early Mississippian	White to light-gray fine- to medium-crystalline limestone and dolomite with chert, and solution features like collapse breccia. Thickness of as much as 825 meters. Deposited in a greenhouse shallow-marine ramp or platform environment.	Martin and others, 2004; Farenbach and others, 2007; Vuke and others, 2007; Murphy and others, 2009	13
Mission Canyon Formation	Mmc	Middle to Early Mississippian	Gray massive limestone and shale, which can be locally pyritic and contain solution breccia zones. Thickness of as much as 520 meters. Deposited in a greenhouse shallow-marine ramp or platform environment.	Vuke and others, 2007	12

Table 1.1. Model units within the northern Great Plains three-dimensional geologic framework model.—Continued

Model unit name	Model characteristics				
	Unit label	Age	Description	Reference(s)	Stacking order
Lodgepole Limestone	Ml	Early Mississippian	Black shale with basal lag conglomerate, light-gray dolomite with fossiliferous lenses, and interbedded cherty gray limestone and calcareous mud. Thickness of as much as 305 meters. Deposited in a greenhouse shallow-marine ramp or platform environment.	Peterson, 1984; Vuke and others, 2007	11
Bakken Formation	MDb	Early Mississippian to Late Devonian	Dark-gray to black carbonaceous shale and light-gray dolomitic siltstone. Thickness of as much as 49 meters. Deposited in an offshore-marine environment.	Murphy and others, 2009	10
Three Forks Shale	MDt	Early Mississippian to Late Devonian	Clean to argillaceous micrite, siltstone, bituminous shale, mottled and pyritic dolomite, and lenses of very fine sand and anhydrite. Thickness of as much as 185 meters. Deposited in restricted-marine, playa-lacustrine, or sabkha environments.	Martin and others, 2004; Farenbach and others, 2007; Murphy and others, 2009	9
Duperow Formation	Dd	Late Devonian	Evaporite sequences interbedded with siltstone, light-crystalline dolostones, and stromatoporod banks capped with anhydrite. Thickness of as much as 533 meters. Deposited in a restricted- to marginal-shallow marine environment.	Murphy and others, 2009	8
Winnepegosis Formation	Dwg	Middle Devonian	Basal brecciated dolostone, red to gray dolostone, interbedded stromatoporoid limestone, and light-gray mudstone. Thickness of as much as 122 meters. Deposited in a deepening-upward sequence from shallow-restricted marine to offshore environments.	Murphy and others, 2009	7

Table 1.1. Model units within the northern Great Plains three-dimensional geologic framework model.—Continued

Model unit name	Model characteristics				
	Unit label	Age	Description	Reference(s)	Stacking order
Interlake Dolomite	SOi	Silurian to Late Ordovician	Light- to dark-brown and gray finely crystalline dolomite, local anhydrite, and red and green dolostone. Thickness of as much as 448 meters. Deposited in shallow-marine environments with a shallowing-upward trend.	Murphy and others, 2009	6
Stony Mountain Formation	Os	Late Ordovician	Grayish-red to buff, fossiliferous limestone and nodular dolomite, with a thickness of as much as 102 meters. Deposited in a shallow marine carbonate environment.	Martin and others, 2004; Farenbach and others, 2007	5
Red River Formation	Or/Oe	Late Ordovician	Yellowish to brown fossiliferous limestone, gray to brown dolomitic limestone, and mottled tan to lavender limestone and dolomite. Thickness of as much as 213 meters. Deposited in shallow- to restricted-marine carbonate environments.	Farenbach and others, 2007	4
Winnipeg Group	Owp	Middle Ordovician	Bioturbated gray to dark-red sand and silt, and greenish-gray to black calcareous shale. Thickness of as much as 161 meters. Deposited in a deepening-upward sequence from fluvial deltaic to offshore open-marine environments.	Murphy and others, 2009	3
Deadwood Formation	O-Cd	Early Ordovician to Cambrian	Brown to light-gray sandstone, shale, limestone, dolomite, and local basal conglomerate. Thickness of as much as 305 meters. Deposited in near-shore, shallow-marine environments.	Martin and others, 2004; Farenbach and others, 2007; Vuke and others, 2007	2
Precambrian basement rock	p€	Precambrian	Crystalline Precambrian crust, including granite, gneiss, schist, and quartzite.	Martin and others, 2004; Anderson, 2009; McCormick, 2010; Bader, 2019a	1

For more information concerning the research in this report, contact the

Center Director, USGS Geosciences and Environmental Change Science Center
Box 25046, Mail Stop 980
Denver, CO 80225
(303) 236-5344

Or visit the Geosciences and Environmental Change Science Center website at
https://www.usgs.gov/centers/geosciences-and-environmental-change-science-center

Publishing support provided by the USGS Science Publishing Network, Denver and Baltimore Publishing Service Centers

USGS

Spangler—**A Three-Dimensional Geologic Framework Model of the Northern Great Plains Region**—SIR 2026–5127

ISSN 2328-0328 (online)
https://doi.org/10.3133/sir20265127